A STUDY OF SECOND-ORDER, $(10\bar{1}1) - (10\bar{1}2)$ TWINNING IN MAGNESIUM

By

WILLIAM HANDY HARTT, III

A DISSERTATION PRESENTED TO THE GRADUATE COUNCIL
THE UNIVERSITY OF FLORIDA
IN PARTIAL FULFILLMENT OF THE REQUIREMENTS FOR THE
DEGREE OF DOCTOR OF PHILOSOPHY

UNIVERSITY OF FLORIDA

August, 1966

DEDICATED TO MY WIFE

HELEN

ACKNOWLEDGMENTS

The author wishes to express his sincere gratitude to the members of the supervisory committee, which included Dr. F.N. Rhines, Dr. R.T. DeHoff, Dr. F.E. Dunnan, and Dr. R.G. Blake. Special thanks are due to Dr. R.E. Reed-Hill, chairman of the committee, for suggesting the topic of this research and for many helpful discussions upon which the success of this work is based.

In addition the author appreciates the helpful suggestions made by Dr. J.J. Hren concerning the electron microscopy phases of this research and the technical assistance on the electron microscope made by Mr. E.J. Jenkins.

The financial support of this work made by the National Aeronautics and Space Administration through an institutional grant is also appreciated.

TABLE OF CONTENTS

		Page
ACKNOWLEDGMENTS		iii
LIST OF TABLES		vi
LIST OF FIGURES		vii
ABSTRACT		xvi
I.	INTRODUCTION	1
II.	EXPERIMENTAL TECHNIQUE	52
III.	Specimen Preparation	52
	Deformation Experiments	54
	Observation of Deformed Surfaces	55
III.	EXPERIMENTAL RESULTS	58
	General Properties of Second-Order Twins	58
	Internal Deformation of $\{10\bar{1}1\} - \{10\bar{1}2\}$ Twins	64
	Shear Accommodation Kinking	80
	Internal Deformation of Shear Accommodation Kinks	88
	Fracture	95
IV.	DISCUSSION PART I; MECHANISM FOR THE SECOND-ORDER, $\{10\bar{1}1\} - \{10\bar{1}2\}$ TWIN HABIT SHIFT	106
	Models for Accommodation of the Second-Order Twinning Shear	116
	Accommodation by kinking	116
	Accommodation by simple slip	124
	Accommodation by dislocation climb	124
	Accommodation by duplex slip	126
V.	DISCUSSION, PART II: INTERNAL DEFORMATION OF SECOND-ORDER, $\{10\bar{1}1\} - \{10\bar{1}2\}$ TWINS	139
	Deformation of Individual, $\{10\bar{1}1\} - \{10\bar{1}2\}$ Twin Lamellae	139

TABLE OF CONTENTS (Continued)

		Page
	Basal slip.	139
	Reorientation of the twinned basal plane by kinking	145
	The Role of Twin Lamellae in the Deformation of a Macroscopic Twin Band.	151
	Grain Boundary Shearing as a Factor in Second-Order Twin Deformation	155
	The Role of Shear Accommodation Kinks in the Deformation Process	163
	Dislocation Models for Shear Accommodation Kinks	165
	Basal dislocations.	165
	Description of the bend plane in terms of two different types of dislocations. .	165
	Slip dislocations on $\{10\bar{1}2\}$	167
	Internal Deformation of Shear Accommodation Kinks	180
VI.	DISCUSSION, PART III: FRACTURE.	190
VII.	CONCLUSIONS.	197
VIII.	APPENDICES	201
	A. INTERNAL DEFORMATION OF $\{10\bar{1}1\}$ - $\{10\bar{1}2\}$ TWINS BY SLIP ON THE BASAL PLANE, 18.5° FROM THE TWIN BOUNDARY.	202
	B. THE LAMELLAE STRUCTURE OF SECOND-ORDER, $\{10\bar{1}1\}$ - $\{10\bar{1}2\}$ TWINS.	205
IX.	BIBLIOGRAPHY	207
X.	BIOGRAPHICAL SKETCH.	216

LIST OF TABLES

Table | Page

1. A comparison of the predicted and observed shear accommodation kink bend plane inclinations based on $\{\bar{1}012\}\ \langle 10\bar{1}1\rangle$ slip . 174

2. The relative inclination of deformation traces within shear accommodation kinks . 181

LIST OF FIGURES

Figure		Page
1.	The geometry of $\langle 10\bar{1}1 \rangle$ $\{11\bar{2}3\}$ slip relative to the close-packed hexagonal unit cell . .	5
2.	A compressive kink band in a single crystal of high purity zinc	7
3.	The distribution of shear strain in the vicinity of the grain boundary of a zinc bicrystal	12
4.	Grain boundary shear in a polycrystalline magnesium tensile specimen.	14
5.	Coherent twin boundary in a face-centered cubic lattice	18
6.	A non-coherent twin boundary in a face-centered cubic lattice.	20
7.	A schematic illustration of a non-coherent twin boundary in a body-centered cubic lattice based on the emmisary dislocation theory of Sleezwyk (55)	21
8.	Accommodation of the shear of a $\{10\bar{1}2\}$ twin in magnesium by kinking on the basal plane . .	25
9.	Accommodation of the shear of $\{11\bar{2}1\}$ twins in zirconium by kinking across a grain boundary	27
10.	Accommodation of the shear of $\{11\bar{2}1\}$ twins in zirconium across a grain boundary by twinning in the adjacent grain	29
11.	Accommodation across a grain boundary of the shear of twins in zirconium by slip in the adjacent grain	31

LIST OF FIGURES (continued)

Figure		Page
12.	Accommodation of the shear of $\{11\bar{2}1\}$ twins in zirconium by formation of a double kink . .	31
13.	A schematic illustration of mechanisms which have been prpposed to account for the nucleation of intercrystalline voids. . . .	32
14.	A schematic illustration of how an obstacle to slip may cause nucleation of a crack . .	34
15.	A schematic illustration of mechanisms by which intercrystalline voids may grow once they are nucleated.	35
16.	A schematic illustration of three basic mechanisms of void coalescence: a) normal rupture. b) shear rupture, and c) tearing. . .	36
17.	Electron micrograph of a normal rupture fracture surface.	38
18.	Electron micrograph of a shear rupture fracture surface.	39
19.	Electron micrograph of a fracture surface which resulted from tearing	40
20.	The temperature dependence of the strain-to-fracture for polycrystalline magnesium. . .	43
21.	The temperature dependence of the strain-to-fracture for single crystals of magnesium oriented with the basal plane parallel to the stress axis	45
22.	Cracking along a second-order, $\{10\bar{1}1\}$ - $\{10\bar{1}2\}$ twin in a grain of a polycrystalline magnesium tensile specimen deformed at 25°C.	48
23.	Electron micrograph of a diffraction grating which illustrates the lens distortion inherently present in the Phillips 100A electron microscope	57
24.	Structure of a typical $\{10\bar{1}1\}$ - $\{10\bar{1}2\}$ twin, as viewed in the optical microscope	59

LIST OF FIGURES (Continued)

Figure		Page
25.	Electron micrograph of $\{10\bar{1}1\}$ - $\{10\bar{1}2\}$ twin lamellae near the front of a second-order twin band	60
26.	Second example of the lamellae structure of $\{10\bar{1}1\}$ - $\{10\bar{1}2\}$ twins	61
27.	The lattice geometry of $\{10\bar{1}2\}$ twinning, as viewed on the $(1\bar{2}10)$ crystal surface (the plane of shear)	63
28.	The lattice geometry of second-order, $\{10\bar{1}1\}$ - $\{10\bar{1}2\}$ twinning	65
29.	The lattice geometry predicted to result from $\{10\bar{1}1\}$ - $\{10\bar{1}2\}$ second-order twinning	66
30.	Composite optical micrograph illustrating the large surface offset and high internal shear strain that may occur in $\{10\bar{1}1\}$ - $\{10\bar{1}2\}$ twins	67
31.	The initial stages of deformation in a region where two $\{10\bar{1}1\}$ - $\{10\bar{1}2\}$ twin lamellae meet	69
32.	The intense shear strain where two twin lamellae meet	70
33.	The interconnection of two $\{10\bar{1}1\}$ - $\{10\bar{1}2\}$ twin lamellae	71
34.	A more advanced stage of the internal deformation of a $\{10\bar{1}1\}$ - $\{10\bar{1}2\}$ twin	72
35.	An example of the intense lattice strain which may occur when two lamellae meet in a region of pronounced internal deformation	73
36.	The flow and cracking along a $\{10\bar{1}1\}$ - $\{10\bar{1}2\}$ twin band after extensive internal shear has occurred	74

LIST OF FIGURES (Continued)

Figure		Page
37.	Example of the deformed structure in a region of intense strain.	75
38.	First example of discontinuous shear along a second-order, $\{10\bar{1}1\}$ - $\{10\bar{1}2\}$ twin . .	78
39.	Second example of discontinuous shear along a second-order, $\{10\bar{1}1\}$ - $\{10\bar{1}2\}$ twin . .	79
40.	The structure of a $\{10\bar{1}1\}$ - $\{10\bar{1}2\}$ twin and its shear accommodation kink.	81
41.	Second example of the appearance of shear accommodation kinks adjacent to second-order, $\{10\bar{1}1\}$ - $\{10\bar{1}2\}$ twins.	82
42.	Electron micrograph of a second-order, $\{10\bar{1}1\}$ - $\{10\bar{1}2\}$ and a shear accommodation kink .	84
43.	Electron micrograph illustrating that shear accommodation kinks remain adjacent to second-order twins by formation of steps along the bend plane.	85
44.	Example of steps which may form along the bend plane of shear accommodation kinks .	86
45.	Schematic illustration of the structure of the shear accommodation kink in Figure 44	87
46.	Example of low shear accommodation kinks remain adjacent to $\{10\bar{1}1\}$ - $\{10\bar{1}2\}$ twins.	89
47.	Small shear accommodation kink in the initial stages of its formation.	90
48.	Example of the deformation which may occur within shear accommodation kinks.	91
49.	Electron micrograph illustrating the distribution of shear strain within a $\{10\bar{1}1\}$ - $\{10\bar{1}2\}$ twin and its shear accommodation kink.	92

LIST OF FIGURES (Continued)

Figure		Page
50.	An example of low shear strain from a {10$\bar{1}$1} - {10$\bar{1}$2} twin is passed into and accommodated within a shear accommodation kink.	94
51.	Example one of shear offset along a deformation trace within a shear accommodation kink	96
52.	Example two of shear offset along a deformation trace within a shear accommodation kink.	97
53.	Example of the large internal shear which may occur within shear accommodation kinks	98
54.	An example of how voids may open up along a {10$\bar{1}$1} - {10$\bar{1}$2} twin.	99
55.	Optical micrograph illustrating how cracks may open up along the macroscopic habit plane of {10$\bar{1}$1} - {10$\bar{1}$2} twins.	101
56.	Structure of the fracture surface which results from cracking along a {10$\bar{1}$1} - {10$\bar{1}$2} twin.	102
57.	Band structure of the fracture surface as observed in the electron microscope	104
58.	Dimple structure of the fracture surface as observed in the electron microscope.	105
59.	Matrix accommodating deformation in the form of kinks resulting from the shear of second-order, {10$\bar{1}$2} twins in zirconium.	112
60.	Schematic illustration of Figure 28 showing the lattice bending induced into a primary, {10$\bar{1}$1} twin tip by the second-order, {10$\bar{1}$2} twinning shear.	114

LIST OF FIGURES (Continued)

Figure		Page
61.	Schematic illustration of how the second-order. $\{10\bar{1}2\}$ twinning shear increases the boundary area of the primary, $\{10\bar{1}1\}$ twin.	115
62.	Accommodation of the second-order, $\{10\bar{1}2\}$ twinning shear by kinking on the matrix basal plane	118
63.	Lattice geometry of $\{10\bar{1}2\}$ twinning in magnesium in terms of the orientations of the first undistorted plane, K_1, and the second undistorted plane, K_2.	119
64.	Effect of the second-order. $\{10\bar{1}2\}$ twinning shear of the orientation of a primary, $\{10\bar{1}1\}$ twin boundary	120
65.	Schematic illustration of successive stages of the compressive deformation of a single crystal by kinking	122
66.	Deformation of a single crystal tensile specimen with end constraints by slip on a single system	123
67.	The effect of dislocation climb on the inclination of a twin relative to the matrix lattice orientation.	125
68.	Deformation of a single crystal tensile specimen by duplex slip on two planes symmetrically oriented with respect to the stress axis	127
69.	Schematic illustration of a magnesium tensile specimen with a $[10\bar{1}0]$ tensile axis showing the relative orientations of the $(10\bar{1}1)$ and $(\bar{1}011)$ lattice planes	129
70.	The effect of matrix glide on $(\bar{1}011)$ on the orientation of the matrix lattice adjacent to a $(10\bar{1}1)$ - $(10\bar{1}2)$ twin. . .	131

LIST OF FIGURES (Continued)

Figure		Page
71.	The effect of matrix glide on $(10\bar{1}1)$ on the orientation of a $(10\bar{1}1)$ - $(10\bar{1}2)$ twin and on the matrix lattice adjacent to a twin .	133
72.	Schematic illustration of the interactions which may occur between dislocations on the $(\bar{1}011)$ and $(10\bar{1}1)$ slip planes.	135
73.	The ultimate dislocation structure in the matrix that is predicted to result from interactions between slip dislocations on $(10\bar{1}1)$ and $(\bar{1}011)$	137
74.	Schematic illustration of the macroscopic shape change observed to accompany the deformation of $\{10\bar{1}1\}$ - $\{10\bar{1}2\}$ twins . . .	141
75.	Schematic illustration of the macroscopic shape change predicted to occur as a $\{10\bar{1}1\}$ - $\{10\bar{1}2\}$ twin deforms by simple slip on the basal plane.	142
76.	Electron micrograph of a $\{10\bar{1}1\}$ - $\{10\bar{1}2\}$ twin on an etched surface.	146
77.	Structure of a kink of 18.5° misorientation that results within a $(10\bar{1}1)$ - $(10\bar{1}2)$ twin as a result of slip on $(\bar{1}011)$.	148
78.	Structure of a kink of 18.5° misorientation that results within a $(10\bar{1}1)$ - $(10\bar{1}2)$ twin as a result of slip on $(\bar{1}011)$ and $(10\bar{1}1)$.	149
79.	Schematic illustration of the misalignment of shear deformation within $\{10\bar{1}1\}$ - $\{10\bar{1}2\}$ twin lamellae relative to that which occurs along the macroscopic band plane	156
80.	Electron micrograph illustrating grain boundary shear in magnesium	158
81.	A highly deformed, $\{10\bar{1}1\}$ - $\{10\bar{1}2\}$ twin in the grain of polycrystalline magnesium tensile specimen	160

LIST OF FIGURES (Continued)

Figure		Page
82.	Schematic illustration of the basal dislocation alignment needed to account for the lattice bending of shear accommodation kinks.	166
83.	The configuration of $\vec{a}_1$ - $\vec{a}_3$, and $\vec{c}$ dislocations needed to describe the bend plane of a shear accommodation kink.	168
84.	Schematic illustration of how $[10\bar{1}1]$ dislocation loops on $(\bar{1}012)$ may account for the structure of shear accommodation kinks . .	171
85.	Structure of a $\{10\bar{1}1\}$ - $\{10\bar{1}2\}$ twin and its shear accommodation kink	175
86.	Second-order twin and its shear accommodation kink.	176
87.	$\{10\bar{1}1\}$ - $\{10\bar{1}2\}$ twin and a highly deformed shear accommodation kink	177
88.	Electron micrograph of a $\{10\bar{1}1\}$ - $\{10\bar{1}2\}$ twin and a shear accommodation kink. . . .	178
89.	Second-order twin and its shear accommodation kink.	179
90.	The relative orientation of two unit cells in a magnesium single crystal tensile specimen with the tensile axis along $[10\bar{1}0]$. The positions of the $(1\bar{1}01)$ and $(0\bar{1}1\bar{1})$ planes are illustrated.	184
91.	The surface offset on the basal plane face of a single crystal which results from $\{10\bar{1}1\}$ - $\{10\bar{1}2\}$ twinning and shear accommodation kinking	186
92.	Electron micrograph illustrating a type of deformation trace within shear accommodation kinks which could not be analyzed .	187

LIST OF FIGURES (Continued)

Figure		Page
93.	Second-order, $\{10\bar{1}1\}$ - $\{10\bar{1}2\}$ twin and its shear accommodation kink as viewed on a $(1\bar{2}10)$ magnesium face which was etched with 20 per cent HCl subsequent to deformation.	188
94.	Schematic illustration of the geometry of the cracks observed at $\{10\bar{1}1\}$ - $\{10\bar{1}2\}$ twin boundaries.	193
95.	Electron micrograph illustrating how cracks may occur normal to the $(1\bar{2}10)$ surface of observation.	195
96.	Schematic illustration of how a single and double twinning shear may give rise to different lamellae structures.	206

Abstract of Dissertation Presented to the Graduate Council in Partial Fulfillment of the Requirements for the Degree of Doctor of Philosophy

A STUDY OF SECOND-ORDER, $\{10\bar{1}1\}$ - $\{10\bar{1}2\}$ TWINNING IN MAGNESIUM

by

William Handy Hartt, III

August, 1966

Chairman: Dr. R.E. Reed-Hill
Major Department: Metallurgical and Materials Engineering

Single crystals of high purity magensium, oriented with the basal plane parallel to the stress axis, were deformed in tension at room temperature and at a strain rate of 0.002 inches/inch/min. in order to form second-order, $\{10\bar{1}1\}$ - $\{10\bar{1}2\}$ twins. The structure and properties of these twins were then investigated using optical and replica electron microscopy techniques. It was concluded that three basic features of these twins are of major importance. The first of these concerns the fact that $\{10\bar{1}1\}$ - $\{10\bar{1}2\}$ twins are inclined approximately 56° to the matrix basal plane, while the orientation of a coherent, $\{10\bar{1}1\}$ twin boundary is at $61^{\circ}54'$. This indicates that a habit shift occurs at some point of the second-order twinning operation. Crocker (Phil. Mag., 7 (1962) 901) has developed a theory for double twinning in an attempt to explain this habit shift phenomenon. However, it is

concluded from the present research that this theory is not applicable to $\{10\bar{1}1\}$ - $\{10\bar{1}2\}$ twinning in magnesium. Instead, five basic conditions are established which any mechanism that is to successfully explain the second-order twin boundary rotation must satisfy, and several models are considered in conjunction with these. In each case it is assumed that the habit shift results from the necessity to accommodate the second-order twinning shear in the matrix. It is concluded that the shift results from duplex slip in the parent lattice adjacent to the twins, and a model is constructed which involves slip on $(10\bar{1}1)$ and $(\bar{1}011)$ planes in $\langle 11\bar{2}3\rangle$ type directions, in good agreement with the experimental observations. The second significant feature of these twins concerns the extensive internal deformation which may occur after the twins form. Experimental observations indicate that after this deformation the basal plane within the second-order twin is oriented nearly parallel to the twin boundary. A non-basal kinking mechanism is postulated that also involves $\{10\bar{1}1\}\langle 11\bar{2}3\rangle$ slip. This rotates the basal plane from its predicted orientation, 18.5° from the boundary, to its observed position. Once this occurs, large strains may result by simple slip on this plane. Additional deformation markings are observed which cannot be described in terms of slip on

previously observed systems. These are best explained by relating the present deformation to grain boundary shear and assuming that similar mechanisms are operative in each case. Also, two processes have been observed whereby the matrix lattice adjacent to these twins may deform. The first of these occurs by shear accommodation kinking. These kinks are most satisfactorily described by a single type of $[10\bar{1}1]$ dislocation in $(10\bar{1}2)$ planes. The second mechanism involves the internal deformation of these kinks subsequent to their formation. Evidence is presented that secondary $\{10\bar{1}1\}$ - $\{10\bar{1}2\}$ twinning and $\langle 10\bar{1}1\rangle$ $\{11\bar{2}3\}$ slip may be responsible. The third feature of importance concerns the fracture which occurs at these twins. This is attributed to large shear strains which develop in these regions. Evidence is presented that small voids open up along the twin boundary during deformation. These grow into microcracks under the influence of the applied stress, and fracture ultimately follows as the interconnecting regions tear apart.

INTRODUCTION

Magnesium has certain properties that justify its application as a structural material. Foremost of these is its high strength-to-weight ratio; that is, it is strong, yet light. But while this may make magnesium favorable for structural application, there are other properties which may sharply limit its usefulness. Most notable of these is its almost complete lack of ductility at room temperature and below. The texture of polycrystalline magnesium which results from most working operations tends to align the basal plane with the axis of working. This applies not only to wrought but also to recrystallized textures. As a consequence, polycrystalline magnesium has a ductility to fracture at room temperature of about 4 per cent (1). In the same manner, single crystal material of similar orientation (with the basal plane parallel to the stress axis) has a ductility to fracture of less than 1 per cent at room temperature (2). However, magnesium should not be classified as a brittle material since, under suitable conditions, it has plastic properties comparable with the most ductile of materials. As evidence of this, Hirsch and Lally (3) recently performed tensile tests on magnesium

single crystals where the basal plane was near the ideal slip orientation and observed shear strains up to 250 per cent in the easy glide region alone. It can only be concluded from this that, with regard to its plastic properties, magnesium is a very anisotropic material.

Slip in Magnesium

Numerous investigators have analyzed the slip properties of magnesium, both in single and polycrystalline form. Here, as in some other close-packed hexagonal metals, glide on the basal plane in the close-packed direction, $(0002)\ \langle 11\bar{2}0\rangle$, is the predominant mode. However, for polycrystalline or single crystalline material with the basal plane parallel to the stress axis, slip on this system is suppressed. For single crystals of this orientation numerous investigators (4,5,6,7) have observed pyramidal $\{10\bar{1}1\}\langle 11\bar{2}0\rangle$ slip above room temperature. On the other hand, slip of the prismatic $\{10\bar{1}0\}\langle 11\bar{2}0\rangle$ type is the prominant non-basal mode below room temperature (2,8). In addition, Reed-Hill and Robertson (7) have observed pyramidal $\{11\bar{2}2\}$ slip on specimens tested at -190°C. Although they were unable to unambiguously determine the slip direction, they did obtain evidence for $\langle 10\bar{1}0\rangle$. Yoshinaga and Horiuchi (9) compressed magnesium single crystals normal to the basal plane and concluded that

$\{11\bar{2}2\}$ slip does not occur. However, judging from their photomicrographs, it is doubtful if the quality of their specimen surfaces was good enough to reveal fine slip traces.

Slip in Other Close-Packed Hexagonal Metals

The slip modes observed in magnesium are characteristic of most close-packed hexagonal metal systems. However, the temperature dependence of non-basal slip in other metals is normally not as pronounced as in magnesium. Consequently, these modes are more significant and operate to increase the low temperature ductility of these metals relative to magnesium.

Slip on $\{11\bar{2}2\}$ planes in a $\langle 11\bar{2}3\rangle$ direction has often been observed in the room temperature deformation of hcp metals such as zinc and cadmium. Gilman (10,11) and Rosenbaum (12) have observed slip of this type in single crystals of zinc. In other experiments with zinc, Bell and Cahn (13) concluded that interaction of this pyramidal mode with basal slip is responsible for the nucleation of $\{10\bar{1}2\}$ twins. Price (14,15,16) has observed that $\{11\bar{2}2\}$ $\langle 11\bar{2}3\rangle$ slip is significant in the deformation and work-hardening behavior of vapor deposited platelets of zinc and cadmium. Also, Baldwin and Reed-Hill(17,18)

have observed slip on $\{11\bar{2}2\}$ planes in polycrystalline specimens of zirconium and hafnium tested in torsion at 77°K. Price (14) observed that $\frac{1}{3}\langle 11\bar{2}3\rangle$ dislocations in the screw orientation may cross glide between $\{11\bar{2}2\}$ and $\{10\bar{1}1\}$ planes. This is possible since planes of this type share a common $\langle 11\bar{2}3\rangle$ direction. The geometry of $\langle 11\bar{2}3\rangle\{10\bar{1}1\}$ slip is illustrated in Figure 1. This figure shows that each $\{10\bar{1}1\}$ plane contains two $\langle 11\bar{2}3\rangle$ slip directions.

Kinking in HCP Metals

Kink bands in general were first observed in metals by Orowan (19) during compression tests on cadmium single crystals. However, their properties were classified as early as 1898 by Mugge (20) for the case of numerous non-metallic crystals. As a result of compression experiments on zinc single crystals, Hess and Barrett (21) were able to describe kink bands in terms of dislocations and normal glide processes. These authors established that, for compressive kink bands pairs of dislocations of opposite sign are nucleated within the volume to be kinked, and these dislocations align into parallel walls nearly normal to the slip plane. Dislocations of one sign enter one wall while those of the opposite sign enter the other. A misorientation in the kinked region then results from

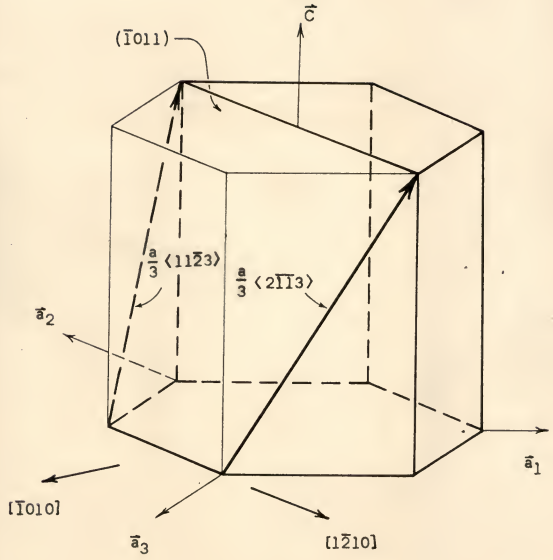

Figure 1: The geometry of $\{10\bar{1}1\}\langle 11\bar{2}3\rangle$ slip relative to the close-packed hexagonal unit cell. The $(\bar{1}011)$ plane and the two Burgers vectors which lie in this plane, a/3 $[11\bar{2}3]$ and a/3 $[2\bar{1}\bar{1}3]$ are shown. Note that this Burgers vector equals an $\vec{a} + \vec{c}$ vector

rotation associated with slip on a single system. Figure 2 is a micrograph of a typical kink of this type from the research of Gilman (22). It is recognized that the nucleation process involves creating dislocation loops on uniformly spaced slip planes. It is also noted that the dislocation walls, or bend planes as they are commonly called, are capable of moving, and that the kink band misorientation may continuously increase by the incorporation of pairs of new dislocations into the bend planes.

Gilman and Read (23) demonstrated that kink bands could also be formed in zinc single crystal tensile specimens, and while the geometry of these kinks was much the same as that observed by Hess and Barrett (21), the morphology was different. In this case kinks were nucleated at some lattice inhomogeniety which had caused a bending moment. This resulted in creating an excess number of edge dislocations of one sign in these regions. These dislocations then form bend planes, as in the case of compressive kink bands. One major distinction between compressive and tensile kinks is that, for the former, the dislocation pairs are created within the kink, while for the latter they are created outside. This is significant since it indicates that for the case of tensile kink bands the dislocations entering each bend plane are nucleated at different sources. Because no conservative mechanism,

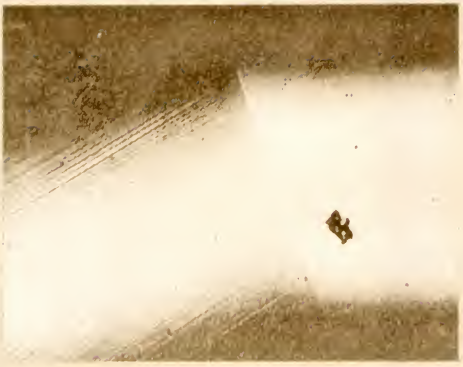

Figure 2: A compressive kink band in a single crystal of high purity zinc. Basal slip traces are observed within the kinked region. The trace of the bend plane is inclined at about 70° from lower right to upper left (after Gilman (22)). 225X

is recognized in dislocation mechanics whereby dislocations of one sign can be created, this implies that somewhere in the lattice there are dislocations, equal in number, but opposite in strength, to those appearing in the bend planes. The specimens of Gilman and Read which formed tensile kinks had crystal orientations from $x_o = 15^o$ to $x_o = 75^o$, where x_o is the angle between the stress axis and the basal plane; so these second sets of dislocations were probably free to glide out of the crystal.

As a result of these and other related experiments (24,25,26,27) two general rules governing the geometry of kink bands, which result from slip on a single plane, were established. These are:

1) The bend plane bisects the angle between the slip plane in the matrix and in the kink.
2) The bend plane bisects the angle between the slip directions of the kink and the matrix.

Gilman and Read (23) showed that any discontinuity in shear strain which results from a simple slip process must necessarily bisect the misorientation angle. If this angle is not bisected, then slip of a second type must occur (28). Since basal slip alone was observed in kink band formation, these investigators were able to account for rule 1 above.

Using the expression for the shear stress of an infinite, vertical array of edge dislocations proposed by Burgers (29), these authors also found that a vertical wall of edge dislocations is self-stabilizing and represents a low energy configuration. This indicates that an attractive interaction exists between the wall and the edge dislocations of the same sign in the lattice. Other authors (30,31,32,33) have since extended the theory of dislocation walls, but the basic qualitative features remain unchanged.

Most of the kink bands studied by the above mentioned investigators (21,23) had a $\langle 1\bar{1}00 \rangle$ bend axis, so that the band plane was nearly normal to a $\langle 11\bar{2}0 \rangle$ slip direction. Kink bands with this axis, whether tensile or compressive, may be completely described in terms of a single dislocation type with Burgers vector $\frac{1}{3}\langle 11\bar{2}0 \rangle$. Hess and Barrett (21), however, also noted examples of bending about a $\langle 11\bar{2}0 \rangle$ axis. For this case the bend plane normal bisected a direction lying midway between two slip directions, and the kink band must have resulted from equal amounts of slip on two basal slip systems. Here the bend plane should be composed of an equal number of two dislocation types.

The Mechanical Effects of Grain Boundaries

It has long been recognized that intercrystalline boundaries increase the strength of a metal crystal. This was concluded by Polanyi and Schmid (34) and by Miller (35), as a result of their classic experiments. The latter thought that the increase in hardness resulted from the fixed nature of the slip planes where they intersected the boundary. Chalmers (36) tested tin bicrystals in tension, where the two crystal orientations were identical with respect to the stress axis, and found that the elastic limit increased linearly as the misorientation angle between the two crystals increased. This implied that the strengthening effect was more involved than originally indicated by Miller (35).

Numerous investigators have also found that the normal slip processes observed in the interior of polycrystalline grains are inhibited in the region adjacent to the boundary. Carpenter and Elam (37) and Yamaguchi (38) concluded from deformation experiments on coarse grained aluminum that less deformation occurs near grain boundaries. The former authors observed this effect up to 2.5 mm. from the boundary. In addition, Hibbard (39) has noted a similar retardation of slip at grain boundaries in copper.

The complex nature of grain boundary hardening has more recently been demonstrated by Galligan, Fenerstein, and Luhman (40). These investigators strained a zinc bicrystal by pure shear parallel to the boundary and observed the relative amounts of strain throughout the specimen. The two crystal orientations were related to one another by a rotation about the basal plane normal, so that the orientation of the close-packed plane was the same in both lattices. In addition, the plane of the boundary was parallel to the basal plane in each crystal. Figure 3 is a micrograph from their original work and shows the shear of a fiducial line which was originally perpendicular to the boundary. This illustrates that the normal crystallographic slip process by which each crystal deforms is inhibited in the region near the grain boundary, even when the active slip plane does not intersect the boundary. As indicated by the arrow, deformation by grain boundary shear, rather than basal slip, has occurred in this region.

However, despite the hardening effect associated with intercrystalline boundaries and its influence on the normal slip processes, polycrystalline materials have an additional means by which they may deform relative to single crystals. This occurs, primarily at elevated temperatures,

Figure 3: The distribution of shear strain in the vicinity of the grain boundary of a zinc bicrystal. The arrow adjacent to the boundary points out that grain boundary shear has occurred (after Galligan, et al. (40)). 238X

by the movement of grains with respect to one another; and this causes large deformation, commonly referred to as grain boundary shear, to be concentrated into small regions adjacent to the boundary. Grain boundary shear has been observed in many metal systems under the proper conditions of temperature and strain rate. Figure 4 is a micrograph illustrating this effect in magnesium deformed 2.2 per cent at room temperature.

The mechanism by which grain boundary deformation occurs is not well understood. Gifkins and Langdon (42) have recently concluded,

> ... that there are two distinct processes: (i) "true" sliding... at the boundary, and (ii) shear near the boundary in a narrow zone....

These authors presented evidence that the first of these may occur independent of the second by showing that the discontinuities in traces which cross a grain boundary in a magnesium - 0.7 per cent aluminum alloy are sharp even at 80,000X. It was also noted that high temperature sliding may occur by a vixcous flow process. However, their investigators demonstrated that this mechanism can not explain the deformation at temperatures well below the melting point. Based on a model for the atomic structure of a grain boundary which combines the "island" theory

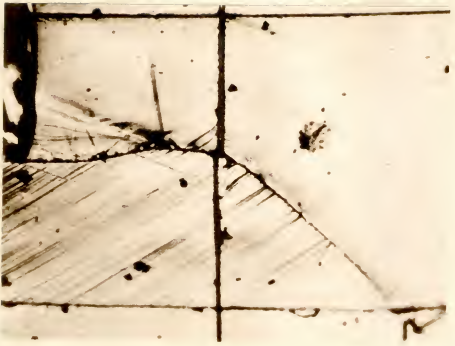

Figure 4: Grain Boundary shear in a polycrystalline magnesium tensile specimen (after Hauser, Starr, Tietz, and Dorn (41)). 140X

of Mott (43) and the defect structure theory of Ké (44), Conrad (45) has concluded that the rate controlling step in sliding is the deformation of jogs on the boundary.

On the other hand, Rhines (46) has contended that sliding per se does not occur, but that grain boundary deformation results from shear in a zone of finite width on one side of the interface. Regarding the mechanism of this shear, Hibbard (39) has stated that the proximity of a boundary may result in slip on systems which would not be operative in a single crystal under similar stress. He referred to this as "forced slip," which is believed to include slip systems that can operate in a single crystal of the same metal. In a discussion of this, Chalmers (47) stated that,

> ... this concept should be extended to include families of planes and directions that are never detected as active slip planes in the single crystal.... There is some evidence that very severely deformed metals no longer deform by slip of the usual kind, even in the interior of grains (48). It is possible that such a wide variety of possible slip planes is available that the main criterion is that of maximum resolved shear stress, in which case the process should be described as "non-crystallographic"....

On this basis it is thought that the shear occurs either by a process of multiple glide or by non-crystallographic flow in a small volume adjacent to the boundary.

Twinning in Magnesium

Mechanical twinning is also a means of plastic deformation available to hexagonal close-packed metals. Unlike twinning in face-centered cubic and body-centered cubic systems, where the twinning shear defines the atom movements exactly, the shear for hcp twinning represents the resultant average movement of a large number of atoms. In order to describe the motion of individual atoms, it is often necessary to postulate movements that occur other than in the twinning direction (49,50,51), and in some cases it is even necessary to include transverse movements.

The most important twinning mode in magnesium is $\{10\bar{1}2\}\langle 10\bar{1}1\rangle$. It is common to most hcp metals and, under the proper conditions of stress and orientation, may occur profusely at a relatively low load. For hexagonal metals, such as magnesium where $c/a = 1.724$ and is, therefore, less than ideal, the conditions for $\{10\bar{1}2\}$ twinning are satisfied by compression parallel to the basal plane. Thus, $\{10\bar{1}2\}$ twinning does not occur when single crystals, oriented with the basal plane parallel to the stress axis, are pulled in tension. $\{10\bar{1}1\}$ and $\{10\bar{1}3\}$ twins have been observed in single crystals of magnesium by Reed-Hill (52,53) under closely controlled conditions of temperature and stress.

These twins never occurred as an independent mode of deformation, but were always retwinned on a $\{10\bar{1}2\}$ plane. The boundary orientation of the second-order $\{10\bar{1}1\}$ - $\{10\bar{1}2\}$ and $\{10\bar{1}3\}$ - $\{10\bar{1}2\}$ twins differed from the coherent position of the primary twin habit, indicating that a habit shift of some type had occurred. Also, the first of these double twinning modes has been observed to significantly influence the deformation and fracture of both single and polycrystalline magnesium, as will be discussed later.

Twin Boundaries

Twin boundaries, in general, may be classified as either coherent or non-coherent. For the case of a coherent boundary, the twin interface is parallel to the first undistorted plane, K_1. In this position the boundary is a mirror plane for the twin and matrix orientations, and the lattice planes meet in a one-to-one correspondence. Figure 5 illustrates schematically a coherent twin boundary in a fcc lattice. Each atom in this boundary retains the equilibrium interatomic spacing with its neighbors.

For the case of a non-coherent twin boundary, where the twin interface is not parallel to the twinning plane, the lattice planes of the two orientations no longer meet in a one-to-one correspondence. Boundaries of this type

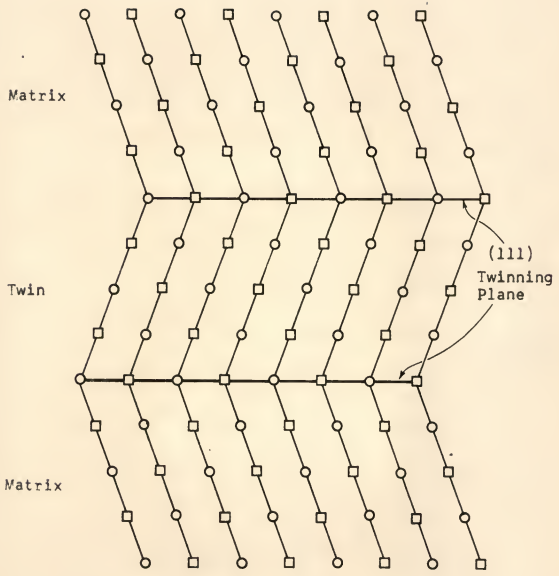

Figure 5: Coherent twin boundary in a face-centered cubic lattice (after C.S. Barrett (49))

are best described by an array of twinning dislocations, as pictured schematically in Figure 6. For a fcc lattice, the Burgers vector of these dislocations is uniquely defined by the twinning shear.

By assuming that every third twinning dislocation in a {112} twin boundary is iron dissociates according to the reaction

$$-\frac{a}{6}\langle 111\rangle \longrightarrow -\frac{a}{2}\langle 111\rangle + \frac{a}{3}\langle 111\rangle ,$$

twin dislocation — slip dislocation — complimentary dislocation

Sleezwyk (55) noted that the stresses present at the twin tip were relieved. The first of the two product dislocations is a normal slip dislocation which is free to glide away from the twin tip on the twinning plane. The second, which was referred to as a "complimentary dislocation," remained in the twin boundary. Sleezwyk noted that the magnitude of the Burgers vector of this latter dislocation was twice that of the original twinning dislocation, and the sense of the two was opposite. The array of twinning and complimentary dislocations which resulted in a non-coherent twin boundary is illustrated in Figure 7. Such a configuration does not have a long-range stress field since the net Burgers vectors for the two dislocation types cancel.

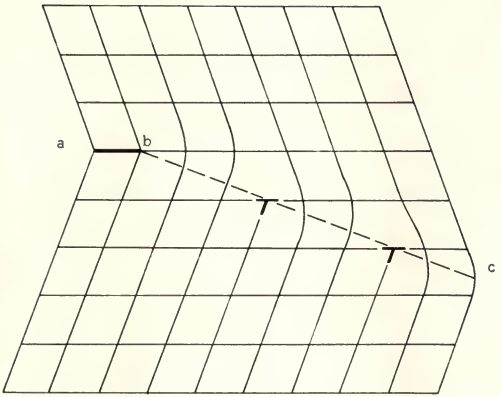

Figure 6: A non-coherent twin boundary in a face-centered cubic lattice. Because the plane of the paper corresponds to the plane of shear for this twin, the twinning dislocations are viewed in the edge orientation. The extra half plane for these dislocations is the K_2 plane for the twinning mode. The segment of the boundary ab is in the coherent orientation, while bc is in the non-coherent.

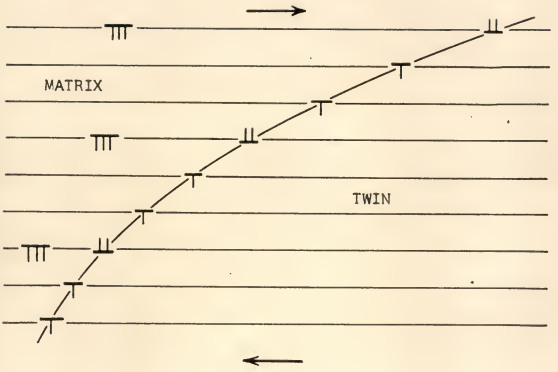

$\perp$ $-\frac{1}{6}\langle 111\rangle$ Twin Dislocation

$\perp\!\!\perp$ $+\frac{1}{3}\langle 111\rangle$ Complementary Twin Dislocation

$\perp\!\!\perp\!\!\perp$ $-\frac{1}{2}\langle 111\rangle$ Slip Dislocation

Figure 7: A schematic illustration of a non-coherent twin boundary in a body-centered cubic lattice based on the emmisary dislocation theory of Sleezwyk (55). Figure from Hull (56)

Twin boundaries in the hcp lattice are more difficult to describe than those in fcc or bcc. Because of the lower symmetry of this crystal class, the shear experienced by successive planes is different. For $\{10\bar{1}1\}$ and $\{10\bar{1}2\}$ twins the shear of individual atoms repeats itself only on every fourth K_1 plane. For this reason it is difficult to define the nature of the individual twinning dislocations for these modes. This, in turn, makes it even more difficult to determine how these interact with one another or with other lattice defects.

Interaction Between Slip and Twinning

Dislocation glide across twin boundaries - Slip and deformation twinning are often closely interrelated phenomena. One example involves cross-glide of dislocations between the matrix and twin lattices. Based on theoretical considerations, Sleezwyk and Verbraak (57) have demonstrated that, for $\{112\}$ twinning in bcc lattices, a properly oriented $\langle 111 \rangle$ slip dislocation may glide across the twin boundary onto the corresponding slip plane in the twin. In so doing, it leaves a step on the boundary equivalent to two twinning dislocations, and under the proper stress these may glide along the boundary resulting in an increase in thickness of the twin. Reed-Hill (58) has also made a

similar observation on $\{11\bar{2}1\}$ twins in zirconium. Here an $\frac{a}{3}\langle 11\bar{2}0\rangle$ basal dislocation in the matrix may dissociate at the twin boundary into an $\frac{a}{3}\langle 11\bar{2}0\rangle$ dislocation on the twin basal plane, plus two $\{11\bar{2}1\}$ twinning dislocations. For these cases twin boundaries do not represent a barrier to slip, and dislocations may glide completely through the twinned structure.

Twin accommodation kinking - A second interrelation that may occur between slip and twinning concerns the accommodation of the shear of a twin within the matrix. A shear cannot end abruptly within a crystal, but must be dissipated gradually if continuity is to be maintained between the sheared and unsheared regions. This continuity is significant in view of the statement by Chalmers (47),

> ...the stress distribution will not in general be uniform, but will be modified so that strain tends to be continuous across the crystal boundary. When there is an abrupt change in strain as a boundary is crossed, intercrystalline fracture may occur....

As evidence of this, Armstrong (59) has pointed out that fracture may occur at twins in cases where there are insufficient deformation modes available in the matrix to permit accommodation of the twinning shear.

Jillson (25), Pratt and Pugh (60), and Moore (61,62) have concluded that lattice kinking is the primary

mechanism of $\{10\bar{1}2\}$ twin accommodation in zinc. Figure 8 is a photomicrograph illustrating that this same type of accommodation kink is associated with $\{10\bar{1}2\}$ twinning in magnesium.

The bend axis of an accommodation kink accompanying a particular type of twin is identical to the axis of rotation associated with the twinning shear (25,60,62). For this reason, twin modes intersecting the basal plane along a $\langle 11\bar{2}0\rangle$ direction, such as $\{10\bar{1}2\}$ and $\{10\bar{1}1\}$ twins, have this same $\langle 11\bar{2}0\rangle$ direction as the bend axis for their accommodation kinks. Thus, the bend planes which support the kink misorientation must be composed of equal numbers of two dislocation types (see page 9).

Accommodation of the Twinning Shear at Boundaries - It was noted on page 23 that the shear of a particular twin cannot end abruptly within a lattice without producing some form of matrix accommodating deformation. This applies not only in single, but also in polycrystalline material; so intersection of a grain boundary by a twin should require that accommodating deformation occur in the grain ahead of the twin. The mechanism by which this accommodating deformation occurs could have a significant bearing on the understanding of second-order twinning. In this case also the shear of a twin (the second twinning mode) intersects a boundary (the primary twin boundary), and this

Figure 8: Accommodation of the shear of a $\{10\bar{1}2\}$ twin in magnesium by kinking on the basal plane (after Reed-Hill (63)).

shear must be accommodated in the matrix lattice across the boundary and ahead of the twin, as discussed above for simple twinning.

In zirconium three different types of matrix lattice deformation, which may occur in one grain as a result of twinning in an adjacent grain, have been observed. These are illustrated in Figures, 9, 10, and 11 where twins are observed to intersect a grain boundary. In each case, accommodating deformation has occurred in the neighboring grain ahead of where the twin intersected the grain boundary. The surfaces of these specimens were polished and anodized (64) in such a manner that small lattice rotations are revealed under polarized light. In the first of these micrographs the twinning shear is accommodated across the grain boundary by formation of a kink band. This type of structure is thought to result from the fact that a slip plane in the neighboring grain was about normal to the shear direction of the twins. The photomicrograph in Figure 10 illustrates a second means of accommodating the twinning shear across a grain boundary. In this case, twinning in the neighboring grain has been induced as a result of twinning in the grain in question. This type of accommodation should normally occur when a twinning plane in the adjacent grain is nearly parallel to the habit of the twin in question. A third type of accommodating deformation is

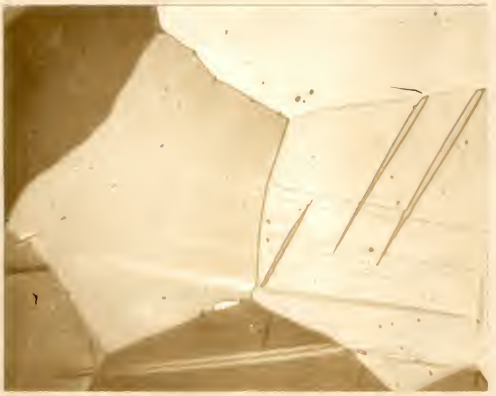

Figure 9: Accommodation of the shear of $\{11\bar{2}1\}$ twins in zirconium by kinking across a grain boundary. The lattice rotation associated with these kinks is revealed by the light areas in the grain where the accommodation is occurring. Specimen strained 3 per cent by rolling at 77°K. (courtesy of R.E. Reed-Hill). 2,000X

Figure 10: Accommodation of the shear of $\{11\bar{2}1\}$ twins in zirconium across a grain boundary by twinning in the adjacent grain. Specimen strained 0.65 per cent by rolling at 77°K. (courtesy of R.E. Reed-Hill). 750X

Figure 11: Accommodation across a grain boundary of the shear of twins in zirconium by slip in the adjacent grain. Specimen strained 12.6 per cent at room temperature and a rate of 0.02 inches/inch/min. (courtesy of R.E. Reed-Hill). 1137X

illustrated in Figure 11. Here slip has been nucleated in one grain as a result of twinning in another. This type of deformation was commonly observed when a slip plane in the neighboring grain was about parallel to the twin habit in question.

In addition, Reed-Hill (58) has observed another mechanism by which the shear of $\{11\bar{2}1\}$ twins may be accommodated at grain boundaries. This is illustrated in Figure 12, where two basal kink bands are observed near the tip of the twins in question. One of these kinks is in the twin and the other in the matrix. This type of accommodation was normally observed when the relative orientation of two adjacent grains was such that the shear of the twin in one grain could not be accommodated in the second by one of the mechanisms discussed above.

Fracture

Conrad (45) has discussed three basic mechanisms by which crack or voids may open up at an intercrystalline boundary. These are illustrated schematically in Figure 13. Figure 13, part a, shows how a wedge-shaped crack may result at a three-grain juncture, according to the fracture theory of Zener (65). In addition, Gifkins (66), Chen and and Machlin (67,68), and McLean (69) have demonstrated how voids may form as a result of jogs or projections on the boundary. This is illustrated in Figure 13, parts a and b. Chen and Machlin (67,68) assumed that projections are an inherent part of the grain boundary structure and that voids may result directly from shearing these parallel to the boundary. Recent observations of grain boundaries (70) in the field-ion microscope have confirmed

Figure 12: Accommodation of the shear of $(11\bar{2}1)$ twins in zirconium by formation of a double kink One kink is observed in the matrix ahead of the twins as a region of darker contrast, while a second kink is revealed within the twins at their tips as a region of lighter contrast. Specimen prestrained 0.65 per cent by rolling at 77°K, and then strained 26.8 per cent in tension at room temperature and a rate of 0.02 inches/inch/min. (courtesy of R.E. Reed-Hill). 2,000X

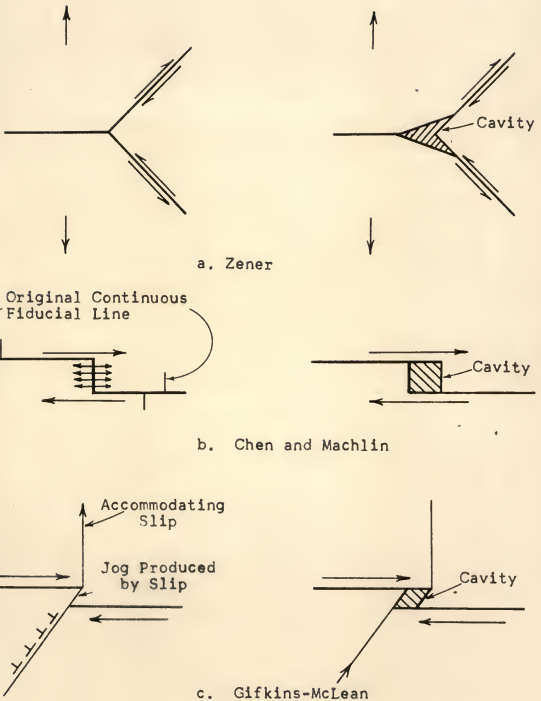

Figure 13: A schematic illustration of mechanisms which have been proposed to account for the nucleation of intercrystalline voids. (after Conrad (45))

that boundary structures of this type do exist. On the other hand, Gifkins (66) and McLean (69) assumed that jogs result from interaction of slip bands with the boundary. Figure 14 illustrates an additional crack nucleation mechanism proposed by Zener (65). Here, an obstacle to slip causes coalesence of edge dislocations of the same sign and nucleates a crack normal to the slip plane. The example shown demonstrates how a grain boundary may act as such an obstacle. Conrad has also considered the various mechanisms by which voids may grow once they form. These are illustrated schematically in Figure 15 from his paper.

It has commonly been observed (71) that metals may fracture in a ductile manner, even though they are brittle on a macroscopic scale. The mechanism by which ductile rupture normally proceeds is coalescence of voids; that is, cracks or voids open up as a result of plastic flow and grow until they interconnect and separate the metal. Electron microscopy is ideally suited for fractography studies because of the high magnification and large depth of field obtainable. Using this as a tool, Beachem (71) has shown that there are three basic mechanisms of void coalescence: normal rupture, shear rupture, and tearing. These are illustrated in Figure 16. The directional

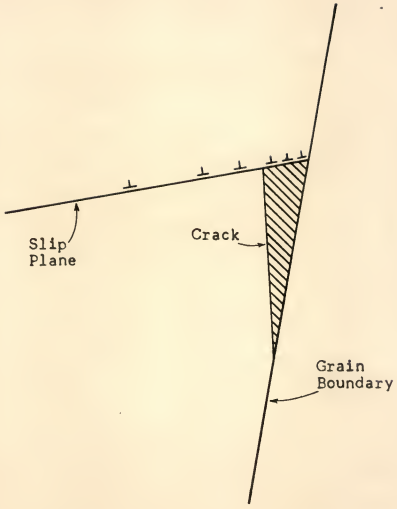

Figure 14: A schematic illustration of how an obstacle to slip may cause nucleation of a crack

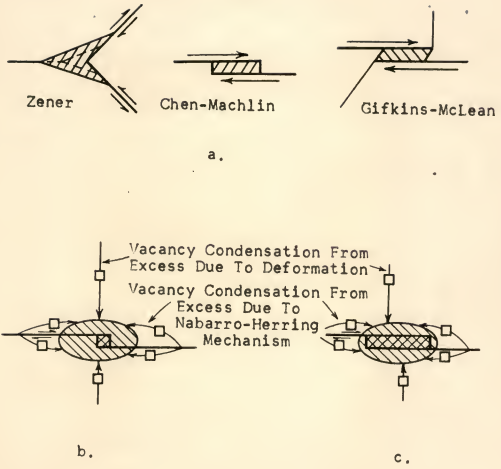

Figure 15: A schematic illustration of mechanisms by which intercrystalline voids may grow once they are nucleated: a) advancement of a crack by continued sliding, b) vacancy condensation on a crack nucleus produced by sliding, and c) combined action of advancement of a crack tip by sliding and vacancy condensation (after Conrad (45))

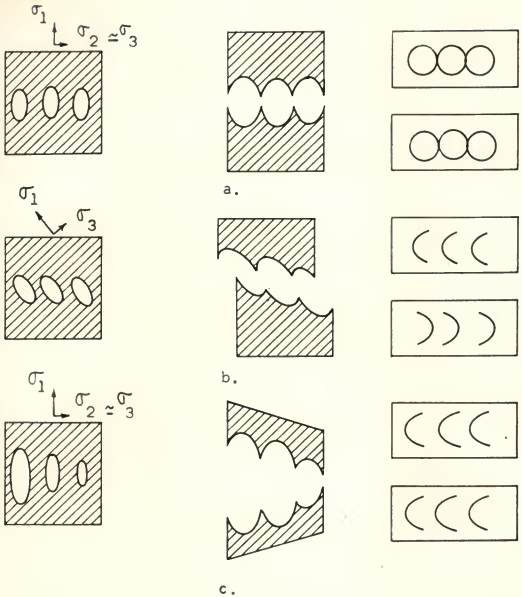

Figure 16: A schematic illustration of three basic mechanisms of void coalesence: (a) normal rupture, (b) shear rupture, and (c) tearing (after Beachem (71)).

characteristics of these voids on the fracture surface is also shown. Figures 17, 18, and 19 are three electron micrographs of fracture surfaces illustrating the actual appearance of these voids for the three observed fracture mechanisms.

Second-Order $\{10\bar{1}1\}$ - $\{10\bar{1}2\}$ Twinning

Reed-Hill and Robertson (72) observed that, upon loading a magnesium single crystal with the basal plane parallel to the tensile axis, a narrow band of intense deformation appeared in regions of concentrated stress shortly after yielding. It was also observed that fracture follows as a direct result of deformation in this band. These bands were originally classified as $\{30\bar{3}4\}$ twins, since their habit was close to this orientation (52,72). However, more extensive investigation revealed that these were actually second-order twins, where a primary $\{10\bar{1}1\}$ twin had undergone retwinning on $\{10\bar{1}2\}$. Second-order twins of this type were first reported by Couling and Roberts (73) and later more thoroughly analyzed by Reed-Hill (53). In the latter research, convincing evidence in support of this double twinning process was obtained in the form of extinction measurements of the basal plane trace using a polarized light microscope. Reed-Hill was able to measure extinctions

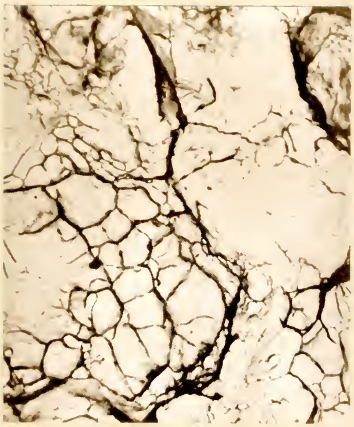

Figure 17: Electron micrograph of a normal rupture fracture surface.(after Beachem (71)).

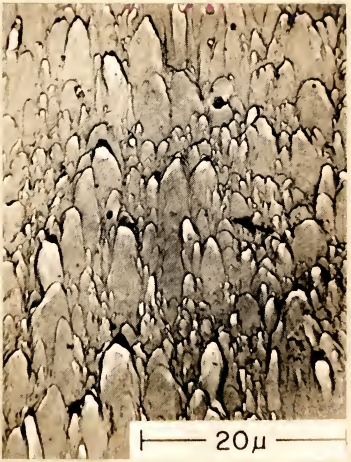

Figure 18: Electron micrograph of a shear rupture fracture surface (after Beachem (71)).

Figure 19: Electron micrograph of a fracture surface which resulted from tearing (after Beachem (71)).

in second-order twins and also in small primary twins at the tips of second-order twins. His measurements of the extinction positions corresponded closely to the predicted positions of the basal plane trace for both the second-order twins and the primary $\{10\bar{1}1\}$ twin tips.

The importance of $\{10\bar{1}1\}$ - $\{10\bar{1}2\}$ twinning extends beyond its role as a mode of deformation in magnesium. A coherent $\{10\bar{1}1\}$ twin boundary makes an angle of $61^{\circ}54'$ with the basal plane. However, second-order twin bands are inclined at about 56° to the basal plane. It follows from this that, in some stage of the second-order twinning process, the habit is shifted toward the basal plane by about 6°. The phenomenon of a habit shift is not new in metallurgical processes, as it has been studied for many years in conjunction with martensite transformations in iron-base (74), as well as in non-ferrous (75,76,77), alloy systems.

Wechsler, Lieberman, and Read (78) were the first to develop a theory for martensite transformations which successfully accounted for the irrational habit plane separating the parent and product structures. Their theory assumed that the transformation occurs as an invariant plane strain; that is, a shear strain parallel to the habit plane, plus a tensile or compressive strain normal to the boundary. Thus, they considered the interface between

the two structures as a plane of zero net distortion. By this theory the habit plane for some martensite reactions can be rationalized. Later extensions of this theory have been made by Bowles and Mackenzie (79), Frank (80), Suzuki (81), and Bullough and Bilby (82), but the fundamental principles originally put forth are essentially the same.

Under the assumption that the double twinning shear is also an invariant plane strain, Crocker (83) has extended this type of approach to the phenomena of second-order twinning in an attempt to explain the observed habit shift. By assuming that no accommodating deformation of either parent or product accompanies the double shear, a habit inclined at $70^{\circ}48'$ to the basal plane was predicted. It was also shown that, by assuming various relative amounts of the shear are accommodated by the parent and the product, a habit inclined anywhere from $61^{\circ}54'$ to $70^{\circ}48'$ could result. This yields a discrepancy between the predicted and observed habit of from 6° to 15°. But more significant is the fact that the theory predicts a habit rotation in the opposite sense than that actually observed.

Deformation and Fracture in Magnesium

The temperature dependence of the strain to fracture for polycrystalline magnesium is illustrated in Figure 20

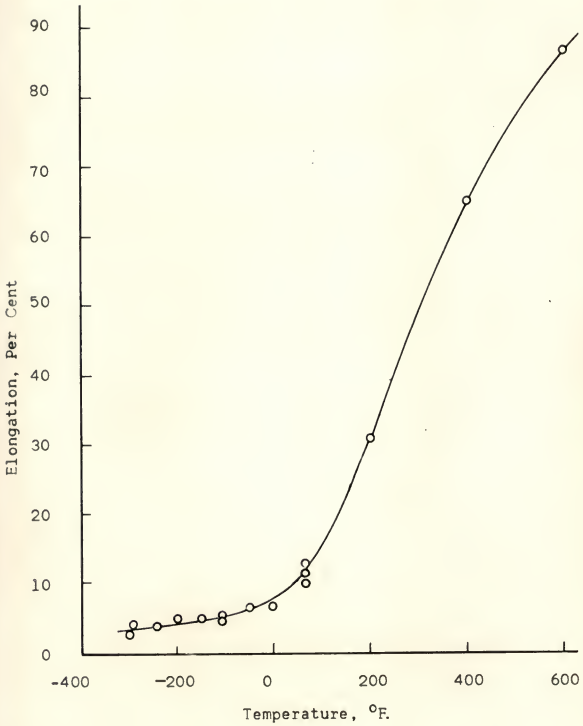

Figure 20: The temperature dependence of the strain-to-fracture for polycrystalline magnesium (after Toaz and Ripling (1)).

and for single crystals with the basal plane parallel to the stress axis in Figure 21. A striking similarity is noted in the curves above room temperature. However, single crystals regain a measure of ductility below room temperature, presumably as a result of prismatic slip. The question then follows as to why the room temperature ductility of magnesium single crystals is so severely limited, and if a relationship exists between the behavior of single and polycrystalline material at this temperature.

The ductility and fracture behavior of polycrystalline magnesium is unique in a number of ways and may be related to the available modes of plastic deformation. Hauser, Landon, and Dorn (8) have observed that the low temperature fracture of polycrystalline magnesium often proceeds intergranularly, a property usually characteristic of high temperature fractures. Taylor (84) has treated the problem of deformation in a polycrystalline aggregate by considering the restraints imposed upon a single grain. He concluded that, for a grain to deform in conjunction with the boundary conditions imposed by its neighbors, it must have available at least five independent modes of deformation. Hauser *et al.* have applied this theory to magnesium and have explained the low temperature brittleness in terms of a lack of enough available deformation modes.

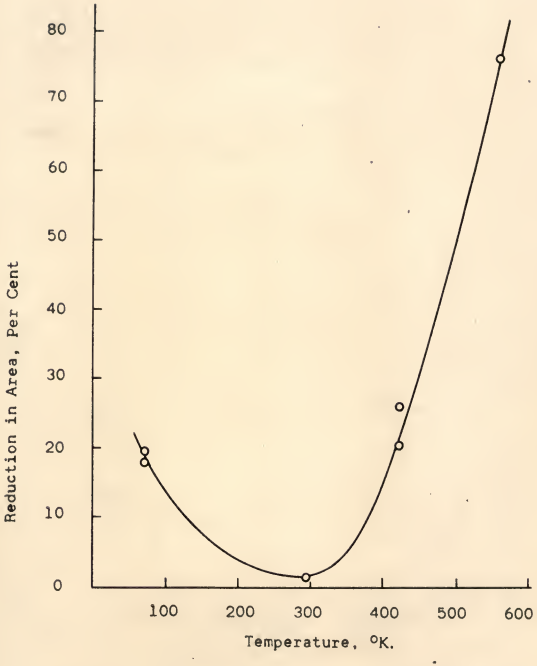

Figure 21: The temperature dependence of the strain-to-fracture for single crystals of magnesium oriented with the basal plane parallel to the stress axis (after Reed-Hill and Robertson (52))

On the other hand, Rhines and Wray (85) have noted that the ductility characteristics of numerous metals are such that the elongation to fracture is often a minimum in the temperature range just below that of recrystallization. In this region grain boundary shearing is an important mechanism of deformation, and as a result fractures often proceed intergranularly. The room temperature brittleness of magnesium may be described in terms of this generalized behavior of other metals, since room temperature coincides with the recovery range of this metal. In addition, grain boundary shearing has been commonly observed near room temperature (41,42). On this basis, fracture of magnesium at room temperature results from an inherent weakness of the grain boundaries and the fact that large, localized deformation occurs in these regions.

The above arguments do not apply to a single crystal; however, the limited ductility of both single and polycrystalline magnesium at room temperature may be interrelated by another cause. Reed-Hill and Robertson (72) concluded as a result of their experiments, that second-order $\{10\bar{1}1\}$ - $\{10\bar{1}2\}$ twins control the room temperature ductility and fracture of magnesium single crystals when the basal plane is parallel to the stress axis. While macroscopically these crystals are brittle and fracture

at less than 1 per cent strain, these authors measured shear strains of up to 1,000 per cent within double twinned regions (52). Thus, it appeared that the fracture in these crystals is actually extremely ductile and results from concentrating large amounts of plastic flow into these small, twinned volumes.

It is also true that many of the room temperature plastic properties of polycrystalline magnesium may be related to $\{10\bar{1}1\} - \{10\bar{1}2\}$ twinning. The occurrence of this double twinning mode in polycrystalline magnesium has been confirmed (86,87,88), and it appears quite possibly to have much the same significance in polycrystalline grains as in single crystals. Cracks may open along second-order twins and spread into grain boundaries. Fracture then proceeds intergranularly. A classical photomicrograph, due to Roberts (88), which illustrates cracking along second-order twins in polycrystalline magnesium is shown in Figure 22. Also, Mote and Dorn (89) have found that second-order twins of this type are important in the fracture of magnesium bi-crystals of certain orientations.

The plastic deformation which occurs in $\{10\bar{1}1\} - \{10\bar{1}2\}$ twins is thought to be responsible for the unlimited cold-rollability of a number of dilute magnesium alloys (90). A study of this phenomenon by Couling, Pashak, and Sturkey (91) revealed that the banded structure characteristic of

Figure 22: Cracking along a second-order, $\{10\bar{1}1\}$ - $\{10\bar{1}2\}$ twin in a grain of a polycrystalline magnesium tensile specimen deformed at 25°C. (after Roberts (88)).

these rolled alloys is due to a high density of small, second-order twins of this type, and the "infinite rollability" has been attributed to deformation of the reoriented material within these twins.

Kinking at second-order twins - Reed-Hill and Robertson (52,72) have observed two different types of kinks associated with $\{10\bar{1}1\}$ - $\{10\bar{1}2\}$ second-order twins. The first of these were lattice accommodation kinks of the type already discussed and commonly observed in hcp twin accommodation (25,60,61,62). The second type, which Reed-Hill and Robertson (52) called shear accommodation kinks, was quite unique in a number of ways and has only been observed in conjunction with this double twinning mode in magnesium. Yosinaga and Horiuchi (92) have also observed these kinks and their observations are in good agreement with those of Reed-Hill and Robertson. The lattice rotations accompanying shear accommodation kinks are quite pronounced, as misorientations of 20° are commonly observed. These kinks have the property that the bend plane does not bisect the angle between the basal plane on either side of the boundary as is the case for most other hcp kinks. In fact, bending occurred about a plane nearly parallel to the second-order twin habit. Reed-Hill and Robertson (52) observed that these kinks were most pronounced where the

internal deformation of second-order twins was a minimum, and that the kinks disappeared where the twin deformation was greatest. On this basis, shear accommodation kinks were thought to accommodate the non-uniform strains existing along second-order twins.

The regions within shear accommodation kinks were often highly plastically deformed. Reed-Hill and Robertson (52) attributed this to small, secondary $\{10\bar{1}1\}$ - $\{10\bar{1}2\}$ twins; however, other traces were observed which could not be explained.

The Purpose of the Present Research

From the foregoing it may be concluded that second-order $\{10\bar{1}1\}$ -$\{10\bar{1}2\}$ twinning, along with its related kinking and deformation, is a very complex phenomenon. It may also be concluded that these twins are significant with regard to the room temperature mechanical properties of magnesium. An understanding of all the processes involved is desirable both for practical and academic reasons. The present work was undertaken, therefore, in order to gain a better understanding of all the mechanisms associated with second-order twinning.

Of primary concern is the $\{30\bar{3}4\}$ habit morphology. The deformation of second-order twins subsequent to their

formation is also of interest because of the mechanism which allows small volumes of metal to undergo such high strains. Also of interest is how these strains are accommodated into a matrix which, for the most part, remains undeformed. Insight into the nature of the shear accommodation kinks which often accompany second-order twins, and a description of these in terms of dislocations, is also desired. In addition, more understanding is needed concerning the processes by which they deform internally. From this it is hoped that the role of these kinked structures in the overall twinning operation may be better understood.

EXPERIMENTAL TECHNIQUE

Specimen Preparation

Tensile specimens for the present experiments were obtained by sectioning a single crystal rod, 1/2 inch in diameter by 8 inches long. This crystal was grown by Conrad (93) using a Bridgman type furnace and was donated for use in the present experiments by Dr. R.E. Reed-Hill. Details of the growing technique, along with the chemical composition of the rod, are listed elsewhere (93). A Laue back reflection X-ray photograph revealed that the basal plane was 4° from the crystal axis and a $\langle \bar{1}100 \rangle$ direction was 6° from this axis.

The crystal was sectioned in such a manner that a number of tensile specimens, oriented with the basal plane parallel to the stress axis, were obtained. This procedure involved mounting the crystal in specially prepared holders, using Trubyte equalizing wax, and cutting along predetermined planes with a jeweler's saw and 03 blades. This technique is essentially the same used by Reed-Hill and is described in greater detail elsewhere (94). Extreme caution was taken throughout to insure that deformation was localized to the region of the saw cut.

The original crystal was cut into 5 cm. lengths normal to the crystal axis, and tensile specimens of 3 x 5 mm. rectangular cross section were obtained from these. The cross section was oriented so that the basal plane was made parallel to the 5 mm. face and a $\{1\bar{2}10\}$ plane made parallel to the 3 mm. face. Specimens of this orientation were desired since $\{1\bar{2}10\}$ is the plane of shear for twinning about the $\langle 1\bar{2}10\rangle$ axis. By observing $\{10\bar{1}1\}$ - $\{10\bar{1}2\}$ twins on the plane of shear, the twinning process may be described in two dimensions with no loss in generality. Subsequent to cutting, each side of the tensile specimen was wet ground successively on 180, 240, 420, and 600 grid carborundum paper to remove deformation from sawing and to obtain smooth, parallel faces. Finally, the specimens were etched in 15-20 per cent HCl to remove surface deformation from grinding. This was followed by thorough rinsing in running water and rapid drying in a warm air stream.

Specimens were then acid machined in 20 per cent HCl to give a reduced gage section. This was done by first masking off the specimen ends and the $\{1\bar{2}10\}$ faces with Unichrome chemical stop. Next, the crystals were placed in the acid machining solution and agitated gently until the desired reduction had occurred; then they were rinsed and dried. By this technique, the basal plane surfaces

were the only faces reduced, and flat $\{1\bar{2}10\}$ faces were obtained along the entire specimen length. Upon loading second-order, $\{10\bar{1}1\}$ - $\{10\bar{1}2\}$ twins usually appeared in regions of high stress concentration. For this reason the fillets separating the specimen shoulder from the gage length were areas of preferential nucleation. By masking the $\{1\bar{2}10\}$ faces, twins which formed at fillets could still be observed on the plane of shear and the crystallographic nature of the twins readily determined. The acid machining procedure resulted in some non-uniform reduction near the masked $\{1\bar{2}10\}$ faces. These formed regions of stress concentration within the gage length, and second-order twins often appeared here also. The non-uniform reduction was desirable, since the primary purpose of the experiments was to study second-order twins and not the stress-strain behavior of the material.

Deformation Experiments

Tensile specimens were extended at room temperature, at a strain rate of 0.002 inches/inch/min. and in the same apparatus used by Reed-Hill (94) for his experiments. Slight modifications were made so that the load could be applied by an Instron Tensile Testing Machine. Second-order twins were observed shortly after yielding in the

regions of stress concentration described above. All specimens that were extended to failure fractured at second-order twins in the manner described by Reed-Hill and Robertson (72). Crystals not extended to failure were unloaded rapidly (20/inches/inch/min.) after being deformed to the desired strain. If they were unloaded slowly, fracture often resulted during the unloading cycle, indicating that the stress to internally deform second-order twins is less than that needed to cause their nucleation.

Observation of Deformed Surfaces

Deformed surfaces were examined with a Leitz polarized light microscope. Significant features of second-order twins were recorded and areas to be studied by electron microscopy were localized. In addition, specimen surfaces were made sensitive to polarized light by an etching technique similar to that of Couling and Pearsall (95). This permitted extinction measurements of the basal plane trace to be made, and the orientation of twinned volumes deduced. Best results were obtained with a modification of the etch suggested by these authors. This etching solution was

10 parts	6 per cent picric acid
2 parts	distilled H_2O
1 part	orthophosphoric acid

With this etch, sharper extinctions of the basal plane trace could be observed, and other effects, which will be discussed later, were also revealed.

Electron microscope observations were made with a Phillips Model 100A using the cellulose acetate, carbon double replica technique. This type of replicating procedure has the added advantage that it reveals microscopic cracks in the metal. By applying a solution of cellulose acetate dissolved in acetone to the surface, cracks may be reproduced on the negative replica. When this replica is shadowed, much more metal is deposited on the portion of the plastic extracted from the crack. In the electron microscope, these cracks appear as dark protrusions on the positive, carbon replica.

Because of the lack of a stigmatizism corrector to compensate for non-uniform magnetic fields in the microscope lenses, an inherent distortion was present in the instrument. Figure 23 is an electron micrograph of a replica from a diffraction grating which illustrates the nature of the distortion. For this reason it was necessary to take certain precautions in analyzing the electron micrographs. By making all angular measurements at the same point, rather than comparing orientations in different areas of the micrographs, this error is minimized.

Figure 23: Electron micrograph of a diffraction grating which illustrates the lens distortion inherently present in the Phillips 100A electron microscope. The grid lines and scratches are actually straight. 5,500X

EXPERIMENTAL RESULTS

General Properties of Second-Order Twins

An optical photomicrograph of a typical second-order, $\{10\bar{1}1\}$ - $\{10\bar{1}2\}$ twin is illustrated in Figure 24. The problems in analyzing these twins are immediately evident from their narrow width and highly deformed structure. This micrograph also indicates the 56° angle between the matrix basal plane and the second-order twin boundary. In addition, it is noted that the matrix adjacent to the twin appears relatively unrotated and strain free although exhibiting some basal slip lines. The detailed structure of these twins is shown most convincingly by the electron micrographs in Figures 25 and 26. These micrographs also indicate that second-order twins occur as small, individual lamellae. This is consistant with the earlier optical microscope observations made on etched surfaces by Reed-Hill and Robertson (52). Figures 25 and 26 also illustrate that, although the lamellae line up along a habit about 56° from the matrix basal plane, the individual lamellae lie near 54°.

From the present experiments added proof was obtained that these bands observed at 56° are actually $\{10\bar{1}1\}$ - $\{10\bar{1}2\}$

Figure 24: Structure of a typical $\{10\bar{1}1\}$ - $\{10\bar{1}2\}$ twin, as viewed in the optical microscope. 910X

Figure 25: Electron micrograph of $\{10\bar{1}1\}$ - $\{10\bar{1}2\}$ twin lamellae near the front of a second-order twin band. The structure of the individual lamellae may be observed, since in this region the internal strain of the twin is small. 4,500X

Figure 26: Second example of the lamellae structure of $\{10\bar{1}1\}$ - $\{10\bar{1}2\}$ twins . 4,000X

twins. This was desired in view of the fact that no acceptable theory accounting for the observed habit shift in terms of these twinning modes has been developed. This confirmation involved observations made on etched surfaces using the electron microscope and is significant because the orientation relationships between twin and matrix may be recorded on micrographs.

The etching solution previously described was found to produce grooves on magnesium surfaces parallel to the basal plane trace. The electron micrograph in Figure 27 illustrates this for the case of $\{10\bar{1}2\}$ twinning. A single crystal of the orientation already described was bent about that $\langle 1\bar{2}10\rangle$ direction normal to the specimen axis. This caused nucleation of $(10\bar{1}2)$ and $(\bar{1}012)$ twins on the compression side of the specimen. The complete crystallographic nature of these twins is revealed by the grooved basal traces in the matrix and twin which make an angle of 86° with each other. In addition, this etch has a tendency to selectively attack areas of high strain, since the twin boundaries, which lie close to 43°, are also observed. Bend planes, indicated at A and B, are a third crystallographic feature revealed in this micrograph. These lie nearly normal to the matrix basal plane and are probably associated with secondary twin accommodation kinking, as described by Moore (62).

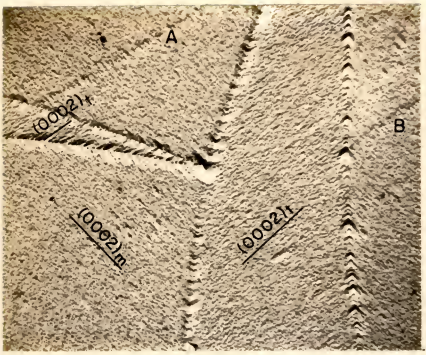

Figure 27: The lattice geometry of $\{10\bar{1}2\}$ twinning as viewed on the $(1\bar{2}10)$ crystal surface (the plane of shear). A small $(\bar{1}012)$ twin is seen intersecting a larger $(10\bar{1}2)$ twin. The basal plane trace in the matrix and in each twin is indicated as $(0002)_m$ and $(0002)_t$, respectively. 5,000X

A twin band of the type presently under investigation is shown in Figure 28. Here the etching procedure was the same as above except that the etching time was less. This resulted in pits parallel to the basal trace rather than grooves. In this micrograph three different pit traces are observed: the first of these is horizontal and corresponds to the matrix basal plane trace, the second, at an angle of $+124^{\circ}$, occurs in the region of the twin tip, and the third, at an angle of -130°, is observed throughout the remaining twin. Also, several bend planes are faintly visible and their significance will be mentioned later. The orientation of these traces compare favorably with the basal plane orientations illustrated schematically in Figure 29 for a second-order, $\{10\bar{1}1\}$ - $\{10\bar{1}2\}$ twin with a primary $\{10\bar{1}1\}$ tip. In addition, the small interface in Figure 28 between the primary and second-order twins closely corresponds to the orientation of a $\{10\bar{1}2\}$ plane in the $\{10\bar{1}1\}$ twin. Thus, with the possible exception of the second-order twin boundary orientation, the lattice geometry in these twinned bands may be completely described by the $\{10\bar{1}1\}$ - $\{10\bar{1}2\}$ double twinning process.

Internal Deformation of $\{10\bar{1}1\}$ - $\{10\bar{1}2\}$ Twins

Figure 30 is an optical photomicrograph that shows the large, total deformation which often accompanies

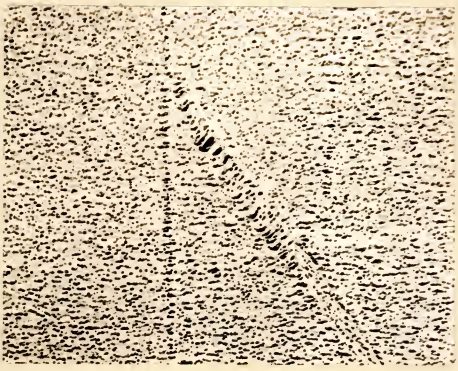

Figure 28: The lattice geometry of second-order, $\{10\bar{1}1\}$ - $\{10\bar{1}2\}$ twinning. The relative lattice orientation in the matrix and in each twinned region is revealed by pits parallel to the basal plane trace. 7,000X

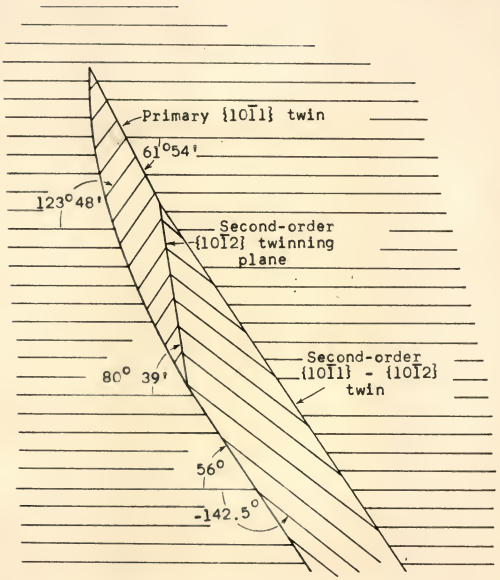

Figure 29: The lattice geometry predicted to result from {10$\bar{1}$1} - {10$\bar{1}$2} second-order twinning

Figure 30: Composite optical micrograph illustrating the large surface offset and high internal shear strain that may occur in $\{10\bar{1}1\}$ - $\{10\bar{1}2\}$ twins. 200X

second-order twinning. Note the pronounced offset of the surface at the specimen edge and the displacement of the dark band that crosses the specimen from lower left to upper right. This is a polishing fault resulting from a small amount of chemical stop that flowed onto this surface from the basal plane face prior to electropolishing. The shear strain in the twin at this band was computed using the ratio of the distance of displacement of the dark band to the width of the twin and was found to be 700 per cent. An electron micrograph of a replica from this area permitted accurate measurement of the twin thickness.

Figures 31 through 37 are electron micrographs illustrating successive stages in the development of the deformation in and around a second-order twin band. In the initial stages of deformation, slip traces are observed nearly parallel to the twin boundary (see Figure 31). In this micrograph the region between two adjacent twin lamellae also shows evidence of strain. While the flow lines within the lamellae are about parallel to the boundaries of the individual twins (54° from the matrix basal plane), flow may also be seen in the parent lattice (point A), where traces are oriented nearly parallel to the macroscopic habit at 56°. Figure 32 shows the

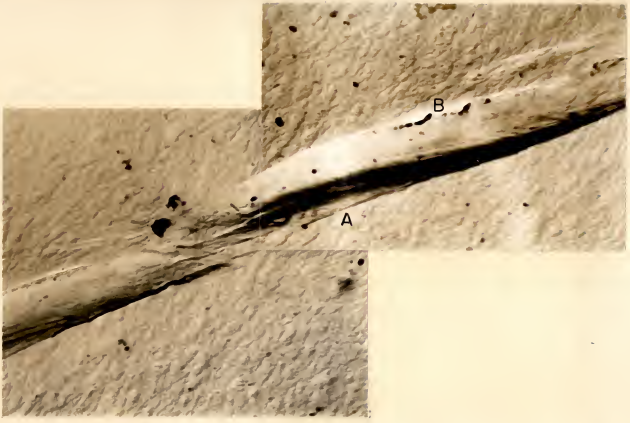

Figure 31: The initial stages of deformation in a region where two $\{10\bar{1}1\}$ - $\{10\bar{1}2\}$ twin lamellae meet. 12.000X

Figure 32: The intense shear strain where two twin lamellae meet. 13,800X

Figure 33: The interconnection of two $\{10\bar{1}1\}$ - $\{10\bar{1}2\}$ twin lamellae. Shear traces are observed parallel to both the habit of the individual lamellae and to the macroscopic twin habit. 14,000X

Figure 34: A more advanced stage of the internal deformation of a $\{10\bar{1}1\}$ - $\{10\bar{1}2\}$ twin. 10,400X

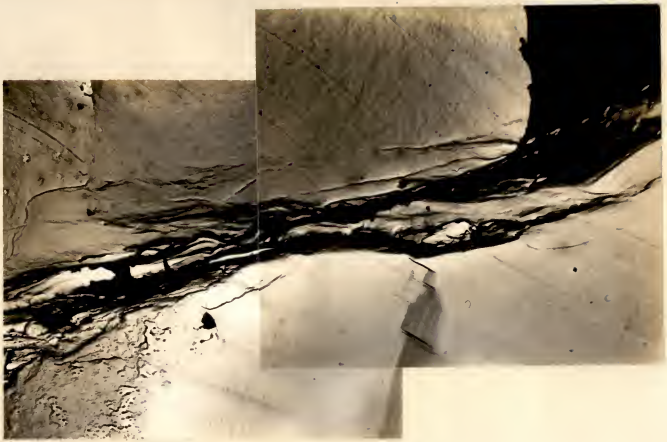

Figure 35: An example of the intense lattice strain which may occur when two lamellae meet in a region of pronounced internal deformation. 10,400X

Figure 36: The flow and cracking along a $\{10\bar{1}1\}$ - $\{10\bar{1}2\}$ twin band after extensive internal shear has occurred. 10,400X

Figure 37: Example of the deformed structure in a region of intense strain. 10,400X

structure a little further from the tip of the twin band. Here the traces within the twin are more pronounced, and the region where the two lamellae join has an appearance of having been subjected to very intense flow. Note that the flow lines within these lamellae are still almost parallel to its boundaries. However, because the individual lamellae are not directly aligned with each other (Figures 25 and 26), some of this shear passed into the matrix. This is evidenced at the lower tip of one lamella (point A) by the flow which extends into the parent lattice, and at the upper tip of the other (point B) through matrix basal slip. Figure 33 is a second example which shows this type of deformation more clearly.

Figure 34 represents another more advanced stage where the individual twin lamellae are no longer recognizable. This probably resulted from the extensive deformation that caused the surface relief to flow together. The structure at point A corresponds to what was probably at one time the tip of a lamella.

The black areas in Figure 34 are cracks that opened along the second-order boundary. Their formation permitted stresses to be relieved in the regions near the voids. The strain is still greater in Figure 35, which shows another region where two lamellae meet. Note that on the upper

side of the twin, flow is observed in the matrix parallel to the twin boundary. The appearance of this deformation is much the same as that which occurred within the twin at an earlier stage of the deformation (Figure 31). Also, on the opposite side of the twin is a region where cross-slip has occurred involving the basal plane and a prism plane. The shear strain in a region adjacent to this was calculated to be about 500 per cent from the relative displacement of the two halves of a corrosion pit intersected by the twin. The deformation within the twin lamellae does not show the intense distortion characteristic of regions such as those where lamellae interconnect. This is illustrated in Figures 36 and 37, where many flow lines nearly parallel to the twin boundary are observed. The shear in these regions is also about 500 per cent. Except for the cracks which are present, these regions do not indicate much more strain than was observed at a much earlier stage of the deformation.

In the preceding micrographs, the internal deformation of the twins occurred by a shearing action that appeared to be distributed uniformly across a twin cross section. However, deformation of a second type was also noted, as shown in the electron micrographs in Figures 38 and 39. Here the specimen surface from which this replica was obtained was

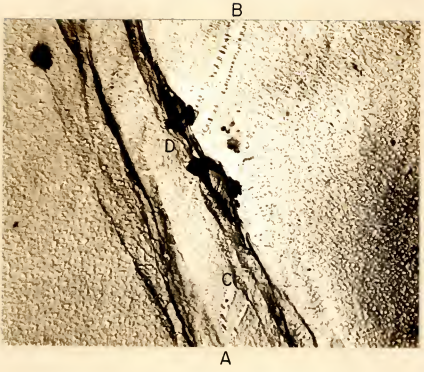

Figure 38: First example of discontinuous shear along a second-order, $\{10\bar{1}1\}$ - $\{10\bar{1}2\}$ twin. 16,500X

Figure 39: Second example of discontinuous shear along a second-order, $\{10\bar{1}1\}$ - $\{10\bar{1}2\}$ twin. 17,000X

rinsed and dried in such a manner that a high density of corrosion pits resulted. These can be used to advantage in analyzing the deformation in the twins, since these spots are sometimes aligned preferentially along the original basal plane trace, as may be observed at A and B in Figures 38 and 39.
By noting the deflection of these traces as they pass through a doubly twinned region, the shear distribution within the twins may be determined.

Both of these micrographs indicate that the shear deformation of second-order twins does not necessarily occur uniformly. Sharp discontinuities of the basal plane trace were observed at points C and D. Although it appears that this offset occurred at the second-order twin boundary, this cannot be stated conclusively because of the highly deformed state of this twin. It is quite possible that discontinuities of this type were also present in the micrographs in Figures 31 through 37 but were not recognizable since the basal plane trace could not be followed through the twin.

Shear Accommodation Kinking

Figures 40 and 41 are two optical photomicrographs of kinks that often occur in the matrix adjacent to second-

Figure 40: The structure of a $\{10\bar{1}1\}$ - $\{10\bar{1}2\}$ twin and its shear accommodation kink. The twin is on the upper side of the band, while the kink, revealed by the deflected basal slip traces, is on the lower. 900X

Figure 41: Second example of the appearance of shear accommodation kinks adjacent to second-order, $\{10\bar{1}1\}$ - $\{10\bar{1}2\}$ twins. 545X

order, $\{10\bar{1}1\}$ - $\{10\bar{1}2\}$ twins. In the first of these the internal twin shear deformation is indicated by the offset of the superficial surface marking in the upper right-hand corner. The second micrograph indicates that these kinks may occur either on one or both sides of the twin. Extinction measurements made in these regions, using a polarized light microscope, revealed that the basal plane trace was parallel to the deflected slip traces observed in these micrographs. This confirmed that these areas are actually kinks and not some form of twinning. Figure 42 is an electron micrograph of the area in Figure 40 where the small, second-order twin intersected the kink. Here pits may be observed along the bend plane trace that possibly indicate the dislocation structure of this boundary.

It was commonly observed that the inclination of the bend plane, relative to the matrix basal plane trace, was slightly greater than that of the second-order twin band. The electron micrograph in Figure 43 illustrates that these kinks remain adjacent to the second-order twin, even when the kink and twin boundaries are not parallel. This occurs by the formation of steps on the bend plane. The nature of these steps was analyzed with the aid of the micrograph in Figure 44, showing the deflected slip traces in greater detail. A corresponding schematic illustration is given in Figure 45 which indicates the bend plane

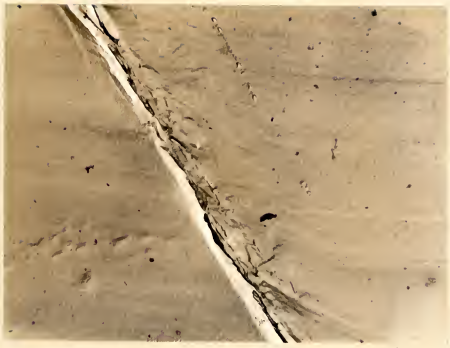

Figure 42: Electron micrograph of a second-order, $\{10\bar{1}1\}$ - $\{10\bar{1}2\}$ twin and a shear accommodation kink. 6,000X

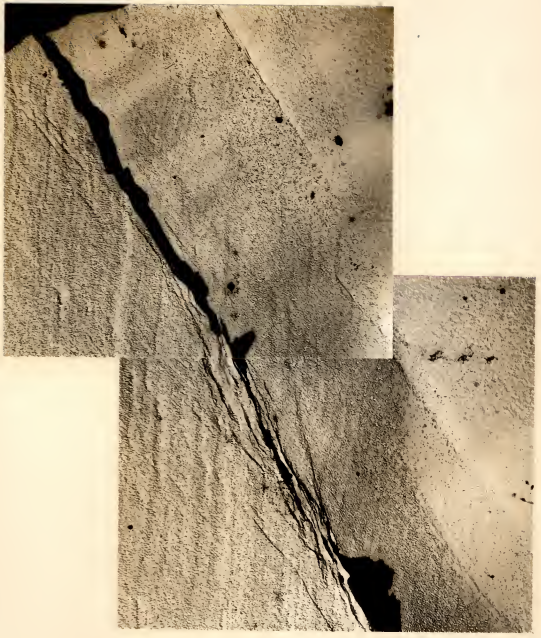

Figure 43: Electron micrograph illustrating that shear accommodation kinks remain adjacent to second-order twins by formation of steps along the bend plane. 4.000X

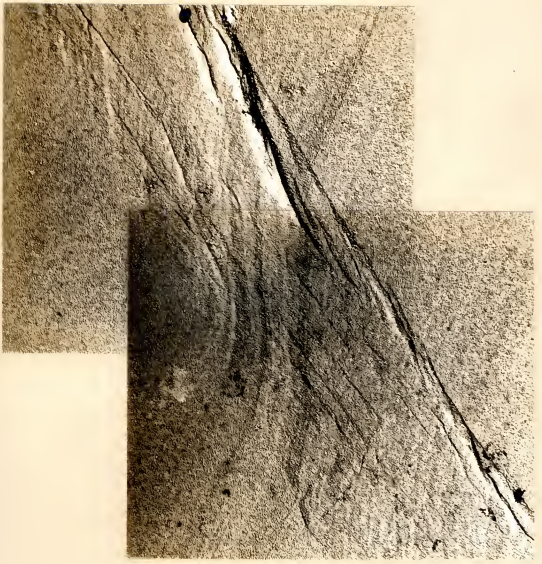

Figure 44: Example of steps which may form along the bend plane of shear accommodation kinks. 3,500X

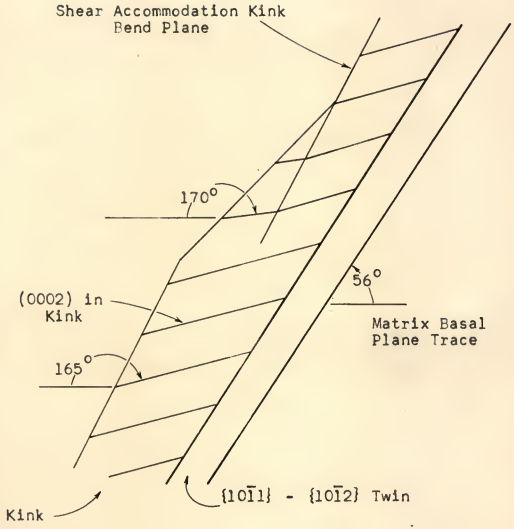

Figure 45: Schematic illustration of the structure of the shear accommodation kink in Figure 44

structure. A third example is shown in Figure 46, where the misorientation of one kink decreases as it goes into the matrix away from the twin, while a second kink has been formed in the immediate area of the twin.

Figure 47 shows what is believed to be a small shear accommodation kink in an initial stage of its formation. The bend plane which surrounds the misoriented region is curved, indicating that the dislocation loops are in an initial phase of their expansion. This is the only case known where a kink has been observed as a circular unit, although Frank and Stroh (96) have referred to this type of structure in their theoretical discussion of kink nucleation.

Internal Deformation of Shear Accommodation Kinks

The optical micrograph in Figure 48 shows that deformation may also occur within shear accommodation kinks. This is revealed by the flow-lines nearly parallel to the second-order twin boundary and the kink bend plane. An electron micrograph of the twin on the left is shown in Figure 49. From this the relative amounts of shear deformation in adjacent regions of the twin band may be determined from the deflection of the rows of corrosion spots that follow the original basal plane trace. These indicate that the internal shear of the actual twinned region which is in

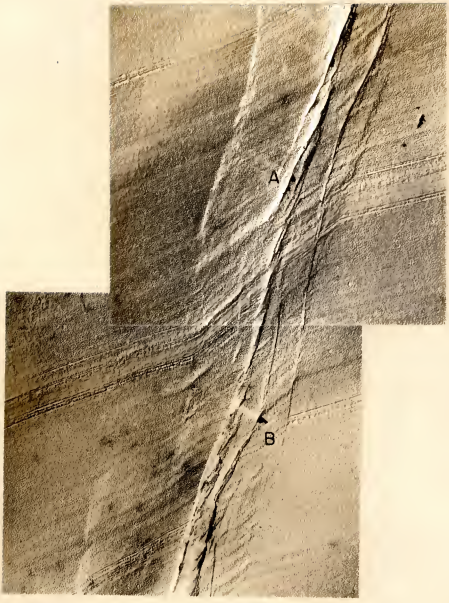

Figure 46: Example of how shear accommodation kinks remain adjacent to $\{10\bar{1}1\}$ - $\{10\bar{1}2\}$ twins. 2,800X

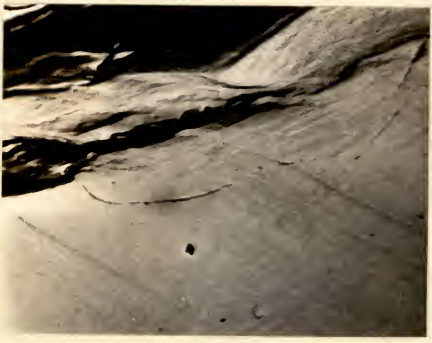

Figure 47: Small shear accommodation kink in the initial stages of its formation. The deformed structure above the kink is a $\{10\bar{1}1\}$ - $\{10\bar{1}2\}$ twin. 22.000X

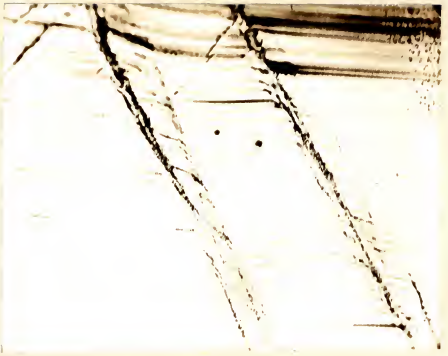

Figure 48: Example of the deformation which may occur within shear accommodation kinks. 545X

Figure 49: Electron micrograph illustrating the distribution of shear strain within a $\{10\bar{1}1\}$ - $\{10\bar{1}2\}$ twin and its shear accommodation kink. 9,000X

the lower portion of this micrograph, is large (note the discontinuity between points A and A'). The twinned area appears to end near point B. From here the shear has been extended into the lattice by a shear accommodation kink and by deformation within this kink. It is from the tip of the twin (point B) that the intense strain has passed from the twin to the kink. This occurred along the trace indicated at point C which separates the strained and unstrained regions of the kink. This observation is in good agreement with the original hypothesis of Reed-Hill (52), that these kinks accommodate non-uniform strains along the second-order twin. In this case, however, the internal deformation of the kink has also contributed to the accommodation.

A second example which illustrates how shear is passed from twin to kink is observed in Figure 50. At the upper position of this micrograph a flow line extends from the tip of a twin lamellae down across the kinked region. As in the previous case, it is difficult to deduce the crystallographic significance of this trace since it is wavy and appears to have no direct relationship to the crystal orientation. The severe strain along this trace is indicated by the cracks near the twin tip (point A).

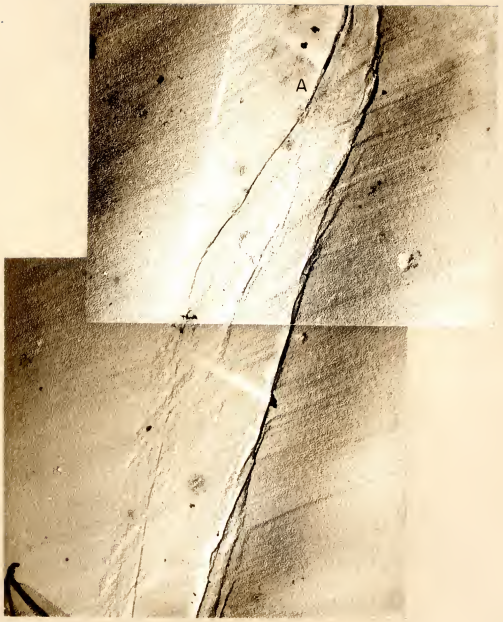

Figure 50: An example of how shear strain from a $\{10\bar{1}1\}$ - $\{10\bar{1}2\}$ twin is passed into and accommodated within a shear accommodation kink. 3,000X

On the opposite side of the kink this trace becomes straight and appears to be the same as the other deformation traces which were observed.

In addition, it was noted that significant offsets may occur along the flow lines within these kinks. This is indicated in Figures 51 and 52 where two halves of the crystal have been displaced along one of these traces. Figure 53 is another example, which indicates the severity of the strain associated with the internal deformation in the kinks. Here, the basal plane trace has been bent sharply in the vicinity of the bend plane.

Fracture

It is thought that the fractures which occur at $\{10\bar{1}1\}$ - $\{10\bar{1}2\}$ twins begin by the formation of small voids at a second-order twin boundary. One example is observed at point B in Figure 31. This indicates that the initial stages of fracture occur when the overall strain within the twin is still relatively small. Another example of voids is given in Figure 54, where they may be observed along a considerable length of the upper twin boundary. Micrographs illustrating cracks along second-order twin boundaries have already been given in Figures 34 through 37. That these areas correspond to cracks in the metal

Figure 51: Example one of shear offset along a deformation trace within a shear accommodation kink. 20,000X

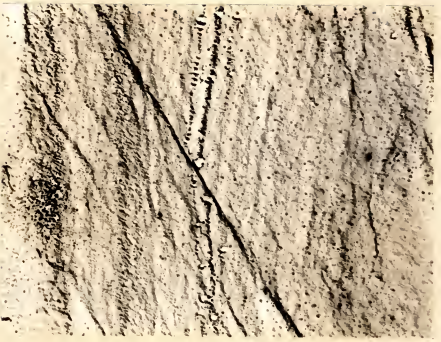

Figure 52: Example two of shear offset along a deformation trace within a shear accommodation kink. 20,000X

Figure 53: Example of the large internal shear which may occur within shear accommodation kinks. 5,000X

Figure 54: An example of how voids may open up along a $\{10\bar{1}1\}$ - $\{10\bar{1}2\}$ twin. This replica was taken from the surface of a polycrystalline magnesium specimen strained 2.5 per cent at 25°C. and a strain rate of 0.002 inches/inch/min. 13,500X

surface is revealed by shadows extending from the black protrusions as are visible in Figure 46. In analyzing these cracks it must be remembered that the shape of the protrusions does not necessarily correspond to the actual crack shape. If the cellulose acetate deposited into the internal voids was extracted cleanly from the crack surfaces, then a true indication of the crack geometry would be given. However, it seems more probable that the negative replicas were separated from the internal crack surfaces in such a manner that not all of the plastic was removed. However, the protrusions are positive indication of the existence of cracks. While it may not be possible to see all of the fissures on the replicas, it is believed that most of them are revealed. An optical micrograph of an edge view of some typical fractures is shown in Figure 55. Here a number of cracks have opened up along $\{10\bar{1}1\} - \{10\bar{1}2\}$ twins which were nucleated at the specimen edge. This is consistent with the electron micrographs in Figures 34 through 37, where cracks were also observed at the second-order twin boundary.

Figure 56 is a low magnification, optical photomicrograph of a fracture surface. The relative shear direction for the metal below this surface is shown. The fracture is characterized by striations parallel to the

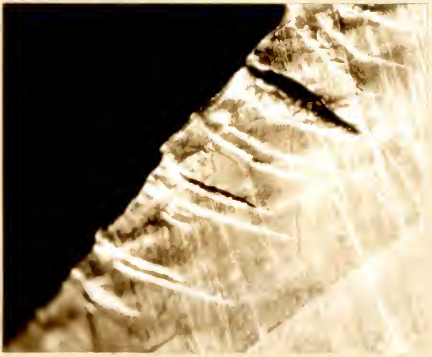

Figure 55: Optical micrograph illustrating how cracks may open up along the macroscopic habit plane of $\{10\bar{1}1\}$ - $\{10\bar{1}2\}$ twins. (Courtesy of R.E. Reed-Hill)

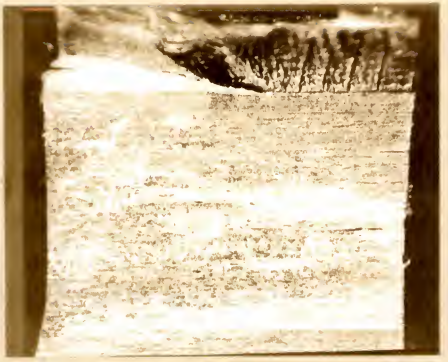

Figure 56: Structure of the fracture surface which results from cracking along a $\{10\bar{1}1\}$ - $\{10\bar{1}2\}$ twin. 28X

trace of the basal plane on this surface and perpendicular to the direction of the resolved shear. Typical electron micrographs of this fracture surface are shown in Figures 57 and 58. The shear direction and the basal plane trace are shown. These micrographs indicate that the structure of the fracture surface may vary greatly from one region to another.

Figure 57: Band structure of the fracture surface as observed in the electron microscope. 3,000X

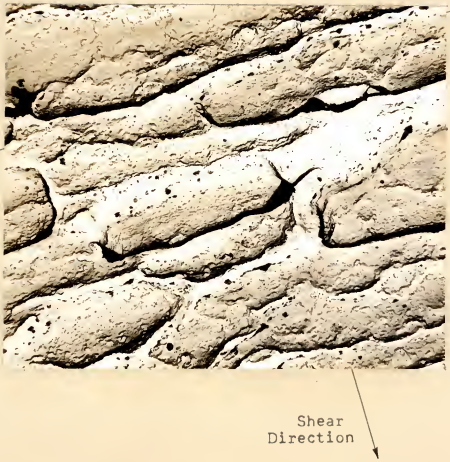

Figure 58: Dimple structure of the fracture surface as observed in the electron microscope. 3.000X

DISCUSSION, PART I: MECHANISM FOR THE SECOND-ORDER, $\{10\bar{1}1\}$ - $\{10\bar{1}2\}$ TWIN HABIT SHIFT

Crocker (83) has attempted to explain in some detail the habit shift phenomenon associated with second-order, $\{10\bar{1}1\}$ and $\{10\bar{1}3\}$ twins in magnesium. He considered two general mechanisms by which a second-order twin may form. The first of these assumed that the primary twin was fully developed before the second-order twin was nucleated. The effect that the shear of this second twin had on the orientation of the primary twin boundary was then considered. Crocker concluded that if the second twinning shear was accommodated wholly within the twinned volume, the macroscopic habit of the double twin should be the same as that of the primary twin. However, if the accommodation occurred completely in the matrix, then the boundary should be rotated from its original inclination by an amount determined by the relative orientations of the primary and second-order shear directions, as well as by the magnitude of the second shear. Upon applying the latter to the $\{10\bar{1}1\}$ - $\{10\bar{1}2\}$ double twinning mode observed by Reed-Hill (53) Crocker predicted that the habit inclination should increase from $61^{\circ}54'$ (the coherent, $\{10\bar{1}1\}$ twin orientation)

to $62^{\circ}38'$. It was also noted that the double twin orientation might lie anywhere between these two limiting values, depending upon the relative fraction of the accommodation that occurred in the twin and matrix respectively. However, this predicted range of angles for the habit plane did not agree with the 56° inclination of the $\{10\bar{1}1\}$ - $\{10\bar{1}2\}$ twins observed by Reed-Hill. Crocker, therefore, considered an alternative explanation. The primary assumption of this second approach was that the total shape deformation could be described as an invariant plane strain and that the resulting double twin boundary was macroscopically unstrained. In this manner no accommodating deformation of the parent or product structure need occur. The growth mechanism on which this theory was based assumed that a primary twin nucleus retwinned on the second-order system at an early stage of the process, and the twin propagated after this under the combined action of two shears. This is interpreted as meaning that the atoms shear directly to the second-order twin lattice sites. For the case of second-order, $\{10\bar{1}1\}$ - $\{10\bar{1}2\}$ twinning in magnesium, this theory predicted a resultant habit plane inclined $70^{\circ}48'$ from the matrix basal plane. However, by assumming that varying amounts of accommodation occur in the parent lattice, it was noted that a habit anywhere between $70^{\circ}48'$

and $62^{\circ}38'$ could result. In discussing the fact that the predicted $70^{\circ}48'$ habit does not agree with that observed by Reed-Hill, Crocker concluded,

> The only possible explanation of this discrepancy appears to be that the $\{10\bar{1}1\}$: $\{10\bar{1}2\}$ mechanism suggested by Reed-Hill (53) is not operative in the formation of these $\{30\bar{3}4\}$ bands.... In view of the importance of these bands...further experimental work on this topic is clearly desirable.

A major goal of the present research has been to re-examine these twin bands, and as a result the original experimental measurements (53) have been confirmed. Evidence was presented on page 64 that the orientation of the basal plane trace in both the primary and double twin regions is in good agreement with that predicted theoretically to result from the $\{10\bar{1}1\}$ - $\{10\bar{1}2\}$, double twinning mechanism. Also, the small interface separating the primary and second-order twin orientations closely corresponds to a $\{10\bar{1}2\}$ plane in the $\{10\bar{1}1\}$ twin lattice. The inclination of the second-order twin boundary relative to that of the primary $\{10\bar{1}1\}$ twin indicates that the habit shift occurs from the coherent, $\{10\bar{1}1\}$ twin boundary orientation $61^{\circ}54'$ from the matrix basal plane to approximately 56°. All of these observations are in good agreement with those made originally by Reed-Hill (53). In addition, the fact that most of the second-order twin bands observed in the

present research have primary $\{10\bar{1}1\}$ twins at the ends where they are growing (Figure 28) indicates that these twins probably do not propogate by the simultaneous action of two twinning shears. The existence of these primary tips implies that the resultant second-order twin boundary is not macroscopically unstrained, as assumed by Crocker's second mechanism, since the shear of the second twinning mode must intersect the boundary established by the first. Further discussion of this will be given later in this section, and evidence will be introduced that the present boundaries are actually strained.

The fact that no existing theory satisfactorily accounts for the habit shift of these twins strongly suggest that the nature of the second-order twinning process should be carefully reconsidered. An analysis of the second-order twins observed in the present research has disclosed five basic conditions which any mechanism adequately explaining the habit shift must satisfy. They are:

1) The proposed mechanism must explain the rotation of the twin boundary from the primary orientation $61^{\circ}54'$ from the matrix basal plane to the second-order orientation at 56°.
2) The mechanism must account for accommodation of the second-order twinning shear.

3) The deformation associated with the accommodation in 2) must leave the matrix lattice unrotated (see Figures 25 and 26).

4) When the shear of a second-order twin intersects a primary twin boundary, the area of this boundary is normally changed. Such a change has to be accommodated on both the twin and matrix sides of the boundary.

5) The deformation which results from the proposed mechanism must be consistent with an applied tensile stress parallel to the basal plane of the original crystal.

Consideration of these five conditions indicates that 1), 3), and 5) are self explanatory and do not need further discussion. The significance of the remaining two, however, is not immediately evident, and it is necessary to elaborate further on their relation to the present research. Concerning the second condition, it may be reasoned that a volume which has undergone simple shear can exist entirely within a crystal without disrupting lattice continuity only if the regions surrounding it are premitted to deform. This is evidenced by Figures 9, 10, and 11, where accommodating deformation may be observed in each case in the grain ahead of a twin that ends at a grain boundary.

It may be reasoned that there is no basic physical difference between normal grain boundaries and the boundaries separating a second-order twin from the matrix. Because of this, deformation similar to that noted above may possibly occur in the matrix where a second-order twin intersects the primary twin boundary. The photomicrograph in Figure 59 of another deformed zirconium specimen is direct evidence of this. Here small, second-order, $\{10\bar{1}2\}$ twins are observed within two larger $\{11\bar{2}2\}$ twins. As a result of the $\{10\bar{1}2\}$ twinning shear, kinks have formed in the matrix from the point where the second-order twins intersected the $\{11\bar{2}2\}$ boundary. In addition, Burrier, Amateau, and Steigerwald (97) have observed that in titanium deformed at temperatures below about -250°F. cracks open up at the interface between the matrix and second-order, $\{10\bar{1}2\}$ twins within primary $\{11\bar{2}2\}$ twins. These cracks are probably the result of a decreasing ability of the matrix to slip with decreasing temperature. Fracture at second-order twin boundaries is thus the natural result of an inability of the matrix to accommodate the second-order twinning shear. It is also very significant that these cracks formed on surfaces that are not normally cleavage planes. This implies that the driving force for strain accommodation is very large and, that at

Figure 59: Matrix accommodating deformation in the form of kinks resulting from the shear of second-order, $\{10\bar{1}2\}$ twins in zirconium Specimen prestrained 3 per cent by cold rolling at 77°K. then strained 23 per cent in tension and a rate of 0.02 inches/inch/min. (Courtesy of R.E. Reed-Hill). 1.000X

least in this case accommodation of a twinning shear inside a twin, as proposed by Crocker in his first example, does not occur naturally.

These examples all imply that some form of matrix deformation should result from the second-order, $\{10\bar{1}2\}$ twinning shear in magnesium. Direct evidence that the surrounding lattice does deform in conjunction with this shear is given in Figure 28. Here bending has occurred within that part of the primary, $\{10\bar{1}1\}$ twin tip adjacent to the second-order twin. The schematic illustration of this in Figure 60 shows that this bending is of the correct sense to be explained in terms of accommodation of the second twinning shear. Also, the fact that the 56° habit is only observed at the second-order twin boundary and not at the primary tips is in good agreement with the assumption that the habit shift results directly from the second-order twinning shear.

The micrographs in Figures 9, 10, 11, and 59 also illustrate that a shear strain, in general, changes the area of a boundary it intersects. Figure 61 illustrates schematically how the area of a $\{10\bar{1}1\}$ twin boundary should increase as a result of the second-order, $\{10\bar{1}2\}$ twinning shear. Condition 4) follows directly from this since the area increase must be consistent with the amount of accommodating deformation in the matrix.

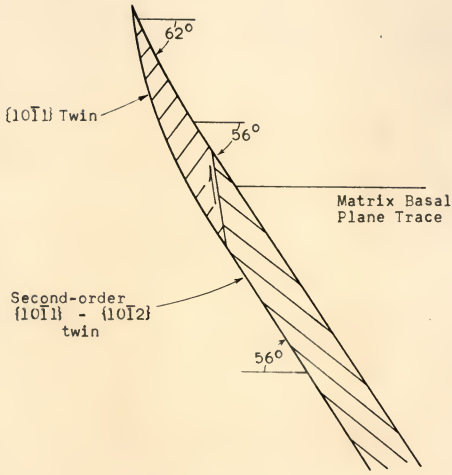

Figure 60: Schematic illustration of Figure 28 showing the lattice bending induced into a primary {10$\bar{1}$1} twin tip by the second-order, {10$\bar{1}$2} twinning shear

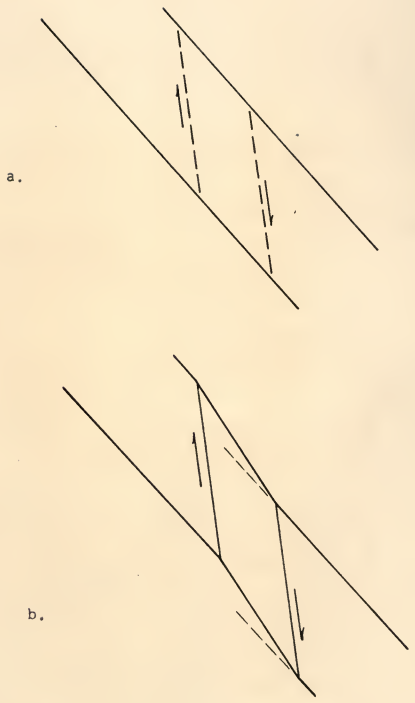

Figure 61: Schematic illustration of how the second-order, $\{10\bar{1}2\}$ twinning shear increases the boundary area of primary, $\{10\bar{1}1\}$ twins a) twin geometry before second-order twinning, and b) after second-order twinning

Models for Accommodation of the Second-Order Twinning Shear

It is thought that the habit shift of $\{10\bar{1}1\}$ - $\{10\bar{1}2\}$ twins results from matrix accommodation of the second-order twinning shear. For this reason several possible mechanisms by which this shear may be accommodated will be considered. Initially only simple models involving basic principles will be discussed; then the conclusions reached from these will be applied to the more general case. These first models will be based on the assumption that a single $\{10\bar{1}1\}$ twin forms and traverses a single crystal. This twin is then permitted to retwin on the second-order, $\{10\bar{1}2\}$ plane. The fact that first-order twins are normally observed at the ends of the double twin regions is in general agreement with this. These models will be discussed critically according to the five conditions proposed above.

Accommodation by kinking - From the examples of the interaction of a twinning shear with a boundary, it was noted that accommodation may occur by formation of a kink on a plane approximately normal to the twinning shear direction (Figures 9 and 59). The relative orientations of the second-order, $\{10\bar{1}2\}$ twin and matrix lattice in the present case are almost ideal for accommodation through

the formation of a basal kink band, since the matrix basal plane is almost perpendicular ($80^{\circ}39'$) to the second-order shear direction. The resulting geometrical relationship between the matrix and twin is shown schematically in Figure 62. The second-order twinning shear direction is only $19^{\circ}45'$ from the primary twin boundary orientation. The magnitude of this shear is calculated to be 0.129 from the two orientations of the second undistorted plane, K_2, in Figure 63. As a result this second twinning shear only reorients the boundary by 40' from its initial position in space, as deduced from the geometry in Figure 64. At the same time, however, a matrix lattice plane which is across the twin boundary and oriented parallel to the initial position of the second undistorted plane, K_2, of the second twinning mode, must be rotated by the full amount of the twinning shear rotation. From Figure 62 this rotation is calculated to be $7^{\circ}24'$. As a result of the relative differences in rotation of the matrix lattice and second-order twin habit, the angle between the basal plane in the kink and the second-order twin boundary becomes $55^{\circ}10'$, which is close to the experimentally observed inclination of these twins. However, the kinking operation indicated here does not conform to conditions 3) and 5) on page 110, that the habit shift mechanism must satisfy.

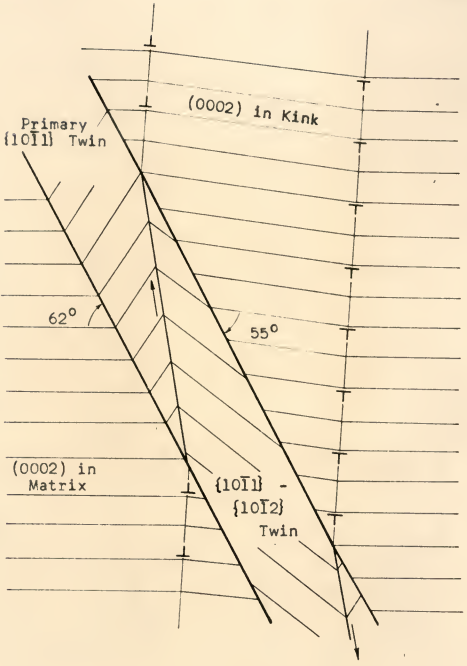

Figure 62: Accommodation of the second-order, (10$\bar{1}$2) twinning shear by kinking on the matrix basal plane

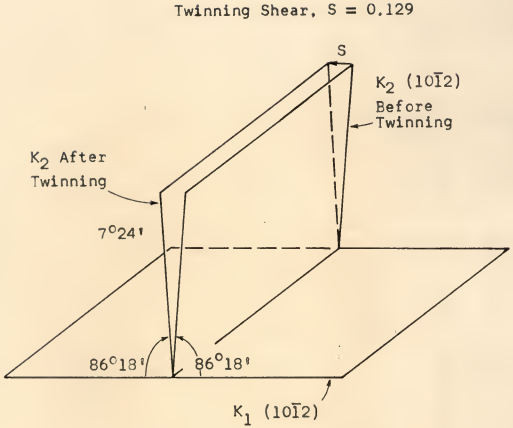

Figure 63: Lattice geometry of $\{10\bar{1}2\}$ twinning in magnesium in terms of the orientation of the first undistorted plane, K_1, and second distorted plane, K_2

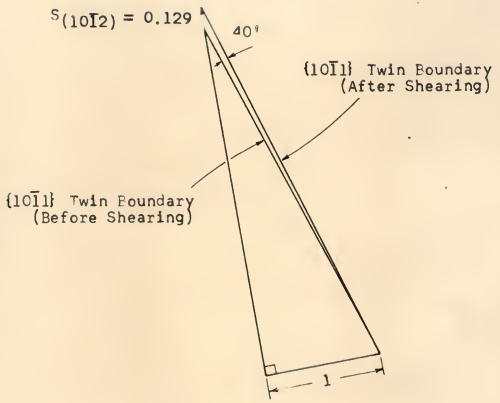

Figure 64: Effect of the second-order, {10$\bar{1}$2} twinning shear on the orientation of a primary, {10$\bar{1}$1} twin boundary

The schematic illustration of this deformation in Figure 62 indicates that a $7^{o}24'$ rotation of the lattice adjacent to the twin is involved. As illustrated by the micrographs of $\{10\bar{1}1\}$ - $\{10\bar{1}2\}$ twins (Figures 24, 25, and 26), no rotation of this magnitude has been observed. Also, the dislocation arrangement of the kink in Figure 62 is similar to that of the compressive kink bands studied by Hess and Barrett (21) (see Figure 65). As shown by Figure 66, tensile deformation of a single crystal by a simple slip process normally rotates the active slip plane toward the stress axis, whereas, the kink band indicated in the present case rotates the active slip plane away from this axis. Formation of a dislocation structure which does not relax the applied stress is normally unacceptable. Unless other deformation processes, which have not thus far been identified, occur to relieve this contractive strain, these kinks should not form.

It is interesting to note that part of the mechanism described here is equivalent to the first mechanism of double twin growth that Crocker (83) considered. In both cases, the second-order twinning shear was predicted to have the same effect on the primary boundary orientation. However, Crocker gave no consideration as to how the shear could be accommodated in the matrix. At any rate this type of accommodation is apparently not feasible.

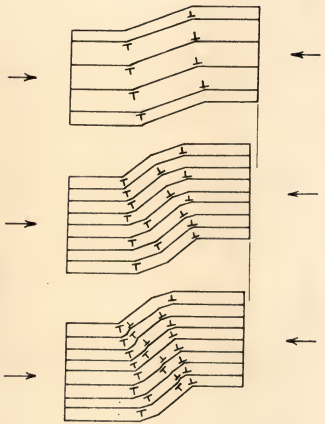

Figure 65: Schematic illustration of successive stages of the compressive deformation of a single crystal by kinking (after Hess and Barrett (21))

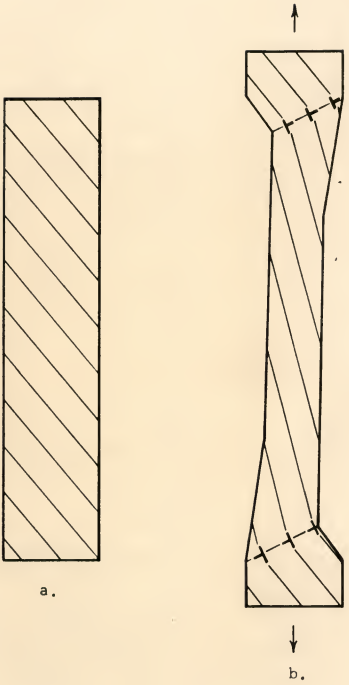

Figure 66: Deformation of a single crystal tensile specimen with end constraints by slip on a single system. In a) the specimen is viewed before straining and in b), after straining. Note that as a result of slip, the active slip plane is rotated toward the tensile axis. The slip plane in the specimen ends has been assumed to bend in the manner observed by Miller (35)

Accommodation by simple slip - It was shown in Figure 11 that, when the shear of a twin intersects a boundary, this shear may be accommodated by slip on a plane nearly parallel to the twinning plane and whose slip direction is approximately colinear with the second-order twinning shear direction. For the present case of $\{10\bar{1}1\}$ - $\{10\bar{1}2\}$ twinning, the second-order shear direction is almost ideally oriented to induce glide on a $\{10\bar{1}0\}$ prism plane in the $\vec{c}$ axis direction. However, while dislocations with a "$\vec{c}$" Burgers vector are known to exist (14), they have never been observed to glide; so it may be concluded that slip on such a system is doubtful.

Accommodation by dislocation climb - Dislocation climb is a third general mechanism by which the orientation of an intercrystalline boundary may be changed. Figure 67 illustrates that introduction of an array of extra half planes into the lattice, both above and below the twin, lowers the inclination of the boundary with respect to the basal plane. These half planes correspond to positive edge dislocations above the twin and negative edge dislocations below. Since dislocations of one sign cannot be created mechanically (page 8). this implies the existence of a vacancy or interstitial mechanism. However, it is doubtful

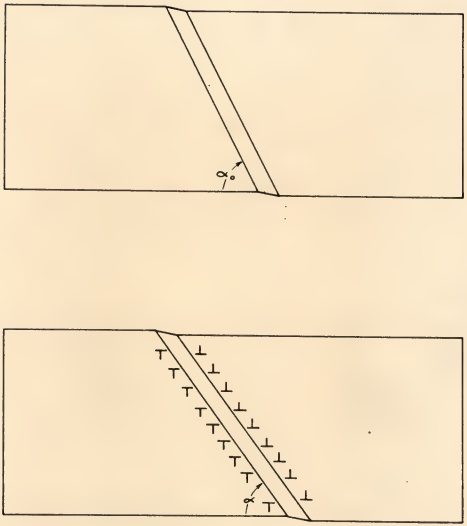

Figure 67: The effect of dislocation climb on the inclination of a twin relative to the matrix lattice orientation. The initial twin is shown in a) inclined at angle α_o, while in b) the twin inclination has been reduced to α.

that a diffusion-controlled process could play a significant roll in the $\{10\bar{1}1\}$ - $\{10\bar{1}2\}$ twin habit shift in magnesium, since this shift may occur in the order of minutes, or less at room temperature ($T \cong 0.3T_{mp}$).

Accommodation by duplex slip - A fourth process by which this habit shift could occur involves slip on two matrix slip systems. In this manner, the lattice can deform by slip without experiencing a general rotation, since the bending associated with slip on one system may be cancelled by the second, thus satisfying condition 3) on page 110. At the same time, however, duplex slip may influence the orientation of a boundary in much the same manner as deformation by simple slip. Figure 68 illustrates how this slip permits a specimen to elongate in the tensile direction and contract in the thickness direction. If a twin is present in this crystal along either of the dashed lines drawn parallel and perpendicular to the tensile axis, its orientation should not be effected by the duxpex slip. This results from the fact that the dislocations on each of these two slip planes shear the twin boundaries in an equal and opposite manner. This is a purely hypothetical case since in this orientation the twin has formed on a plane with no resolved shear stress. If, however, the twin

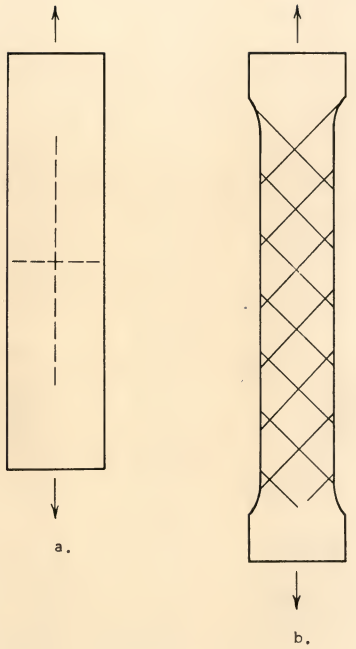

Figure 68: Deformation of a single crystal tensile specimen by duplex slip on two planes symmetrically oriented with respect to the stress axis

is in some random orientation as duplex slip occurs, it should be sheared more by the dislocations on one of the slip planes than on the other; and a net rotation should occur. The amount of this rotation should, in general, be a maximum when the twin is parallel to one of the slip planes. At the same time, slip on one of these systems may be correctly oriented to accommodate the second-order twinning shear. Thus, duplex slip may satisfy all five of the necessary habit shift conditions, provided the slip systems are properly chosen in conjunction with the lattice geometry involved. If it is assumed that duplex slip occurs on $\{10\bar{1}1\}$ planes in $\langle 11\bar{2}3\rangle$ directions, a habit shift mechanism can be constructed that is in good agreement with experimental observations. The existence of $\frac{1}{3}\{10\bar{1}1\}\langle 11\bar{2}3\rangle$ slip dislocations (14) in magnesium must be postulated, however, and evidence supporting their existence will be presented in the following section.

For a magnesium crystal with a $\langle 10\bar{1}0\rangle$ tensile axis, there are two symmetrically oriented $\{10\bar{1}1\}$ planes on which slip could occur. These are indicated as $(\bar{1}011)$ and $(10\bar{1}1)$ in Figure 69. The dislocation types on each plane which should result from the applied tensile load are also shown. In addition, it is noted from Figure 1 that there are two $\langle 11\bar{2}3\rangle$ slip directions on each of these slip planes. These are symmetrical with respect to the

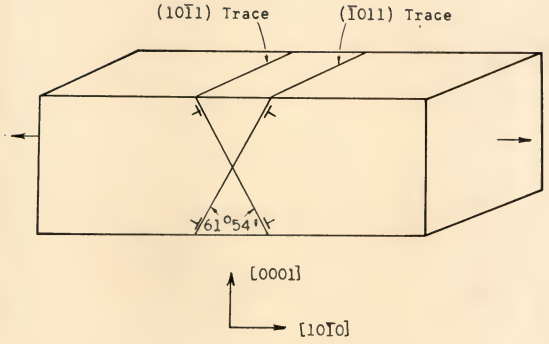

Figure 69: Schematic illustration of a magnesium tensile specimen with a [10$\bar{1}$0] tensile axis showing the relative orientations of the (10$\bar{1}$1) and ($\bar{1}$011) lattice plane

tensile axis, so slip on each plane should involve approximately equal numbers of two dislocation types.

The effect on the second-order twin boundary orientation of equal amounts of slip on the $(\bar{1}011)$ and $(10\bar{1}1)$ planes will be determined by considering each system separately. The most favorably oriented plane to accommodate the second-order twinning shear by a slip mechanism is $(\bar{1}011)$. Although this plane lines 37° from the second-order twinning shear direction, this places the acting slip direction closer to the shear direction than for any other known crystallographic slip system in a hcp lattice. It is assumed that the second-order twinning shear has the same effect on the primary boundary orientation as discussed on page 117, where it was shown that a 40' rotation should result. The accommodating deformation which results from glide on $(\bar{1}011)$ is illustrated in Figure 70. The rotation associated with a single slip process is indicated. This structure is actually that of a kink band, although no bend planes are shown. The spacing of dislocations needed to produce the $7^{\circ}24'$ matrix rotation in conjunction with the second-order twinning shear rotation, may be calculated from the equation of Read (28).

$$D = \frac{b}{2\sin \theta/2} \qquad (1)$$

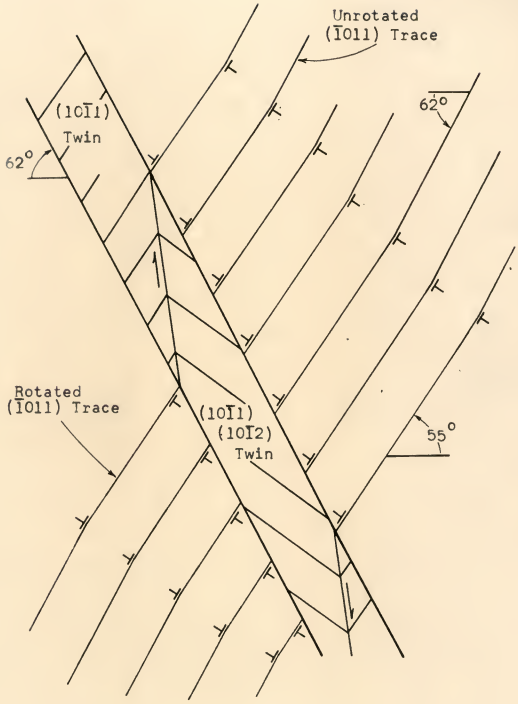

Figure 70: The effect of matrix glide on (1̄011) on the orientation of the matrix lattice adjacent to a (10$\bar{1}$1) - (10$\bar{1}$2) twin. As a result of this glide the angle between the twin habit and the basal plane in the slipped region is reduced to 55°

where D is the vertical spacing of dislocations, b is the magnitude of the Burgers vector component normal to the bend plane, and θ is the lattice rotation produced. On this basis, an array of $\frac{1}{3}[11\bar{2}3]$ and $\frac{1}{3}[2\bar{1}\bar{1}3]$ dislocations on $(\bar{1}011)$ planes spaced 49.7Å apart produces the required $7^{\circ}24'$ bend of the lattice. As discussed on page 117, deformation which rotates the matrix lattice clockwise by this amount with respect to the twin also automatically reduces the inclination of the second-order boundary in the deformed region to 55° relative to the matrix basal plane.

It is now necessary to consider the effect of an equal amount of slip on $(10\bar{1}1)$. Because the $\langle 11\bar{2}3\rangle$ slip directions on $(10\bar{1}1)$ are nearly parallel to the second-order twin boundary, intersections of $\frac{1}{3}[\bar{2}113]$ and $\frac{1}{3}[\bar{1}\bar{1}23]$ dislocations with the boundary occur at widely spaced intervals. For this reason the boundary rotation induced by glide of this type is about the same as the lattice rotation itself. This is illustrated in Figure 71 where, as a result of slip on this second system, both the matrix and twin boundary are rotated clockwise by $7^{\circ}24'$. In this manner the angular relationship between the second-order boundary and the matrix lattice established by slip on $(\bar{1}011)$ is maintained. The net effect of slip on these two systems is thus to produce about a 7° rotation of the

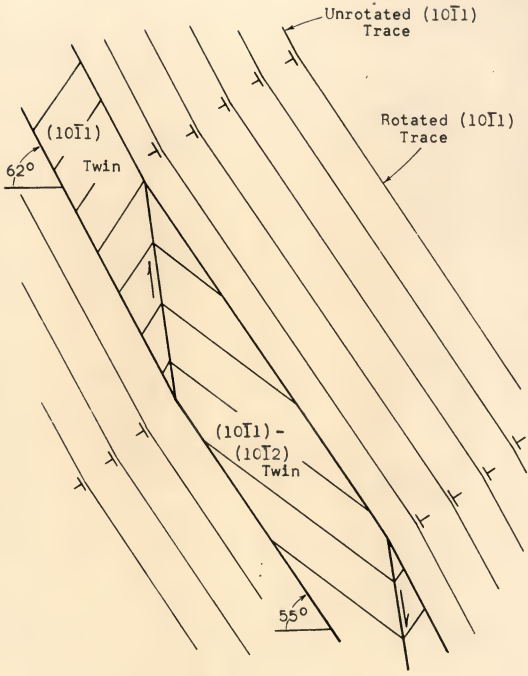

Figure 71: The effect of matrix glide on (10$\bar{1}$1) on the orientation of a (10$\bar{1}$1) - (10$\bar{1}$2) twin and on the matrix lattice adjacent to a twin

second-order twin boundary toward a lower angle with the matrix basal plane. In practice the $(\bar{1}011)$ and $(10\bar{1}1)$ slip systems are assumed to operate simultaneously; so at any one time there is no actual lattice rotation in the matrix, as implied in the above discussion.

Interaction of $\frac{1}{3}\langle 11\bar{2}3\rangle$ Dislocations

The fact that slip on two systems has been assumed in this accommodation process implies that interactions may occur between dislocations on the two planes, as pictured schematically in Figure 72. It is assumed that these interactions occur along the basal plane and the $(\bar{1}010)$ prism plane. This geometry for the interactions was chosen only because of the simplicity which is introduced. Equations (2), (3), (4), and (5) indicate the product dislocations that result from interactions along the $(\bar{1}010)$ plane.

$$\frac{1}{3}[2\bar{1}\bar{1}3] + \frac{1}{3}[\bar{1}\bar{1}23] \longrightarrow \frac{1}{3}[1\bar{2}10] + [0001] + [000\bar{1}] \quad (2)$$

$$\frac{1}{3}[2\bar{1}\bar{1}3] + \frac{1}{3}[\bar{2}113] \longrightarrow [0001] + [000\bar{1}] \quad (3)$$

$$\frac{1}{3}[11\bar{2}3] + \frac{1}{3}[\bar{1}\bar{1}23] \longrightarrow [0001] + [000\bar{1}] \quad (4)$$

$$\frac{1}{3}[11\bar{2}3] + \frac{1}{3}[\bar{2}113] \longrightarrow \frac{1}{3}[\bar{1}2\bar{1}0] + [0001] + [000\bar{1}] \quad (5)$$

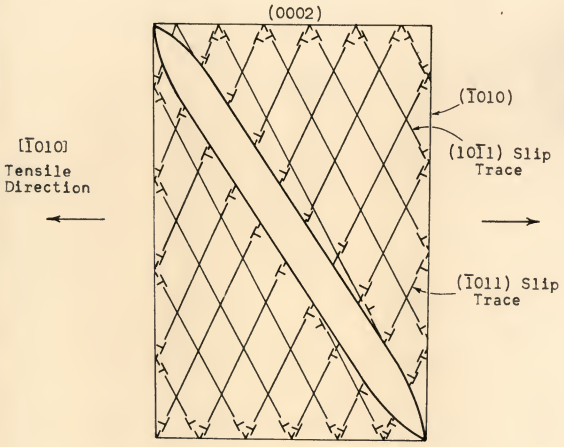

Figure 72: Schematic illustration of the interaction which may occur between dislocations on the (Ī011) and (10Ī1) slip planes

If it is assumed that the energy of a dislocation is proportional to the square of its Burgers vector, then it may be shown that each of these reactions is energetically feasible. Since the same number of product dislocations should result from (2) and (5), the $[1\bar{2}10]$ and $[\bar{1}2\bar{1}0]$ dislocations cancel; and the net Burgers vector of these four reactions is along the $\vec{c}$ axis.

From the interactions which may occur along the basal plane (Figure 72), the following reactions should result:

$$\frac{1}{3}[\bar{1}\bar{1}23] + \frac{1}{3}[\bar{1}\bar{1}2\bar{3}] \longrightarrow \frac{1}{3}[\bar{1}\bar{1}20] + \frac{1}{3}[\bar{1}\bar{1}20] \qquad (6)$$

$$\frac{1}{3}[\bar{1}\bar{1}23] + \frac{1}{3}[\bar{2}113] \longrightarrow [\bar{1}010] \qquad (7)$$

$$\frac{1}{3}[\bar{2}11\bar{3}] + \frac{1}{3}[\bar{1}\bar{1}23] \longrightarrow [\bar{1}010] \qquad (8)$$

$$\frac{1}{3}[\bar{2}11\bar{3}] + \frac{1}{3}[\bar{2}113] \longrightarrow \frac{1}{3}[\bar{2}113] + \frac{1}{3}[\bar{2}110] \qquad (9)$$

Energy considerations indicate that these also may occur. Since the Burgers vector component normal to $[1\bar{2}10]$ in Equations (6) and (9) cancel, the net Burgers vector is parallel to $[\bar{1}010]$. Because the $(\bar{1}011)$ and $(10\bar{1}1)$ planes intersect along $[1\bar{2}10]$, the $\vec{a}$ and $\vec{c}$ product dislocation lines should also lie along this direction. A schematic illustration of these dislocations relative to a $(10\bar{1}1)$ - $(10\bar{1}2)$ twin is given in Figure 73. It is noted that this

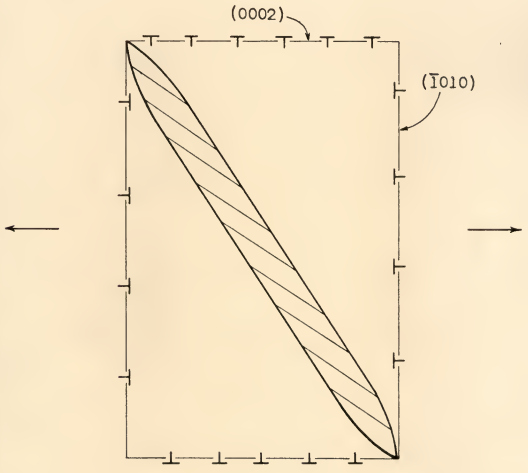

Figure 73: The ultimate dislocation structure in the matrix that is predicted to result from interactions between slip dislocations on $(10\bar{1}1)$ and $(\bar{1}011)$. The dislocations lying on (0002) have a net Burgers vector along $[1\bar{2}10]$ .while those on $(10\bar{1}0)$ have their vector in the $\vec{c}$ axis direction

resultant structure is consistant with the concept of duplex slip, since the region bounded by these dislocations has been elongated in the tensile direction and contracted in the transverse. Also, the density of these dislocations should decrease with increasing distance from the twin. This is consistent with the fact that the effect of the second-order twinning shear, and thus the intensity of $(\bar{1}011)$ and $(10\bar{1}1)$ slip, should decrease away from the twin. That no specimen contraction has been experimentally observed in the vicinity of second-order twins which have propagated completely through a crystal may also be explained by this.

DISCUSSION, PART II: INTERNAL DEFORMATION OF SECOND-ORDER, $\{10\bar{1}1\} - \{10\bar{1}2\}$ TWINS

In order to understand the large internal strains of second-order $\{10\bar{1}1\} - \{10\bar{1}2\}$ twins, which occur subsequent to their formation, two basic features of this deformation must be explained. The first of these concerns the mechanism which permits shear strains of up to 1,000 per cent (52) to occur within these narrow bands. The second involves the necessary continuity of material which must occur between the matrix and twin lattices at the second-order twin boundary if fracture is not to immediately result. The mechanism of deformation which is operative within the individual twin lamellae will be considered first, and then the significance of this in the general twin band deformation will be discussed.

Deformation of Individual, $\{10\bar{1}1\} - \{10\bar{1}2\}$ Twin Lamellae

Basil slip - As a result of $\{10\bar{1}1\} - \{10\bar{1}2\}$ double twinning, the basal plane is realigned 37.5° from the stress axis (Figure 29). This is close to the ideal slip orientation. It seems most probable that the internal deformation of these twins could occur by extensive slip on the basal plane. Certain difficulties are encountered, however,

when a narrow volume of material such as these twins is sheared on a single system which is not exactly parallel to the boundary. This may be realized by considering the macroscopic shape change which results from the deformation of $\{10\bar{1}1\}$ - $\{10\bar{1}2\}$ twins. The micrographs in the preceding section indicate that this internal strain is occurring by a shear directed nearly parallel to the second-order twin boundary. This should produce a shape deformation of the type illustrated schematically in Figure 74. One notable feature of this deformation is that the width of the sheared volume, w, is the same both before and after the shear. This is consistent with the experimental observation that the thickness of second-order twins in regions of intense strain is not significantly greater than in regions of small strain (compare Figure 31 with Figure 37). In view of the magnitude of the shear strains involved. this change may probably be considered as negligible. This implies that the observed deformation is equivalent to a shear on a plane aligned parallel with the sides of the twin.

An attempt will now be made to rationalize the shape change in Figure 74 in terms of simple slip on the second-order twin basal plane. Figure 75, part a, shows schematically a volume of material in the double twin orientation as it lies relative to the stress axis. The basal

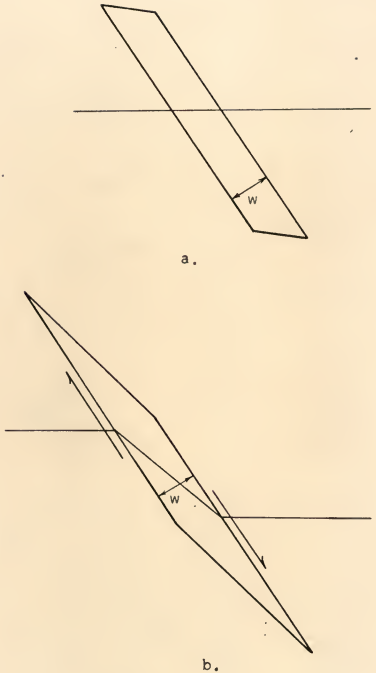

Figure 74: Schematic illustration of the macroscopic shape change observed to accompany the deformation of $\{10\bar{1}1\}$ - $\{10\bar{1}2\}$ twins. The initially undeformed twin volume is shown in a) and the deformed in b)

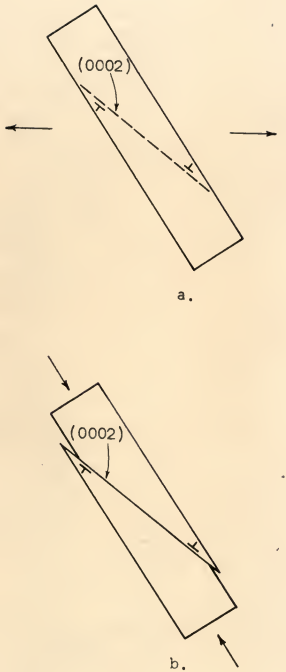

Figure 75: Schematic illustration of the macroscopic shape change predicted to occur as a $\{10\bar{1}1\} - \{10\bar{1}2\}$ twin deforms by simple slip on the basal plane. The initially undeformed twin volume is shown in a) and the deformed in b)

plane trace, indicated by the dashed line, is at the predicted inclination 18.5° from the boundary. The macroscopic shape change which should result from slip on this system is shown in Figure 75, part b. It is noted that this is not a shear deformation but is analogous to what should result from a compressive load directed along the length of the twin. This indicates that the deformation described by Figure 74 cannot result from slip on this plane. If large deformations do occur in this manner, then there should be considerable thickening of the twin and the basal plane should be rotated toward the stress axis. The amount of rotation which should necessarily accompany a strain within the twin of 500 per cent was computed to be about 30° from the equation in Schmid and Boaz (98). This would align the basal plane about 7° from the tensile axis. However, analysis of the orientation of the basal plane traces within second-order twin lamellae indicates that this plane is not rotated toward the tensile axis but away from it. This is shown by the micrograph in Figure 29 of an etched $\{1\bar{2}10\}$ magnesium face where the basal plane trace in the second-order twin is about 50° from the matrix basal plane. As discussed on page 121 a rotation of the active slip plane in this sense implies that the crystal has been stressed in compression parallel to the basal plane rather than tension. This is further evidence that the internal

strain of these twins cannot occur by slip on the twinned basal plane, as described, but must involve some other mechanism of deformation. Additional arguments which support this fact are discussed in Appendix A.

Couling, Pashak, and Sturkey (91) have attributed the infinite rollability of certain magnesium base alloys to basal slip within small $\{10\bar{1}1\}$ - $\{10\bar{1}2\}$ second-order twin bands. Based on extinction measurements made with a polarized light microscope, these authors concluded that the basal plane within these twins was parallel to the boundary, thus permitting deformation by shear on this plane. They stated that,

> Although this double twinning process does not reorient the basal plane to a position exactly parallel to the band plane, it does reorient the basal plane to a position where basal slip will operate and consequently rotate the basal plane into the band plane.

However, as discussed above, slip on the basal plane, which occurs in conjunction with the applied stress, does not produce a rotation in this direction.

In the present experiments the doubly twinned basal plane was often observed to make a steeper angle with the matrix basal plane than the predicted 37.5°, as was illustrated in Figure 28. Many of the second-order twin basal traces observed were inclined near this same orientation

(50^{o} from the matrix basal plane). Figure 76 shows an example where the twinned basal plane is almost exactly parallel to the second-order twin habit. This is in agreement with the observations of Couling, et al., and indicates that the same mechanism may be responsible for the deformation of double twins in pure magnesium and in rolled magnesium base alloys. Reorientation of the twinned basal plane may be a significant step in the overall deformation process, since once the basal plane becomes aligned parallel to the twin boundary, extensive shear strains may occur by simple slip on this plane.

Reorientation of the twinned basal plane by kinking - A mechanism which could operate in both pure magnesium and in the rolled alloys and that rotates the twinned basal plane in the correct sense involves non-basal kinking within the twin. In this case the twin boundary is considered as an asymetrical tilt boundary which may be formed as discussed by Read (28) using two different types of edge dislocations. The macroscopic stress level as these twins deform in between 15,000 and 20,000 pounds/square inch, which is significantly greater than the critical resolved shear stress for basal slip in magnesium

Figure 76: Electron micrograph of a $\{10\bar{1}1\}$ - $(10\bar{1}2)$ twin on an etched surface. The pits within the twin, which correspond to the basal plane trace, are aligned nearly parallel to the twin boundary. Matrix bend planes of a small orientation (1^{o} or less) are also observed in this micrograph. It is thought that these play a minor role in accommodating non-uniform strains within the twins. 5,000X

of 65 pounds/square inch (6). This high stress and the proximity of the two boundaries to each other, may direct a concentrated shear along the twin length. These conditions are then ideal for kinking on a plane approximately normal to the twin boundary. The two planes most suitably oriented for this are $(\bar{1}011)$ and $(\bar{1}012)$ which lie 25° and 6° from the stress axis, respectively, and 99° and 118° from the twin boundary. The existence of $\frac{1}{3}\{10\bar{1}1\}\langle 11\bar{2}3\rangle$ dislocations has already been discussed in conjunction with the proposed habit shift mechanism. Evidence that $\langle 10\bar{1}1\rangle$ dislocations on $\{10\bar{1}2\}$ exist in magnesium will be presented later in this section. Based on this, slip within second-order twins could probably occur on either of these two planes. If it is assumed that a kink forms as a result of slip on $(\bar{1}011)$, then two types of dislocations, $\frac{1}{3}[2\bar{1}\bar{1}3]$ and $\frac{1}{3}[11\bar{2}3]$, are involved, as shown by Figure 1. The structure of a kink with an 18.5° misorientation which results from $(\bar{1}011)$ slip is shown schematically in Figure 77.

If a second set of $\frac{1}{3}\langle 11\bar{2}3\rangle$ dislocations on $(10\bar{1}1)$ planes is introduced, the orientation of the bend planes in Figure 77 may be made parallel to the second-order twin boundary, as indicated in Figure 78. By requiring that the bend planes be parallel to the twin boundaries and assuming that each may be treated as an asymetrical

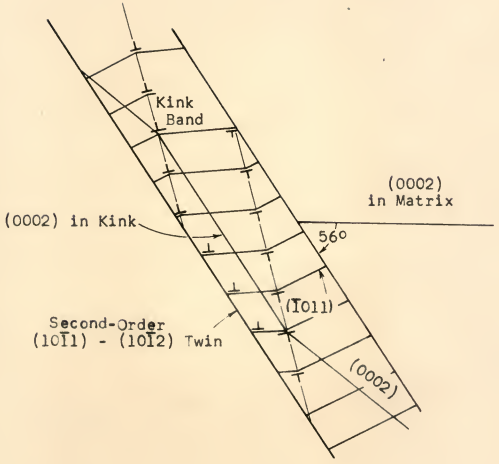

Figure 77: Structure of a kink of 18.5° misorientation that results within a (10$\bar{1}$1) - (10$\bar{1}$2) twin as a result of slip on ($\bar{1}$011)

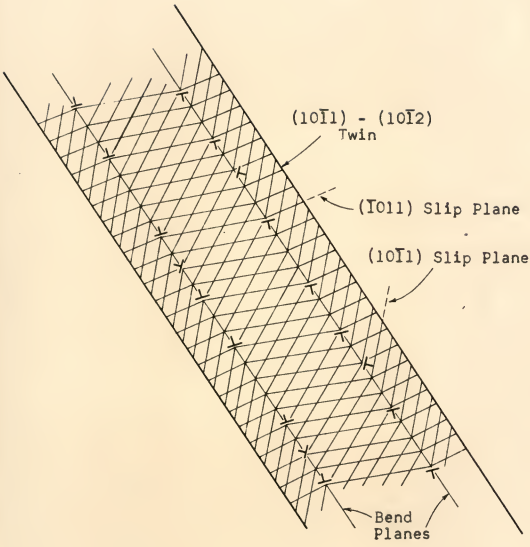

Figure 78: Structure of a kink of 18.5° misorientation that results within a (10$\bar{1}$1) - (10$\bar{1}$2) twin as a result of slip on ($\bar{1}$011) and (10$\bar{1}$1)

tilt boundary (28), the orientation of the second-order twin habit should not change as the bend planes expand out to the twin boundaries and the two interact. Also, no matrix lattice strains should result from the two types of dislocations entering the twin boundary.

As a result of this kinking operation, the basal plane within the twin is rotated toward the second-order twin boundary. For a kink misorientation of 18.5°, the twinned basal plane and twin boundary become effectively parallel. At the same time this kink contributes to the overall tensile elongation of the crystal, since both of the active slip planes are rotated toward the tensile axis and a shear strain of 0.33 occurs parallel to the twin boundary. The spacing of each dislocation type needed to produce this bending was calculated from the two equations in Read (28),

$$D_{(\bar{1}011)} = \frac{b}{\theta \sin \phi} \qquad (\underline{10})$$

$$D_{(10\bar{1}1)} = \frac{b}{\theta \cos \phi} \qquad (\underline{11})$$

The terms here are the same as defined on page 132, except for ϕ, which is the bend plane inclination relative to the mean orientation of $(\bar{1}011)$ planes. On this basis $\frac{1}{3}\langle 11\bar{2}3\rangle$ dislocations spaced 19.2 Å apart on $(\bar{1}011)$ and 58.4 Å apart on $(10\bar{1}1)$ are required.

The flow lines observed within second-order twins are often nearly parallel to the twin boundary. This applies both in regions where the strain is small (Figure 13) and where it is extensive (Figure 37), and indicates that the deformation mechanism produces a net shear in this direction. This is consistent with the present model where the twinned basal plane is aligned parallel to the plane of the boundary, since with the close-packed plane in this orientation the large internal strains of these twins may occur by basal slip.

The Role of Twin Lamellae in the Deformation of a Macroscopic Twin Band

It is now necessary to consider how the deformation within separate twin lamellae is related to the total macroscopic deformation of a second-order twin band. The mechanism proposed for the deformation of individual lamellae, where extensive slip occurs on the reoriented basal plane, does not adequately describe the overall deformation process. The micrographs of typical $\{10\bar{1}1\}$ - $\{10\bar{1}2\}$ twins which have been sheared extensively (Figures 34 through 37) are evidence of this, since they indicate that the deformation is too complex to be interpreted by simple slip on a

plane parallel to the twin boundary. It is thought that these complexities are a consequence of two characteristic features of the $\{10\bar{1}1\}$ - $\{10\bar{1}2\}$ twin lamellae structure. The first of these results from the fact that these individual twins are separated from one another by the matrix lattice (Figures 25 and 26). The manner in which the internal deformation proceeds from one lamellae to the next, Figures 31 and 33, indicates that the flow often occurs continuously through this matrix. The appearance of the flow lines in these interconnecting regions is complex, and on the basis of the information in these micrographs an exact mechanism could not be deduced. However, the net effect of this deformation is a shear strain effectively directed along the macroscopic twin band habit 56° from the matrix basal plane. In view of the large stresses along the twin length and the fact that the lamellae themselves probably strain with relative ease by slip on the basal plane, these interconnecting regions of matrix orientation may be stressed to extremely high values, and the driving force for them to relax may be great. There is evidence that the adjacent lamellae do not interconnect during deformation by twin growth. If the two did join by the mutual growth of each, then simple slip on the basal plane could occur along the entire twin length. However,

the electron micrograph in Figure 76 of a deformed second-order twin on an etched $\{1\bar{2}10\}$ magnesium surface indicates that the lamellae have retained their individual identity up to this late stage of deformation. For this reason it is difficult to explain the flow where two lamellae meet (Figures 32 and 34) in terms of any normal crystallographic slip process.

The second structural feature of second-order twin bands which complicates the deformation process is thought to result from the fact that the individual twin lamellae are not exactly parallel to the macroscopic habit plane. A possible explanation for this misalignment is presented in Appendix B. The glide traces within these lamellae are nearly parallel to the twin boundary (Figure 31), indicating that the deformation produces a net shear in this direction. However, because of the misalignment of individual lamellae, the shear from adjacent twins is not colinear, and some strain must be transmitted into the matrix and accommodated there. The resulting type of deformation is illustrated by Figure 32. Here, it is noted that the ends of the two lamellae (at points A and B) have been sheared about three microns past one another. The intense deformation in each twin is indicated by the contours of the flow lines where the two interconnect. This

micrograph also illustrates that two types of matrix deformation may occur in order to accommodate the strain from the lamellae tips. The first of these takes the form of a shear parallel to the macroscopic twin habit, as observed at point A; and the second occurs as slip on the matrix basal plane, which is noted at point B.

Another form of matrix deformation, thought to result from the misalignment of individual, second-order twin lamellae , is illustrated at point A in Figure 31. Here a long, narrow shear trace is observed parallel to the macroscopic twin habit (56^{o} to the matrix basal plane). It is thought that this resulted from a stress relaxation along the twin length, which caused the matrix to be sheared in this direction. A second example of this which illustrates the effect even more convincingly, is noted in Figure 33, where extensive shear has occurred in this same direction on the upper side of the right lamellae. The deformation mechanism which could operate in the matrix and permit this shear at 56^{o} to the basal plane must be complex and is not easily deduced. It is difficult to interpret this strain in terms of dislocation motion on slip systems which have been previously reported. Deformation of the type observed here may be instrumental, however, in directing the net shear strain parallel to the macroscopic twin habit. This is

illustrated schematically in Figure 79, where it is shown how the twin lamellae are sheared parallel to their length, and at the same time the interconnecting matrix lattice is sheared along the macroscopic twin habit. In this manner the shear traces in Figure 37, which illustrate an advanced stage of the deformed structure, can be explained.

Grain Boundary Shearing as a Factor in Second-Order Twin Deformation

It was mentioned in the preceding section that, in general, a second-order twin boundary has symmetry properties similar to a general grain boundary. On this basis the atomic configuration of such a twin boundary may be identical to that of a high-angle boundary of the same inclination separating two crystals of the same relative misorientation. Thus, the structure of a magnesium single crystal containing a single $\{10\bar{1}1\}$ - $\{10\bar{1}2\}$, second-order twin is comparable to that of a tricrystal with two grain boundaries inclined 56° to the stress axis. These separate a long, narrow grain of the double twin orientation from two grains of the matrix orientation. It was pointed out on page 10 that the presence of an intercrystalline boundary may increase the strength of a material in addition to surpressing the normal slip processes in the vicinity of the boundary. This was demonstrated most

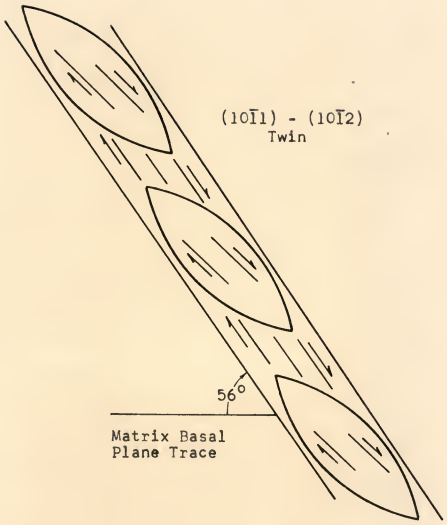

Figure 79: Schematic illustration of the misalignment of shear deformation within (10$\bar{1}$1) - (10$\bar{1}$2) twin lamellae relative to that which occurs along the macroscopic band plane. The angular misorientation of the two shear traces is exaggerated for emphasis

convincingly by Figure 3, where it was observed that no measurable basal slip has occurred in the vicinity of the boundary of a zinc bicrystal although the macroscopic shear strain was 150 per cent. This hardening effect was so pronounced that grain boundary shear, rather than basal slip, was the preferred mechanism of deformation, despite the fact that the basal plane did not intersect the boundary. When applied to the present case of $\{10\bar{1}1\}$ - $\{10\bar{1}2\}$ twinning in magnesium, these facts suggest that realignment of the second-order twin basal plane parallel to the twin boundary does not necessarily permit deformation to occur by simple glide on this plane. Instead, it is possible that the internal deformation of these twins proceeds by an alternate means, namely the same mechanism that is responsible for grain boundary deformation in polycrystalline materials. Based on the tricrystal model proposed above, this implies that deformation of the small, narrow grain, which corresponds to the second-order twin, occurs by grain boundary shear.

Several authors (41,42) have observed grain boundary shear in magnesium at room temperature. Figure 80 is an electron micrograph illustrating this type of deformation on the deformed surface of a polycrystalline magnesium

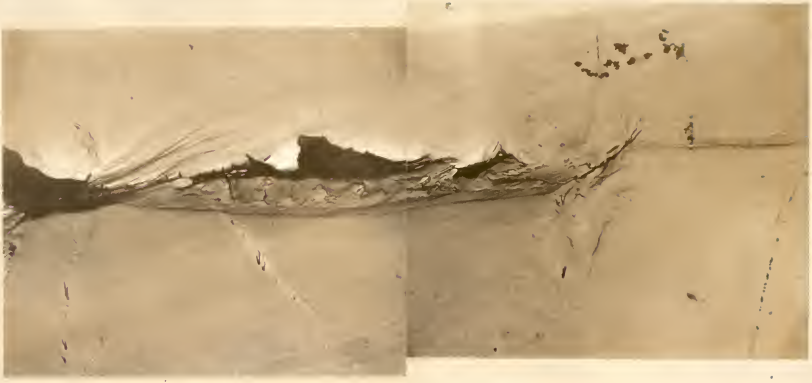

Figure 80: Electron micrograph illustrating grain boundary shear in magnesium. 5,500X

specimen, strained 2.5 per cent at 25°C. Cracks, revealed by the black projections, are observed at the edge of the sheared region, and extensive basal slip proceeds from here into the lower grain. These probably resulted from a discontinuity in strain between these two regions. This micrograph points out the striking difference between a region deformed solely by basal slip and one which has undergone grain boundary shear. Figure 81 is a second electron micrograph showing a highly deformed $\{10\bar{1}1\}$ - $\{10\bar{1}2\}$ twin in the same grain where the boundary shear was observed. The deformed structure of this second-order twin has much the same appearance as the shear observed at the grain boundary in Figure 80. This implies that identical mechanisms may have been operative in both cases. In comparing the deformation in Figures 80 and 81 with that observed in second-order twins in single crystals (Figures 31 through 37), it must be pointed out that in the former case the shear is viewed on a $\{10\bar{1}3\}$ plane, while in the latter it is seen on the $\{1\bar{2}10\}$ plane of shear.

The deformation mechanism discussed here is consistent with the intermediate temperature ductility minimum theory proposed by Rhines and Wray (85) and discussed on page 46. These authors recognized that in numerous metal systems

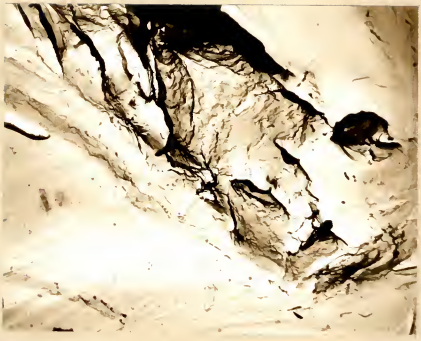

Figure 81: A highly deformed, $\{10\bar{1}1\}$ - $\{10\bar{1}2\}$ twin in the grain of a polycrystalline magnesium tensile specimen. 5,500X

fracture results from grain boundary shear in the temperature range corresponding to that of recovery. This may explain the fact that $\{10\bar{1}1\}$ - $\{10\bar{1}2\}$ twins are important in the deformation and fracture of magnesium at ambient temperatures alone, since this type of shear mechanism may only be significant in this range. However, the fact that the present deformation is observed only at room temperature may not be a consequence of the temperature dependence of grain boundary shear, but may be due to the nucleation characteristics of the particular twin types that are involved.

Deformation of the type observed in Figures 31 through 37 gives the appearance of "viscous" or "turbulent" flow. However, these terms imply that the material behaves as if it were amorphorous, and that once it yields it deforms continuously without work hardening. It is thought that such an implication should not be attached to the present deformation observed in magnesium. Chalmers (47) has postulated that the mechanism of grain boundary deformation may be best described as "non-crystallographic." He stated that this results from the large concentrated stress in these localized regions and the fact that this stress surpasses the critical resolved shear on a large number of planes. He also pointed out that the availability of such a large number of possible slip planes

would permit flow to occur in the direction of maximum resolved shear. Applied to the present case of second-order twinning, this shear direction is nearly parallel to both the boundary and the doubly twinned basal plane.

The term non-crystallographic deformation implies that the operating mechanism is in no way related to the structure of the crystalline lattice. For this reason it seems more proper to consider the flow mechanism as crystallographic, but under the assumption that the active slip planes and directions may have higher indices than normally would be expected to operate. In this manner it is implied that the deformation has a direct relationship to the crystal lattice structure, although the net flow direction which results may be the same as the direction of maximum shear.

The flow traces observed in second-order twins are also interesting in view of the theory of Bauwens, Homès, and Pankowski-Fern (99). These authors have considered the problem of uniaxial extension of a homogeneous, isotropic material under a continuously increasing tensile load. They calculated that flow should first occur along the surface of a cone whose axis corresponds to the tensile direction and whose semiapex angle is 55°. These authors noted that cup-cone fractures in certain steels

occur along a cone at about this same inclination. Also, in steels, where deformation proceeds by propagation of a Luder's band, the band front is often inclined 55° from the stress axis (100).

Although the structure of second-order twins in magnesium cannot be classified as homogeneous and isotropic, the observed flow direction is close to 55° from the stress axis. This result may be fortuitous; however, it is interesting to note the good agreement between the theory and experiment.

The Role of Shear Accommodation Kinks in the Deformation Process

The previous discussion has been concerned primarily with the mechanism of deformation within $\{10\bar{1}1\}$ - $\{10\bar{1}2\}$ twins. With regard to this, it was mentioned on page 153 that this deformation may introduce accommodating strains into the matrix along the length of the twin. An additional form of accommodating deformation which has been observed in the matrix will now be considered. This involves a complex kinking phenomenon of the type noted in Figures 40 through 48. Reed-Hill and Robertson (52) referred to these as shear accommodation kinks, since they were thought to accommodate non-uniform shear deformation within the twins. They based this on the observation that

these kinks were most pronounced where the internal shear of the twin was small and that the kinks disappeared where the shear was greatest. The kinks observed in the present experiments confirmed this; however, it is thought that their role may be of greater significance. In this respect it is thought that these kinks are important in accommodating strains in the matrix which may result from the deformation in the individual twin lamellae. Figure 35 is a micrograph of intensely strained region where two lamellae interconnect. It is noted from this that matrix flow has occurred on the upper side of this strained band. The basal plane trace in this region appears to be misoriented, indicating that some kinking may also have occurred. Figure 47 is a second example which indicates the necessity of matrix accommodation adjacent to second-order twins. In this case the shear from the individual lamellae is quite pronounced, as it leaves the twin and enters the matrix. This is indicated at points A and B. It is noted that a shear accommodation kink of significant misorientation has developed along the length of this twin, thus suggesting that there may be a relationship between the two. It is thought that additional factors which have thus far not been recognized may also be important in the

morphology of these kink structures. In this respect more experimental investigations are still desired.

Dislocation Models for Shear Accommodation Kinks

Basal dislocations - The kinks observed in Figures 40 through 48, where the bend plane is almost parallel to the second-order twin boundary, are difficult to describe in terms of basal slip alone. Figure 82 illustrates schematically the bending which results from aligning basal slip dislocations at a 60° inclination. Such an array has a long range stress field (101); and, therefore, its energy is greater than a vertical array of the same dislocations. Also, if these kinks result solely from basal slip, then the active slip plane has been rotated away from the stress axis. As discussed on page 121, this makes a negative contribution to the overall tensile strain. In addition, Figure 82 indicates that a skewed dislocation wall introduces a change in the interplanar spacing as the wall is traversed.

Description of the bend plane in terms of two different types of dislocations - It is possible to describe the kinks adjacent to second-order twins by assuming that the bend planes are composed of two sets of dislocations.

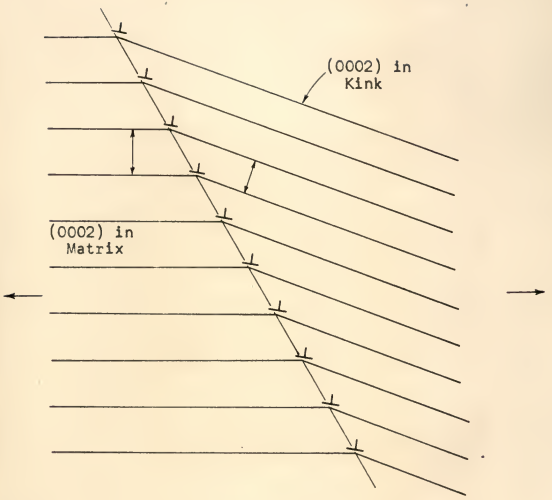

Figure 82: Schematic illustration of the basal dislocation alignment needed to account for the lattice bending of shear accommodation kinks

This is similar to the kink band boundary discussed in the preceding section, where $\frac{1}{3}\langle 11\bar{2}3\rangle$ dislocations on $(\bar{1}011)$ and $(10\bar{1}1)$ were used to describe a bend plane. Figure 83 illustrates that the proper combination of $\vec{a}_1$, $-\vec{a}_3$, and $\vec{c}$ dislocations may completely describe a bend plane inclined 60° from the basal plane. The density of each dislocation type needed to produce bending about this plane may be calculated in the same manner as on page 132 Assuming a kink misorientation of 10°, $\vec{a}_1$ and $-\vec{a}_3$ dislocations spaced 39Å. apart and $\vec{c}$ dislocations spaced 52Å. apart are required. A similar model may be constructed which involves dislocations with a $\frac{1}{3}\langle 11\bar{2}3\rangle$ Burgers vector on the $(10\bar{1}1)$ and $(\bar{1}011)$ planes.

Slip dislocations on $\{10\bar{1}2\}$ - A third model may be constructed which assumes the bend plane is composed of $[10\bar{1}1]$ dislocations on $(\bar{1}012)$. While dislocations of this type have never been observed, there is strong evidence for their presence in the bend planes of shear accommodation kinks. $[10\bar{1}1]$ dislocations may be formed by interaction of two basal dislocations with a $\vec{c}$ dislocation according to the reaction

$$\frac{1}{3}[2\bar{1}\bar{1}0] + \frac{1}{3}[11\bar{2}0] + [0001] \longrightarrow [10\bar{1}1] \qquad (12)$$

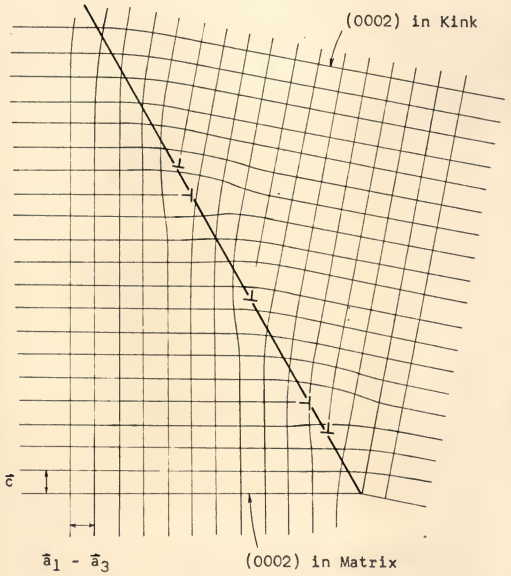

Figure 83: The configuration of $\vec{a}_1$, - $\vec{a}_3$, and $\vec{c}$ dislocations needed to describe the bend plane of a shear accommodation kink

This same product dislocation may result from a second type of reaction, which involves interaction of a pryamidal $\frac{1}{3}\langle 11\bar{2}3\rangle$ dislocations, as shown by the Reactions (13) and (14)

$$\frac{1}{3}[2\bar{1}\bar{1}3] + \frac{1}{3}[11\bar{2}0] \longrightarrow [10\bar{1}1] \qquad (13)$$

$$\frac{1}{3}[11\bar{2}3] + \frac{1}{3}[2\bar{1}\bar{1}0] \longrightarrow [10\bar{1}1] \qquad (14)$$

Based on the criteria that the dislocation energy is proportional to the square of its Burgers vector, it was found that both Reactions (13) and (14) involve an increase in energy. However, this does not mean that the reactions cannot occur, since the localized stress conditions in the lattice may also be significant. The reactant pyramidal dislocations must lie on $(\bar{1}011)$ if the product dislocation is to be glissile on $(\bar{1}012)$ Since the $(\bar{1}011)$ and (0001) planes share the $[1\bar{2}10]$ direction, it is along this line that the two dislocations interact. This direction is also common to $(\bar{1}012)$; so the product dislocation is theoretically glissile on this plane, since it contains both the dislocation line and the Burgers vector. If, however, the reactant $\frac{1}{3}\langle 11\bar{2}3\rangle$ dislocations lie on a $\{11\bar{2}2\}$ plane. the reaction

occurs along $(\bar{1}010)$, and the product dislocation is not glissile on $(\bar{1}012)$.

If shear accommodation kinks do result from slip on $(\bar{1}012)$ in the $(10\bar{1}1)$direction, there are several ways that this dislocation structure could occur. One of these assumes that $[10\bar{1}1]$ dislocation loops are nucleated on equally spaced $(\bar{1}012)$ planes in a manner similar to that proposed by Hess and Barrett (21) for basal kinks. This is illustrated schematically in Figure 84. A second mechanism for kink formation involves interaction of $\frac{1}{3}\langle 11\bar{2}3\rangle$ matrix glide dislocations with the basal bend planes observed adjacent to second-order twins (Figure 76). The presence of these bend planes was discussed in conjunction with this Figure. It was also noted (page 4) that the dislocation walls associated with a kink band should always occur in pairs. On this basis the bend planes in Figure 78 should correspond to approximately equal numbers of positive and negative dislocation arrays. Thus, the $[10\bar{1}1]$ dislocations could form from interaction of $\frac{1}{3}\langle 11\bar{2}3\rangle$ dislocations. This mechanism predicts that $[\bar{1}01\bar{1}]$ and $[10\bar{1}1]$ dislocations on $(\bar{1}012)$ should result. The positive $[10\bar{1}1]$ dislocations occur by Reactions (13) and (14), while the negative dislocations form from interactions between dislocations of opposite sign, as expressed by the reactions

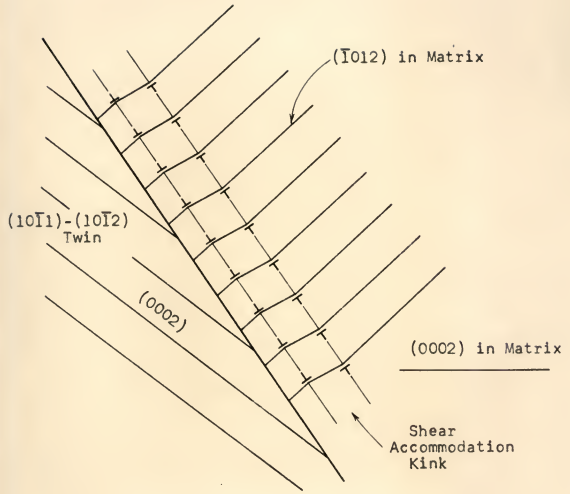

Figure 84: Schematic illustration of how [10$\bar{1}$1] dislocation loops on (1̄012) may account for the structure of shear accommodation kinks

$$\frac{1}{3}[\bar{2}11\bar{3}] + \frac{1}{3}[\bar{1}\bar{1}20] \longrightarrow [\bar{1}01\bar{1}] \qquad (15)$$

$$\frac{1}{3}[\bar{1}\bar{1}23] + \frac{1}{3}[\bar{2}110] \longrightarrow [\bar{1}01\bar{1}] \qquad (16)$$

Under the applied stress the positive dislocations align into the bend planes observed in the micrographs (Figures 40 through 48), while the negative move into the second-order twin boundary. It is noted that while the basal plane is rotated away from the stress axis, the $(\bar{1}012)$ plane, on which the kink was assumed to form, has been rotated toward this axis. Thus, this mechanism is consistent with the applied tensile load.

Rosenbaum (12) has postulated a similar dislocation reaction involving $\langle 10\bar{1}1\rangle$ dislocations in order to explain the pile-up of pyramidal dislocations at basal twin accommodation kinks in zinc. However, because the pyramidal $\frac{1}{3}\langle 11\bar{2}3\rangle$ dislocations he observed were on $\{11\bar{2}2\}$ planes, the resultant dislocations could not have been glissile on $\{10\bar{1}2\}$.

There is considerable evidence in support of this non-basal kinking mechanism. Read (28) has pointed out that a tilt boundary composed of a single set of dislocations has only one degree of freedom. He demonstrated

that for this case the boundary orientation and the relative tilt misorientation between the two lattices are interrelated, so that only one of these is an independent variable. A test of the theory that the present kinks result from glide of a single dislocation type on $(\bar{1}012)$ was made based on this fact. From observing the position of the basal trace in the kink and matrix, the orientation of the $(\bar{1}012)$ plane in each may be determined. The orientation of the bend plane can then be predicted on the assumption that $(\bar{1}012)[10\bar{1}1]$ dislocations are involved. Table 1 indicates that in every case the predicted and observed positions of the bend plane are in good agreement with each other. The micrographs which were used for these measurements and which, thus far, have not been introduced are shown in Figures 85 through 89. It is also noted that some of the measurements were made on micrographs from previous research. All measurements were made in regions where the internal deformation of the kinks was a minimum, so that the kink misorientation could be measured accurately. In only one example, which is shown in Figure 89, was the bend plane inclined at a smaller angle to the matrix basal plane than the second-order twin boundary. However, the misorientation of this kink was only 13°, which was less than for any of the other kinks observed, and for

TABLE 1

A Comparison of the Predicted and Observed Shear Accommodation Kink Bend Plane Inclinations Based on $\{10\bar{1}2\}\langle 10\bar{1}1\rangle$ Slip

Kink Misorientation	Observed Inclination of Bend Plane	Predicted Inclination of Bend Plane	Figure Number
23°	60°	58.5°	41
25°	58°	59.5°	42
31°	63°	62.5°	85*
13°	53°	53.5°	86*
30°	64°	63°	87*
24°	57°	59°	88
25°	60°	59.5°	89*

*Indicates micrographs from research by Dr. R.E. Reed-Hill

Figure 85: Structure of a $\{10\bar{1}1\}$ - $\{10\bar{1}2\}$ twin and its shear accommodation kink (after R.E. Reed-Hill (94). 230X

Figure 86: Second-order twin and its shear accommodation kink (after R.E. Reed-Hill (94)). 230X

Figure 87: $\{10\bar{1}1\}$ - $\{10\bar{1}2\}$ twin and a highly deformed shear accommodation kink (after R.E. Reed-Hill (94)). 230X

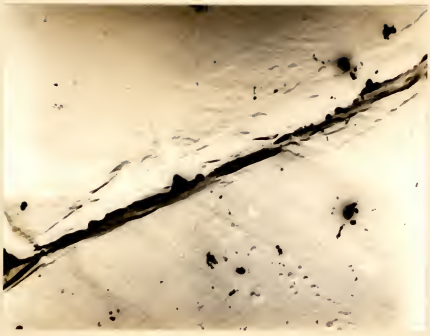

Figure 88: Electron micrograph of a $\{10\bar{1}1\}$ - $\{10\bar{1}2\}$ twin and a shear accommodation kink. 7,000X

Figure 89: Second-order twin and its shear accommodation kink (after R.E. Reed-Hill (52)). 450X

this reason the bend plane orientation is still consistent with the theory of slip on $(\bar{1}012)$.

Internal Deformation of Shear Accommodation Kinks

The phenomenon of $\{10\bar{1}1\}$ - $\{10\bar{1}2\}$ twin band deformation is further complicated by the fact that shear accommodation kinks are often internally deformed. This gives an additional means by which the matrix may deform and accommodate the strains of the twins. Analysis of the deformation traces observed within shear accommodation kinks is difficult because of the complex geometry involved. In most cases these traces were nearly parallel to the second-order, $\{10\bar{1}1\}$ - $\{10\bar{1}2\}$ twin, irrespective of whether the kink misorientation was large or small. Measurements of the angular relationship of these deformation traces relative to the kinked basal plane are listed in Table II. The greatest scatter was observed in regions where the kink deformation was pronounced, as exemplified by readings number 5 and 7 in this table. The low angle measurement in the latter case was characteristic of the highly strained region, while the 55° measurement was made in an area of relatively small strain.

These factors indicate that the internal deformation of these kinks may occur as the kink misorientation is being established. This follows since the inclination

TABLE 2

The Relative Inclination of Deformation Traces within Shear Accommodation Kinks

Number	Inclination of Deformation Trace to Kink Basal Plane	Micrograph from which Measurement was made
1	42°	Figure 42
2	44°	44
3	41°	45
4	44°	48
5	34°	50
6	49°	85
7	55° 32°	87
8	43°	89

of a twin boundary or slip trace, relative to an active glide plane, may be altered as a result of slip on this plane. However, the orientation of the trace with respect to a fixed reference system should, in general, change only slightly. This could explain the angular discrepancy observed for the present deformation traces; since if they formed after the kink misorientatin was established, they should occur at their characteristic crystallographic inclination inside the kink. However, if the kink misorientation continued to increase after the traces formed, then their inclination relative to the kinked basal plane may be decreased. On this basis the true crystallographic orientation of this deformation should be the largest angular inclination recorded in Table 2, which is about 55°. It is also significant that traces of this same inclination were observed on etched as well as deformed surfaces. This indicates that the deformation traces are probably associated with twinning rather than slip. From the inclination of these twins, which was discussed above, it appears that they are of the second-order, $\{10\bar{1}1\}$ - $\{10\bar{1}2\}$ type. Kink deformation by the mechanism of double twinning is also supported by the intense strain which was often observed at these

regions (Figures 50, 54 and 87). This is in good agreement with the conclusions of Reed-Hill and Robertson (52), which were discussed on page 50.

It is possible that additional deformation mechanisms may also be operating in shear accommodation kinks. This is indicated by the traces observed in the small kink in Figure 48, which appear much more like fine slip lines than twins. Also, they are inclined at about 45° to the kinked basal plane, which is probably close to their true crystallographic inclination, since the kink is in the initial stages of its formation.

These traces may be interpreted in terms of $\frac{1}{3}\langle 11\bar{2}3\rangle\{10\bar{1}1\}$ slip on the $\{10\bar{1}1\}$ planes which are inclined obliquely to the $(1\bar{2}10)$ surface of observation. Because $(1\bar{1}01)$ and $(0\bar{1}1\bar{1})$ are both symmetrically oriented to the stress axis, this slip should occur in equal amounts on each of these two planes. From the geometry in Figure 1, this indicates that dislocations with four different Burgers vectors are involved. These planes and their respective slip directions are illustrated in Figure 90, relative to the surface of observation. It is indicated that $(1\bar{1}01)$ and $(0\bar{1}1\bar{1})$ intersect the plane of observation 43° from the basal plane, which is close to the inclination of the traces measured under readings 1 - 4 and 8 in

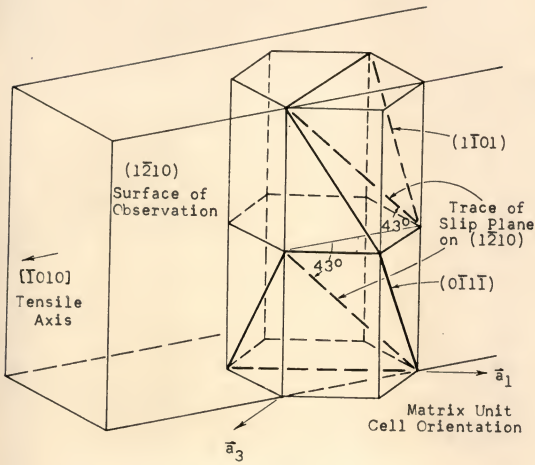

Figure 90: The relative orientation of two unit cells in a magnesium single crystal tensile specimen with the tensile axis along [10$\bar{1}$0]. The positions of the (1$\bar{1}$01) and (0$\bar{1}$1$\bar{1}$) planes are illustrated

Table 2. Further evidence in support of this slip system is given in Figure 91. Here a second-order twin and its shear accommodation kink are viewed on the basal plane face of the specimen. Slip traces are observed in a portion of the kink, and these are consistent with $\frac{1}{3}\langle 11\bar{2}3\rangle \{10\bar{1}1\}$ slip on one of the pyramidal planes discussed above (Figure 90).

Additional deformation traces were also observed which could not be explained. An example of these is shown at point A in Figure 92. Surface markings such as this cannot be interpreted in terms of either the twinning or slip mechanism proposed above. In addition, Reed-Hill (72) observed etch pit traces within these kinks which also are difficult to classify. These are illustrated at point A in Figure 93. These factors indicate that more extensive investigations are desirable if the internal deformation of these kinks is to be completely understood.

Summary: The foregoing discussion demonstrates that the overall process by which $\{10\bar{1}1\}$ - $\{10\bar{1}2\}$ twin bands deform is quite complex. It was found that the deformation could be treated as three distinct but interrelated operations. The first of these is concerned with the shear strain within the individual twin lamellae, which occurs parallel to the twin boundary, while the second involves

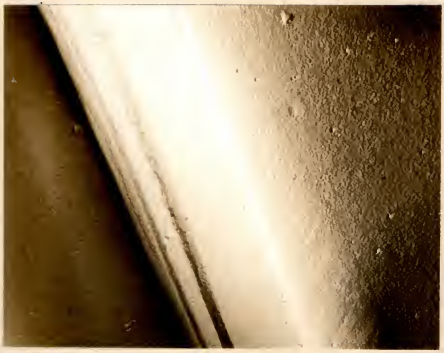

Figure 91: The surface offset on the basal plane face of a single crystal which results from $\{10\bar{1}1\}$ - $\{10\bar{1}2\}$ twinning and shear accommodation kinking. The twin and kink are parallel to the $\langle\bar{1}2\bar{1}0\rangle$ direction. Traces are observed within the kink about 60° from this. 7,400X

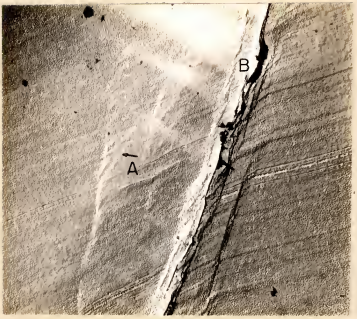

Figure 92: Electron micrograph illustrating a type of deformation trace within shear accommodation kinks which could not be analyzed. 3,000X

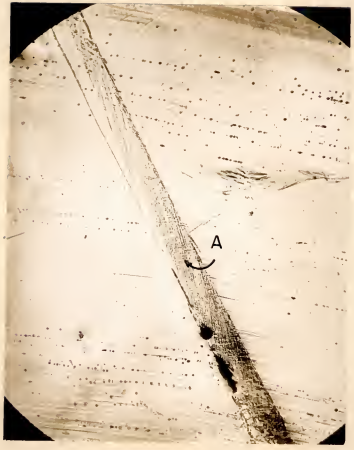

Figure 93: Second-order, $\{10\bar{1}1\}$ - $\{10\bar{1}2\}$ twin and its shear accommodation kink as viewed on a $(1\bar{2}10)$ magnesium face which was etched with 20 per cent HCl subsequent to deformation (courtesy of R.E. Reed-Hill). 75X

a shear in the matrix lattice immediately adjacent to these lamellae. This deformation is thought to be significant in directing the large concentrated strains which are observed along the band length. The third phase of the deformation is concerned with shear accommodation kinking in the adjacent matrix and the subsequent deformation in these kinks. These last two factors permit the matrix to deform and accommodate the deformation in the twin, and for this reason they may be significant in prolonging the time when fracture occurs.

DISCUSSION, PART III: FRACTURE

The micrograph in Figure 55 illustrates that the crystals extended in the present experiments fractured along second-order, $\{10\bar{1}1\}$ - $\{10\bar{1}2\}$ twins. The mechanism by which this fracture occurred is thought to proceed in three basic steps. The first of these involves formation of small voids of the type observed in Figures 31 and 54. The second step occurs as the strain increases and these voids grow and interconnect to form microcracks, as observed in Figures 34 through 37, where the doubly twinned region is heavily deformed. Third, the ultimate fracture results in a "postage-stamp" manner as a direct consequence of the development of these cracks into a linear network across the entire specimen cross section.

It is thought that there are two general mechanisms which could account for nucleation of the voids and cracks observed at $\{10\bar{1}1\}$ - $\{10\bar{1}2\}$ twins. The first involves pile-up of dislocations at the second-order boundary, thus giving rise to cracks as proposed by Zener (65) and described on page 33. The second assumes void formation as a result of the relative shear displacement of the lattice on either side of the twin boundary. This involves a mechanism similar to that proposed by Gifkins (66), Chen

and Machlin (67,68), or McLean (69). It is possible that both processes are operative in the present case, but the fact that cracks have been observed along narrow shear flow lines gives direct evidence in support of the second (Figures 38 and 39). In the latter example there is a good indication that the crack at point D results from shear, since the discontinuity in the basal plane trace AB indicates that the two crystal halves have been displaced about two microns past one another. In applying a mechanism similar to that of Gifkins, Chen, et al., or McLean to the present shear cracks, it is not necessary to postulate steps on the atomic scale. Instead, as evidenced at point B in Figure 92 larger discontinuities may be involved. This shows that the cracks are not necessarily parallel-sided but may have bends or steps along their length. However, there is no way of knowing if these were instrumental in the crack formation or whether they are a consequence of subsequent deformation after the crack formed. Also, it must be noted that although the micrographs in Figures 38 and 39 were taken at magnifications of 16,500X and 17,000X, the observed shear traces may still correspond to a finite width on the atomic scale. In this case the mechanism of Zener (65) which involves piled-up dislocations, could also be significant.

From Figures 57 and 58 it was noted that different areas of the fracture surface may differ greatly in appearance. One possible interpretation of this is that different mechanisms are responsible for fracture at different parts of the double twin. Also, while the fracture probably follows the macroscopic twin habit in most regions, as discussed on page 100 , it is possible that in others it propagates through the matrix adjacent to the twins. That the latter may actually occur is evidenced by the cracks observed within shear accommodation kinks at point A, Figure 50.

Figure 57 illustrates that some areas of the fracture surface are characterized by straight bands parallel to the basal plane trace on this surface. This micrograph is generally consistent with the optical micrograph of this same surface (Figure 56), since both exhibit this directional structure. These dark bands are thought to correspond to regions of the twin which tore apart under the influence of the tensile stress once the crack structure was sufficiently developed. On this basis the region between the bands corresponds to what was once the face of a crack. The fact that these bands are long and straight indicates that the cracks may have had their edges parallel to the basal plane trace, as shown schematically in Figure 94.

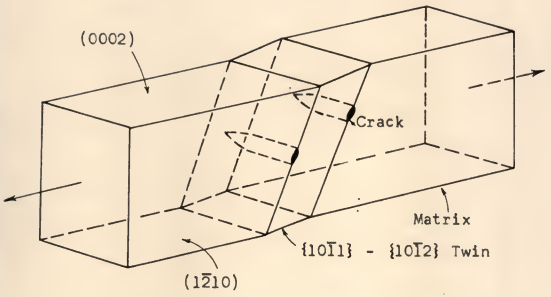

Figure 94: Schematic illustration of the geometry of the cracks observed at {10$\bar{1}$1} - {10$\bar{1}$2} twin boundaries

This is consistent with the fact that the twin structure is essentially two dimensional; so once a crack is nucleated at the twin boundary it may propagate very rapidly along the interface in the direction parallel to the basal plane trace on the fracture plane. As noted on page 100 the shape of the black protrusions on the replicas from the $\{1\bar{2}10\}$ prism face do not necessarily give a true indication of the crack geometry. However, several examples were observed where the edges of these protrusions appeared to be normal to the surface of observation (and thus parallel to the basal plane trace on the fracture plane). The best example of this is seen in Figure 95. This substantiates the proposed geometry of these cracks in Figure 94.

From Figure 58 it was observed that some areas of the fracture surface are characterized by a type of "dimple" structure. Beachem (71) has pointed out that the relative shape of dimples on a shear rupture surface is dependent upon the ratio of normal strain to shear strain as the voids open, grow, and coalesce. Thus, a high ratio of these strains gives rounded dimples (approaching the shape of the normal rupture dimples shown in Figure 17), while a low ratio should produce dimples elongated in the shear direction, as shown in Figure 18. It is apparent that neither of these rupture modes adequately describe the

Figure 95: Electron micrograph illustrating how cracks may occur normal to the $(1\bar{2}10)$ surface of observation. 4,000X

present fracture, since the dimples observed in Figure 58 are elongated in the direction of the basal plane trace (normal to the resolved shear direction). This is also consistent with the assumption that once these cracks are nucleated, they grow rapidly in a direction parallel to $[1\bar{2}10]$. However, it is thought that more extensive investigations are needed to fully understand the nature of these dimples. Also, more work is desired in order to relate the structure on both types of fracture surfaces (Figures 57 and 58) to the geometry of $\{10\bar{1}1\}$ - $\{10\bar{1}2\}$ twins.

CONCLUSIONS

Additional confirmation has been obtained that the bands of intense deformation observed by Reed-Hill and Robertson (72) and by Reed-Hill (53) are $\{10\bar{1}1\}$ - $\{10\bar{1}2\}$, second-order twins. These twins are nucleated in magnesium by straining a single crystal, oriented with the basal plane parallel to the stress axis, in tension at room temperature. Under the influence of the applied load, the twins may deform extensively subsequent to their formation and thus lead to fracture. In this manner they control the room temperature deformation and fracture of single crystals of this orientation.

As a result of the present research, the following conclusions have been reached:

1) The habit shift from the primary twin orientation at $61^{\circ}54'$ to the second-order twin orientation at approximately 56° cannot be explained by the double twinning theory of Crocker (83).
2) The $\{10\bar{1}1\}$ - $\{10\bar{1}2\}$ twin habit shift can be explained if it is assumed that duplex slip occurs in the matrix lattice adjacent to the twin. On this basis a model has been constructed involving

slip on $(\bar{1}011)$ and $(10\bar{1}1)$ planes in $\langle 11\bar{2}3\rangle$ directions, and this satisfactorily accounts for the shift.

3) The internal deformation of second-order twins occurs by three distinct but interrelated processes.

a) The first of these involves deformation which occurs within individual twin lamellae. Experimental observations reveal that the twinned basal plane is nearly parallel to the second-order twin boundary, indicating that the close-packed plane has been re-oriented from its predicted inclination 18.5° from the boundary. A kinking mechanism, which also involves slip on $(\bar{1}011)$ and $(10\bar{1}1)$ planes in $\langle 11\bar{2}3\rangle$ directions has been postulated to account for this. Once the twinned basal plane becomes aligned parallel to the twin boundary, extensive deformation of the individual lamellae may occur by simple slip on this plane.

b) The second process involves deformation which occurs along the entire macroscopic twin band. The shear markings in the matrix

which are parallel to the twin lamellae and which interconnect them are difficult to explain in terms of slip on previously observed systems. This deformation is thought to be similar to that which occurs during grain boundary shearing. The directionality of these traces results from the concentrated shear stress parallel to the twin boundaries.

c) The last phase of twin deformation concerns the mechanisms by which the matrix lattice adjacent to $\{10\bar{1}1\}$ - $\{10\bar{1}2\}$ twins can deform. Generally, this deformation may be considered to occur in two parts. The first of these involves shear accommodation kinking. These kinks are best described by a single set of $[10\bar{1}1]$ dislocations on $(\bar{1}012)$ planes. The second involves the internal deformation of these kinks subsequent to their formation. It is thought that this occurs by secondary $\{10\bar{1}1\}$ - $\{10\bar{1}2\}$ twinning and by $\{10\bar{1}1\}\langle 11\bar{2}3\rangle$ slip on the two planes of this type obliquely inclined to the stress axis.

4. The fracture which occurs at $\{10\bar{1}1\}$ - $\{10\bar{1}2\}$ twins is thought to initiate by formation of

small voids at the twin boundary. A boundary shearing mechanism similar to that proposed by Chen and Machlin (67) may be responsible. As deformation continues, these voids grow into microcracks, and fracture ultimately results from tearing apart of the interconnecting regions.

APPENDICES

APPENDIX A

INTERNAL DEFORMATION OF $\{10\bar{1}1\}$ - $\{10\bar{1}2\}$ TWINS BY SLIP ON THE BASAL PLANE, 18.5° FROM THE TWIN BOUNDARY

The following arguments are given to substantiate those on page 140 that the large internal strains of second-order twins cannot occur by slip on the basal plane. Based on the assumption that a twin is sheared 500 per cent and that the strain is distributed uniformly through the twinned lattice, it may be calculated that this corresponds to approximately five dislocations at the end of every slip plane. These dislocations may interact with the twin boundary in one of two ways. First, they may enter the boundary, in which case this boundary may be treated as an asymetrical kink bend plane (28). This type of approach is discussed in greater detail on page 145 Application of Equation (1)* indicates that the kink misorientation which would produce 500 per cent strain is much greater than 180°, which is unrealistically large. This is especially true in view of the fact that this rotation is toward the stress axis, while experimental

---

*This equation, in the strictest sense, should only be used where the kink misorientation is small. However, the present application is made only to demonstrate the general magnitude of the rotation.

observations indicate a rotation in the opposite sense that is never greater than 18.5°. Second, if the dislocations become piled up at the boundary, a rotation in the same sense as that discussed above for kinking should result. It can only be concluded that the large strains often observed within these twins cannot be explained by basal slip.

Extensive deformation of second-order twins could result from the mechanism of basal slip, however, if some added phenomenon occurred to relieve the stresses of dislocation pile-ups at the twin boundary. One mechanism which permits this involves passage of basal edge dislocations out of the twin into the matrix in the manner proposed for {112} twinning in body-centered cubic lattices by Sleezwyk and Verbraak (57) and for $\{11\bar{2}1\}$ twinning in zirconium by Reed-Hill (58). By a related mechanism the basal dislocations piled-up at the second-order, $\{10\bar{1}1\}$ - $\{10\bar{1}2\}$ twin boundary could conceivably pass into the matrix, thus permitting the large internal strains of these twins to occur. However, because of the complex geometry between the $\{10\bar{1}1\}$ – $\{10\bar{1}2\}$ doubly twinned and matrix structures, no simple relationship exists between the Burgers vectors of slip dislocations in the twin and matrix. Also, a mechanism such as this

should involve a measurable increase in the twin thickness due to the large number of twinning dislocations created at the boundary as the slip dislocations pass through it. An estimate was made of the increase in twin thickness which should result from a shear strain of 500 per cent within the twin. It was concluded that the width of a twin 10 microns long should increase by approximately 10 microns as a result of this slip. This is not verified experimentally, since twin thicknesses at regions of intense strain are not significantly greater than near the undeformed tips (page 140). In addition, this mechanism predicts that an equal amount of basal slip should occur in both the matrix and twin, since basal dislocations from the twin enter the parent lattice. This also is not observed experimentally.

Theoretically, it is also possible for basal dislocations in the screw orientation with an $\frac{a}{3}$ $[1\bar{2}10]$ Burgers vector to cross glide between the matrix and second-order twin orientations, in the same manner observed by Price (102) for $\{10\bar{1}2\}$ twins in zinc. This is possible since this Burgers vector lies in the plane of the $\{10\bar{1}1\}$ - $\{10\bar{1}2\}$ twin boundary. However it is noted that the Burgers vector for these dislocations is normal to the observed shear direction of these twins, and for this reason their movement should not contribute to the observed shear strain.

APPENDIX B

THE LAMELLAE STRUCTURE OF SECOND-ORDER, $\{10\bar{1}1\}$ - $\{10\bar{1}2\}$ TWINS

From Figures 25 and 26 it was noted that $\{10\bar{1}1\}$ - $\{10\bar{1}2\}$ twins occur as individual lamellae which are not exactly aligned with the macroscopic twin habit (page 58) This structure may be explained in terms of the two twinning shears which are invoved. Figure 96 illustrates that when a single twin forms the twinning shear is propagated into the matrix lattice in exact alignment with the pre-existing twin band. On this basis the next lamella would normally be expected to form along this same line. However, for the case of second-order, $\{10\bar{1}1\}$ - $\{10\bar{1}2\}$ twinning the net twinning shear vector is inclined about 71° from the matrix basal plane, as shown in Figure 96, part b. This is approximately 15° from the observed habit plane for these twins. Thus, the lattice strains induced into the matrix by a double twin lamella should be greatest in a direction about 71° above and to the right of the pre-existing twin. This region of the matrix should then be the preferred site for nucleation of the next twin lamella, as illustrated in Figure 96, part c.

a.

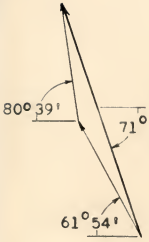

b.

c.

Figure 96: Schematic illustration of how a single and double twinning shear may give rise to different lamellae structures. a) the lamellae structure predicted from a simple shear, b) the geometry of the second-order $\{10\bar{1}1\}$ - $\{10\bar{1}2\}$ twinning shears, and c) the lamellae structure predicted from two shears of the $\{10\bar{1}1\}$ - $\{10\bar{1}2\}$ type

BIBLIOGRAPHY

1. M.W. Toaz and E.J. Ripling, "Correlation of the Tensile Properties of Pure Magnesium and Four Commercial Alloys with Their Mode of Fracturing," Trans. AIME, 206 (1956) 936; Journal of Metals, August, 1956.

2. R.E. Reed-Hill and W.D. Robertson, "Deformation of Magnesium Single Crystals by Nonbasal Slip," Trans. AIME, 209 (1957) 496; Journal of Metals, April, 1957.

3. P.B. Hirsch and J.S. Lally, "The Deformation of Magnesium Single Crystals," Phil. Mag., 12 (1965) 595.

4. E. Schmid and G. Wasserman, Handbuch der Physikalische, und technische Mechanik, 4 (Part 2) (1931) 319.

5. P.W. Bakarian and C.H. Mathewson, "Slip and Twinning in Magnesium Single Crystals of Elevated Temperature," Trans. AIME, 152 (1943). 226; Metals Technology, April, 1943.

6. E.C. Burke and W.R. Hibbard, "Plastic Deformation of Magnesium Single Crystals," Trans. AIME, 194 (1952) 295; Journal of Metals, March, 1952.

7. R.E. Reed-Hill and W.D. Robertson, "Pyramidal Slip in Magnesium," Trans. AIME. 212 (1958) 256.

8. F.E. Hauser, P.R. Landon, and J.E. Dorn, "Deformation and Fracture Mechanisms of Polycrystalline Magnesium at Low Temperatures," Trans. ASM, 48 (1956) 986.

9. H. Yoshinaga and R. Horiuchi, "On the Nonbasal slip in Magnesium Crystals," Trans. Jap. Inst. Metals, 5 (1964) 13.

BIBLIOGRAPHY (Continued)

10. J.J. Gilman, "Study of a New Mode of Plastic Deformation in Zinc Crystals," Trans. AIME, 203 (1955) 206; Journal of Metals, January, 1955.

11. J.J. Gilman, "Etch Pits and Dislocations in Zinc Monocrystals," Trans. AIME, 206 (1956) 998; Journal of Metals, August, 1955.

12. H.S. Rosenbaum, "Non-Basal Slip and Twin Accommodation in Zinc Crystals," Acta Met., 9 (1961) 742.

13. R.L. Bell and R.W. Cahn, "The Dynamics of Twinning and the Interrelation of Slip and Twinning in Zinc Crystals," Proc. Roy. Soc. (London), A239 (1957) 494.

14. P.B. Price, "Pyramidal Glide and the Formation and Climb of Dislocation Loops in Nearly Perfect Zinc Crystals," Phil. Mag., 5 (1960) 873.

15. P.B. Price, "On Dislocation Loops Formed in Zinc Crystals During Low Temperature Pyramidal Glide," Phil. Mag., 6 (1961) 449.

16. P.B. Price, "Nonbasal Glide in Dislocation-Free Cadmium Crystals. II. The $11\bar{2}2$ $11\bar{2}3$ System," Journ. App. Phys., 32 (1961) 1750.

17. D.H. Baldwin and R.E. Reed-Hill, "Some Obervations of the Deformation Modes of Polycrystalline Hafnium and Zirconium," Trans. AIME, 233 (1964) 248.

18. R.E. Reed-Hill and D.H. Baldwin, "Slip and Twinning in Zirconium," Ninth Quarterly Report, November 1963, AEC Contract AT938-1)-252, "An Evaluation of the Role of Deformation Twinning in the Plastic Deformation of Zirconium."

19. E. Orowan, "A Type of Plastic Deformation New in Metals," Nature, 149 (1942) 643.

20. O. Mugge, "On Slip and Related Phenomena in Crystals," Neues. Jahr. f. Miner., 7 (1898) 71.

BIBLIOGRAPHY (Continued)

21. J.B. Hess and C.S. Barrett, "Structure and Nature of Kink Bands in Zinc," Trans. AIME, 185 (1949) 599; Journal of Metals, September, 1949.

22. J.J. Gilman, "Mechanism of Ortho Kink-Band Formation in Compressed Zinc Monocrystals," Trans. AIME, 200 (1954) 621.

23. J.J. Gilman and T.A. Read, "Bend Plane Phenomena in the Deformation of Zinc Monocrystals," Trans. AIME, 197 (1953) 49; Journal of Metals, January, 1953.

24. N.K. Chen and C.H. Mathewson, "Structural Studies of Plastic Deformation in Aluminum Single Crystals," Trans. AIME, 191 (1951) 653; Journal of Metals, August, 1951.

25. D.C. Jillson, "An Experimental Survey of Deformation and Annealing Processes in Zinc," Trans AIME, 188 (1950) 1009; Journal of Metals, August, 1950.

26. R.W. Honeycombe, "Inhomogeneities in the Plastic Deformation of Metal Crystals, I and II," Journal Inst. of Metals, 80 (1951) 45,49.

27. R.W. Cahn, "Slip and Polygonization in Aluminum," Journal Inst. of Metals, 18 (1951) 129.

28. W.T. Read, Dislocations in Crystals, McGraw-Hill, (1953) 173.

29. J.M. Burgers, "Some Considerations on the Fields of Stress Connected with Dislocations in a Regular Crystal Lattice I," Kon. Neder. Akad. v. Weten., Proc., 42 (1939) 293.

30. F.R.N. Nabarro, "Mathematical Theory of Stationary Dislocations," Advances in Physics, 1 (1952) 269.

31. S. Amelinckx and W. Dekeyser, "The Structure and Properties of Grain Boundaries," Solid State Physics, 8 (1960) 296.

32. J.C.M. Li, "The Interaction of Parallel Edge Dislocations with a Simple Tilt Dislocation Wall," Acta Met., 8 (1960) 296.

BIBLIOGRAPHY (Continued)

33. J.C.M. Li, "Some Elastic Properties of an Edge Dislocation Wall," Acta Met., 8 (1960) 563.

34. M. Polanyi and E. Schmid, "Uber die Struktuz bearbeiteter Metalle," Ztsch. f. tech. phys., 5 (1924) 580.

35. R.F. Miller, "Influcence of a Grain Boundary on the Deformation of a Single Crystal of Zinc," Trans. AIME, 111 (1934) 135.

36. B. Chalmers, "The Influcence of the Difference of Orientation of Two Crystals on the Mechanical Effect of Their Boundary," Proc. Roy. Soc. (London), A162 (1937) 120.

37. H.C.H. Carpenter and C.F. Elam, "The Production of Single Crystals of Aluminum and Their Tensile Properties," Proc. Roy. Soc., A100 (1921) 329.

38. K. Yamaguchi, Sci. Papers Inst. Phys. Chem. Research (Tokyo), 6 (1927) 271.

39. W.R. Hibbard, "Plastic Deformation of Large-Grained Copper Specimens," Trans. AIME, 180 (1949) 52.

40. J.M. Galligan, S. Fenerstein, and W. Luhman, "Shear in Zinc Bicrystals," Acta. Met. 8 (1960) 135.

41. F.E. Hauser, C.D. Starr, L. Tietz, and J.E. Dorn, "Deformation Mechanisms in Polycrystalline Aggregates of Magnesium," Trans. ASM, 47 (1955) 102.

42. R.C. Gifkins and T.G. Langdon, "On the Question of Low-Temperature Sliding at Grain Boundaries," Journal Inst. of Metals, 32 (1965) 347.

43. N.F. Mott, "Slip at Grain Boundaries and Grain Growth in Metals," Proc. Phys. Soc., 60 (1948) 391.

44. T.S. Kè, "A Grain Boundary Model and the Mechanism of Viscous Intercrystalline Slip," Jour. App. Phys., 20 (1949) 274.

45. H. Conrad, Mech. Behavior of Materials at Elevated Temperatures, (ed., J.E. Dorn), McGraw-Hill (1961) 218.

BIBLIOGRAPHY (Continued)

46. F.N. Rhines, W.E. Bond, and M.A. Kissel, "Grain Boundary Creep in Aluminum Bicrystals," Trans. ASM, 48 (1956) 919.

47. B. Chalmers, "Mechanical Effect of Interfaces," ASM Seminar, (1952) 299.

48. B. Chalmers, Pittsburgh Symposium on Plastic Deformation, (1950), 193.

49. C.S. Barrett, "The Crystallographic Mechanisms of Translation, Twinning, and Banding," ASM Seminar (1949) 78.

50. H. Kiho, "The Crystallographic Aspects of the Mechanical Twinning in Metals," J. Phys. Soc. Japan, 9 (1954) 739.

51. M.A. Jaswon and D.B. Dove, "Twinning Properties of Lattice Planes," Acta Cryst. 9 (1956) 621.

52. R.E. Reed-Hill and W.D. Robertson, "Additional Modes of Deformation Twinning in Magnesium," Acta Met., 5 (1957) 717.

53. R.E. Reed-Hill, "A Study of the $\{10\bar{1}1\}$ and $\{10\bar{1}3\}$ Twinning Modes in Magnesium," Trans. AIME, 218 (1960) 554.

54. R. Siems and P. Hassen, "Die Geschwindizkeit der Zwillingsbildung in Zink-Einkristallen," Zeits fur Metal., 49 (1958) 213.

55. A.W. Sleezwyk," Emissary Dislocations: Theory and Experiments on the Propagation of Deformation Twins in α-Iron," Acta Met., 10 (1962) 705.

56. D. Hull, Deformation Twinning , (ed. R.E. Reed-Hill, J.P. Hirth, and A.C. Rogers), Gordon and Breach, (1963) 151.

57. A.W. Sleezwyk and C.A. Verbraak, "Incorporation of Slip Dislocations in Mechanical Twins - I" Acta Met., 9 (1961) 917.

BIBLIOGRAPHY (Continued)

58. R.E. Reed-Hill and W.A. Slippy, "Double Accommodation Kinking in Zirconium," Ninth Quarterly Report, November 1963, AEC Contract AT(38-1)-252, "An Evaluation of the Role of Deformation Twinning on the Plastic Deformation of Zirconium," 8.

59. R.W. Armstrong, Deformation Twinning (ed. R.E. Reed-Hill, J.P. Hirth, and H.C. Rogers), Gordon and Breach, (1963) 356.

60. P.L. Pratt and S.F. Pugh, "Twin Accommodation in Zinc," Journal Inst. Metals, 80(1952) 653.

61. A.J.W. Moore, "Accommodation Kinking Associated with the Twinning of Zinc," Proc. Phys. Soc., B65 (1952) 956.

62. A.J.W. Moore, "Twinning and Accommodation Kinking in Zinc," Acta Met., 3 (1955) 163.

63. R.E. Reed-Hill, Physical Metallurgy Principles, van Nostrand, (1964) 417.

64. M.L. Picklesimer, Oak Ridge National Laboratory, Oak Ridge, Tenn., private communication.

65. C. Zener, "The Micromechanism of Fracture," ASM Seminar (1947) 3.

66. R.C. Gifkins, "A Mechanism for the Formation of Intergranular Cracks When Grain Boundary Sliding Occurs," Acta Met., 4 (1956) 98.

67. C.W. Chen and E.S. Machlin, "On the Mechanism of Intergranular Cracking," Acta Met., 4 (1956) 655.

68. C.W. Chen and E.S. Machlin, "On a Mechanism of High Temperature Intercrystalline Cracking," Trans. AIME, 209 (1957) 829.

69. D. McLean, Grain Boundaries in Metals, Oxford, London (1957).

BIBLIOGRAPHY (Continued)

70. D.G. Brandon, B. Ralph, S. Ranganathan, and M.S. Wald, "A Field Ion Microscope Study of Atomic Configuration at Grain Boundaries," Acta Met., 12 (1964) 813.

71. C.D. Beachem, "An Electron Fractographic Study of the Influence of Plastic Strain Conditions upon Ductile Rupture Processes in Metals," Trans. ASM, 56 (1963) 318.

72. R.E. Reed-Hill and W.D. Robertson, "The Crystallographic Characteristics of Fracture in Magnesium Single Crystals," Acta Met., 5 (1957) 728.

73. S.K. Couling and C.S. Roberts, "New Twinning Systems in Magnesium," Acta Cryst., 9 (1956) 972.

74. L. Kaufman and M. Cohen, "The Martensite Transformation in the Iron-Nickel System." Trans. AIME, 206 (1956) 1393.

75. A.B. Greninger and V.G. Mooradian, "Strain Transformation in Metastable Beta Copper-Zinc and Beta Copper-Tin Alloys," Trans, AIME, 128 (1938) 337.

76. M.W. Burkart and T.A. Read, "Diffusionless Phase Change in the Indium-Thallium System," Trans. AIME, 197 (1953) 1616.

77. L. Chang and T.A. Read, "Plastic Deformation and Diffusionless Phase Changes in Metals: The Gold-Cadmium Beta Phase," Trans. AIME, 189 (1951) 47: Journal of Metals, January, 1951.

78. M.S. Wechsler, D.S. Lieberman, and T.A. Read, "On the Theory of the Formation of Martensite," Trans. AIME, 197 (1953) 1503.

79. J.S. Bowles and J.K. Mackenzie, "The Crystallography of Martensite Transformations I and II," Acta Met., 2 (1954) 129, 138.

80. F.C. Frank, "Martensite," Acta Met., 1 (1953) 15.

BIBLIOGRAPHY (Continued)

81. H. Suzuki, Sci. Rep. Res. Inst. Tohoku Univ., 6A (1954) 30.

82. R. Bullough and B.A. Bilby, "Continuous Distributions of Dislocations: Surface Dislocations and the Crystallography of Martensite Transformations," Proc. Phys. Soc., 69B (1956) 1276.

83. A.G. Crocker, "Double Twinning," Phil. Mag., 7 (1962) 901.

84. G.I. Taylor. "Plastic Strain in Metals," Journal Inst. of Metals, 62 (1938) 307.

85. F.N. Rhines and P.J. Wray, "Investigation of the Intermediate Temperature Ductility Minimun in Metals," Trans. ASM. 54 (1961) 117.

86. C.S. Roberts, Discussion of Reference 41, Trans. ASM. 47 (1955) 130.

87. H. Asada and H. Yoshinaga. "Nonbasal Slip and Twinning in Large Magnesium Grains." Nippon Kinzoku Gakkai-Si, 23 (1959) 67.

88. C.S. Roberts, Magnesium and Its Alloys, John Wiley and Sons, (1960).

89. J.D. Mote and J.E. Dorn, "Deformation and Fracture of Magnesium Bicrystals," Trans. AIME, 218 (1960) 491.

90. J.C. McDonald, "Anomalous Behavior During Cold Working and Subsequent Heat Treating of Certain Magnesium Base Alloys," Trans. AIME, 212 (1958) 45.

91. S.L. Couling, J.F. Pashak, and L. Sturkey, "Unique Deformation and Aging Characteristics of Certain Magnesium-Base Alloys," Trans. ASM. 51 (1959) 94.

92. H. Yoshinaga and R. Horiuchi, "Deformation Mechanisms in Magnesium Single Crystals Compressed in the Direction Parallel to the Hexagonal Axis," Trans. Jap. Inst. Metals, 4 (1963) 1.

BIBLIOGRAPHY (Continued)

93. H. Conrad and W.D. Robertson, "Effect of Temperature on the Flow Stress and Strain-Hardening Coefficient of Magnesium Single Crystals," Trans. AIME 209 (1957) 503.

94. R.E. Reed-Hill. "The Mechanism of Fracture in Single Crystals of Magnesium," Ph.D. Thesis, Yale University, (1956).

95. S.L. Couling and G.W. Pearsall. "Determination of Orientation in Magnesium by Polarized Light Examination." Trans. AIME, 209 (1957) 939.

96. F.C. Frank and A.M. Stroh, "On the Theory of Kinking," Proc. Phys. Socl. 65 (1952) 811.

97. H.I. Burrier, M.F. Amateau, and E.A. Steigerwald, "The Relationship between Plastic Deformation and Fracture in Alpha Titanium," Tech. Rept. AFML-TR-65-239, July, 1965, Wright-Patterson Air Force Base, Ohio.

98. E. Schmid and W. Boaz. Kristallplastizat, Springer (Berlin). (1935) 62.

99. J.C. Bauwens. G.A. Homès. and R. Pankowski-Fern, "Aur l'amorce des bandes de deformation dans les Materiaux homogenes et isotropes," Compt. rend., 250 (2) (1960) 290.

100. R.B. Liss. "Luder's Bands." Acta Met., 5 (1957) 341.

101. J. Weertman and J.R. Weertman. Elementary Dislocation Theory. MacMillan. (1964) 190.

102. P.B. Price. "Nucleation and Growth of Twins in Dislocation-Free Zinc Crystals." Proc. Roy. Soc. (London). A260 (1961) 251.

BIOGRAPHICAL SKETCH

William Handy Hartt, III, was born April 28, 1939, at Long Beach, California. He was graduated from Woodrow Wilson High School in Portsmouth, Virginia, in January, 1957. In June, 1961, he received the degree of Bachelor of Science from Virginia Polytechnic Institute and was commissioned an officer in the United States Army. In September, 1961, he began graduate studies at the University of Illinois and worked as a research assistant in the Department of Metallurgical Engineering. In April, 1963, he enrolled in the graduate school of the University of Florida where he worked as a graduate assistant in the Department of Metallurgical and Materials Engineering. From this date until the present he has pursued his work toward the degree of Doctor of Philosophy.

William Handy Hartt is married to the former Helen Fensom Moore of Richmond, Virginia, and is the father of one child. He is a member of the American Society for Metals, Alpha Sigma Mu, Tau Beta Pi, Omicron Delta Kappa, Who's Who in American Colleges and Universities and Sigma Xi.

This dissertation was prepared under the direction of the chairman of the candidate's supervisory committee and has been approved by all members of that Committee. It was submitted to the Dean of the College of Engineering and to the Graduate Council, and was approved as partial fulfillment of the requirements for the degree of Doctor of Philosophy.

August, 1966

Dean, College of Engineering

Dean, Graduate School

Supervisory Committee:

Chairman